Application of the Stability of Proteins from Rates of Oxidation Technique to the Analysis of Mouse Models of Aging and Parkinson's Disease

by

Julia Hamilton Roberts

Department of Chemistry
Duke University

Date:_____

Approved:

_____
Michael C. Fitzgerald, Supervisor

_____
Qiu Wang

_____
Terrence G. Oas

_____
Jennifer L. Roizen

Dissertation submitted in partial fulfillment of the requirements for the degree of Doctor of Philosophy in the Department of Chemistry in the Graduate School of Duke University

2017

ABSTRACT

Application of the Stability of Proteins from Rates of Oxidation Technique to the Analysis of Mouse Models of Aging and Parkinson's Disease

by

Julia Hamilton Roberts

Department of Chemistry
Duke University

Date:_____

Approved:

_____
Michael C. Fitzgerald, Supervisor

_____
Qiu Wang

_____
Terrence G. Oas

_____
Jennifer L. Roizen

An abstract of a dissertation submitted in partial fulfillment of the requirements for the degree of Doctor of Philosophy in the Department of Chemistry in the Graduate School of Duke University

2017

Abstract

Recently, several mass spectrometry-based proteomics techniques have been developed for the large-scale analysis of thermodynamic measurements of protein stability. This has created the possibility of characterizing disease states via differential thermodynamic stability profiles. Described here is the application of the Stability of Proteins from Rates of Oxidation (SPROX) technique to characterize mouse models of disease. The mouse models studied here are of normal aging and two genetically induced Parkinson's Disease (PD) models.

Thermodynamic stability profiles were generated for 809 proteins in brain cell lysates from C57BL/6 mice at age 6- (n=7) and 18-months (n=9). The biological variability of the protein stability measurements was low, and within the experimental error of the SPROX technique. Remarkably, the large majority of the 83 brain protein hits were destabilized in the old mice, and the hits were enriched in proteins that have slow turnover rates ($p<0.07$). Furthermore, 70% of the hits have been previously linked to aging or age-related disease.

One of the PD mouse models involved characterizing the protein interactions induced by mutated leuceine-rich repeat kinase 2 (LRRK2) at a pre-symptomatic time point (3 months old). The models used were a control, overexpressed wildtype LRRK2, and overexpressed R1441G mutated LRRK2 (n=2 for all models). Comparative analyses

on thermodynamic stability profiles of ~470 proteins revealed relatively few differences. In fact, the observed hit rate in each comparative analysis was close to that associated with the biological variability of the mice. However, four protein hits, dihydropyrimidinase-related protein 2, eukaryotic translation initiation factor 4A2, Rap1 GTP-GDP dissociation stimulator 1 and myelin basic protein, were identified with consistent thermodynamic stability in multiple mice within a biological state and as hits in multiple comparisons suggesting they are the most likely to be true positives.

The second PD mouse model studied was one in which the human α-synuclein protein, containing the known PD mutation A53T, was overexpressed. To characterize the disease progression of PD induced by this mutation, mice were sacrificed at 1 month (n=4), 6 months (n=4) and when they became symptomatic at 10-16 months (n=3). Thermodynamic stability profiles were generated for >850 proteins at each time point. The relative stabilities of these proteins were assayed in a series of comparative analyses involving mice at the different time points and the normally aged mice from above. In total 244 peptides were found to be differentially stabilized during PD progression. A subset of 52 peptide hits was identified to be of particular interest. Of these 52 peptides 22 were identified with early disease progression, 5 peptides showed late disease progression, 5 peptides reported a gradual difference in stability over disease progression and 20 peptides indicated no disease progression trend. More than 90% of

the 32 peptides indicating a trend in disease progression showed progression related destabilization.

The results of this thesis help validate the use of thermodynamic stability measurements to capture disease-related proteomic differences in mice. Furthermore, these results establish a new biophysical link between the hit proteins identified and their role in aging, LRRK2 protein interactions, and PD progression.

Dedication

This thesis is dedicated to my wonderful and selfless mother, Margaret Roberts. Thank you for always loving and supporting me through everything. I would not be the person I am today without you by my side.

Contents

List of Tables

List of Figures

Acknowledgements

First, I must thank my advisor Professor Michael C. Fitzgerald for his guidance, support and trust throughout my time at Duke. It has been an incredible experience to work in the Fitzgerald Lab over the past 5 years. I am very thankful that Michael trusted me to become the 'mouse lady' of the lab and to take SPROX into this exciting new direction. I would also like to thank the other members of my committee Professors Qui Wang, Terrence Oas, and Jennifer Roizen for their advice and assessment of my graduate work. I am thankful for the energy and time they have spent to help me achieve this dissertation.

I would also like to thank the members of the Fitzgerald lab (past and present) who have contributed to my education and scientific pursuits. Dr. M. Ariel Geer-Wallace and Dr. Jagat Adhikari were my mentors when I joined the lab. They always answered my questions, pushed me to consider how and why I was doing experiments and provided friendship and laughter. To Ryenne Ogburn—who has been my friend, support system, and scientific partner—thank you. I cannot imagine my journey through graduate school without you and your friendship. I have been lucky to work with many other members of the Fitzgerald Lab: Dr. Yingrong Xu, Lorrain Jin, Fang Liu, He Ming and Arthur Ma. It has been a pleasure to work alongside you and I am excited to see your future contributions to science.

To my WiSE Ladies—Emily, Paige Caroline, Jacqueline and Candise—there are not enough words to express how lucky I am to have found you at Duke. Thank you for your constant encouragement, support, laughter, tears, coffee breaks and love. I have been so inspired by all of you and you have given me a confidence that I will cherish forever. To my Girl Squad—Catherine and Kathleen—you have been my Durham family and my life lines throughout this process. Thank you for always knowing when I need to just take a night off and enjoy your company and always having the best motivational GIF. To Alyson—thank you for being my best friend and support system since college. You always know how to find the right animal video to make me feel better and making me laugh until I cry. Thank you for being such a great role model of a lady boss. To my Farm Family—thank you for supporting me in everything I have attempted since before I can remember. I cannot explain how honored I feel to call you family and know that I would not be the woman I am today without each and every one of you. To the Ball Women—I'm so inspired by the role models of successful women that you have been in my life. I am so excited to be another success from the Ball line!

Finally, I would like to thank my sister Kathryn, my parents Margaret and Kenrick and my fiancée Erik. Katey, I am so lucky to be your older sister. You are always the brightest person in a room and your thoughtfulness, love, support and encouragement have meant more to me than you know. To my mother, Margie, I am constantly in awe of your selflessness and dedication to our family. I would never have accomplished this

degree without you. Thank you for believing in me even when I did not believe in myself and for being my role model. To my father, Ken, thank you for instilling a love of science in me since childhood. You were always willing to answer my detailed 'why' questions and force me to think deeply about how and why our world works the way that it does. Even though I hate to admit it, I probably would not be getting this degree if you had not forced me to read Genome on a family vacation! To my incredible fiancée, Erik, I am so lucky and honored to be your partner. Thank you for always being my biggest supporter and confidant. Thank you for always making me laugh, for taking long hikes with me and for being my calm in this crazy storm over the past five years.

My mantra throughout this process has been "She believed she could, so she did". To all of you—thank you for helping me believe. We did it!

1. Introduction

Portions of this chapter can also be found in the paper "Discovery of Age-Related Protein Folding Stability Differences in the Mouse Brain"(1)

1.1 Protein Thermodynamic Stability Measurements

Proteins are molecules that exist in a dynamic equilibrium, constantly folding and unfolding. In order to perform their biological function, proteins interact with small molecules and other proteins. Proteins can undergo a wide range of conformational changes from more local unfolding of specific regions of secondary structure to more global unfolding of protein domains or even the entire protein structure. The free energies and rate constants associated with these different conformational changes are fundamental biophysical properties of proteins. These properties have been measured on numerous purified proteins to characterize ligand-binding interactions. Understanding how this biophysical property is different across biological states will provide a new avenue for molecular characterization of disease.

The work in this thesis is focused on the evaluation of the protein folding free energies (ΔG_f) associated with more global folding and unfolding reactions of proteins. The equilibrium measured by such ΔG_f values is typically described as between two states: the fully folded native form of the protein and the random coil like structure of the unfolded form. Changes in this thermodynamic measurement due to a ligand interaction (such as a drug) or differences in the nature of the protein (such as a disease

related post-translational modification (PTM) or amino acid mutation) are closely tied to the functionality of a protein. These disease related differences are of particular significance to the work in this dissertation.

This dissertation focuses on a new application of ΔG_f values to characterize mouse models of disease. To date, the large-scale analysis of such disease-state models has largely relied on gene and protein expression levels(2-5). Studying the thermodynamic stability differences induced by disease specific mutations or in disease specific comparative analyses has the potential to better identify functionally relevant changes in complex biological systems. These differences may be induced by a direct interaction with the disease specific mutated protein or may be indicative of a downstream effect on thermodynamic stability due to altered protein-protein interactions or PTMs.

1.2 Proteomic Techniques for Probing Protein Energetics

Over the past decade several different techniques have been developed to study protein folding on the proteomic scale via mass spectrometry. The use of mass spectrometry allows for the analysis of hundreds to thousands of proteins within an experiment. Probing such a large number of proteins in one experiment allows for a more thorough characterization of protein thermodynamic stabilities than was previously accessible. The different techniques probe the different equilibrium

unfolding/refolding properties of proteins using one of three different strategies: limited proteolysis, protein precipitation or covalent modification.

Two techniques have been developed to probe the more local folding/unfolding properties of proteins by exploiting a limited proteolysis reaction at very low concentrations of denaturant (or in the absence of denaturant): Drug Affinity Responsive Target Stability (DARTS) and Limited Proteolysis (LiPS)(6, 7). Another limited proteolysis technique, Pulse Proteolysis(8), involves the incubation of proteins in increasing amounts of chemical denaturant followed by a limited proteolysis reaction to probe the more global the unfolding/folding reaction. Stability of Proteins from Rates of Oxidation (SPROX) is a chemical denaturant based technique that uses the covalent oxidation of methionine residues to characterize the more global folding/unfolding behavior of proteins(9). The last group of techniques are those that quantify the extent of temperature induced protein precipitation to report on the folding/unfolding equilibrium (thermal proteome profiling (TPP)(10), target identification by ligand stabilization (TILS)(11) and thermal stability shift-based fluorescence difference in two dimensional gel electrophoresis (TS-FITGE)(12)).

The above strategies have largely been developed in the context of protein-ligand studies where the goal was to quantify ligand-induced thermodynamic stability shifts. These strategies have been developed using a number of well-studied protein ligand systems(6, 8-22). They have also been used in an increasing number of protein target

discovery efforts(6, 11, 12, 23-36). More recently they have begun to be used for disease state characterization (**Table 1).** The studies summarized in **Table 1** are important because they indicate the ability of thermodynamic stability measurements to differentiate disease states. The techniques in this field are all relatively new and researchers are still investigating the benefits and drawbacks of using a specific technique in a given context. As shown in **Table 1** half of the experiments reported thus far on disease state characterization utilize the SPROX technique. The work in this dissertation involves extending the application of SPROX to the characterization of mouse models of disease.

Table 1: The current experiments that have studied differential protein energetics in biological states via proteomic techniques.

Technique	Biological State	Protein Sample (cell lysate)	Coverage (Proteins)	Hits (Proteins)	Ref
SPROX	Breast Cancer	MCF7, MCF-10A, MDA-MB-231	~800	~170	(37)
Hybrid-SPROX	Allergens	Dust Mites	675	N/A	(38)
SPROX	Aging	Mouse Brains	809	83	(1), Ch. 3
LiPs	Metabolism	Yeast	>1000	~300	(7)
LiPs	Breast Cancer	MCF7, MCF-10A	556	203	(39)
DARTS	Oxidative Stress	THP-1	N/A	2	(40)

1.3 Stability of Proteins from Rates of Oxidation (SPROX)

1.3.1 SPROX Methodology

The SPROX strategy involves distributing protein samples into increasing concentrations of a denaturant and allowing the proteins to equilibrate. Hydrogen peroxide is added to the samples and reacted for three minutes. These reaction conditions have been tuned in order to ensure that only exposed methionine residues are modified and the reaction is pseudo-first order. The reaction time and hydrogen peroxide concentration are set to ensure that the reactions of an unprotected methionine residue proceeds for three half-lives. The hydrogen peroxide reaction conditions are also set such that the system exists in so-called EX2 reaction conditions (i.e. the modification reaction rate is much slower than the folding/unfolding rate of the protein)(41). The hydrogen peroxide reaction is ultimately quenched with an excess of reducing agent, typically methionine. The relative quantity of unoxidized methionine or oxidized methionine can be measured through a number of labeling techniques—isobaric mass tagging (TMT or iTRAQ-8plex)(9) or SILAC labeling of cells(20). A critical aspect of the SPROX methodology is the detection of and quantitation of methionine containing peptides in the bottom up proteomics experiments. To facilitate this, a methionine-containing peptide enrichment strategy has been incorporated into the SPROX protocol(19, 42). Full experimental protocol described below in **Figure 1**.

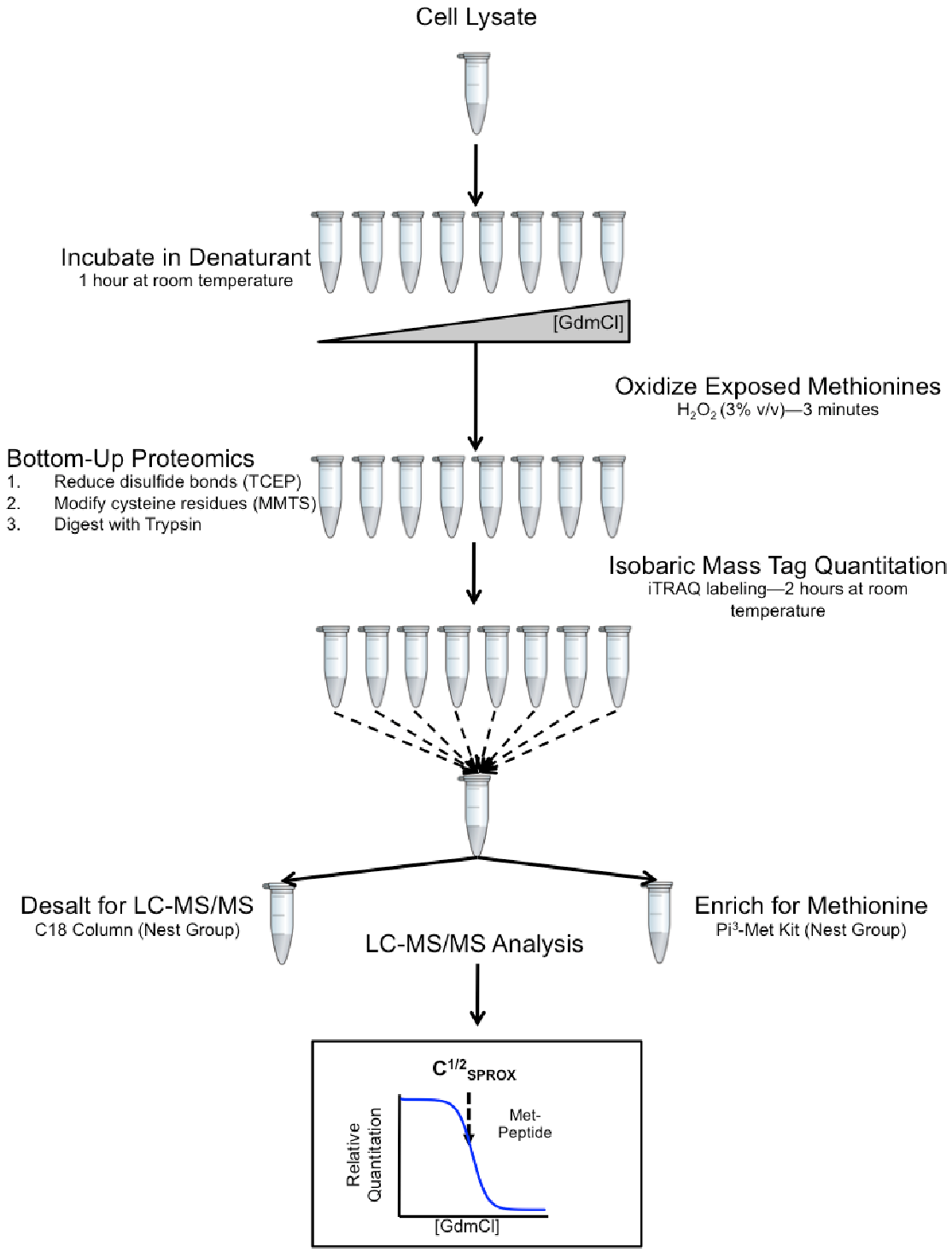

Figure 1: Schematic of the standard iTRAQ-SPROX protocol used for all experiments in this thesis.

1.3.2 SPROX Development

The SPROX technique was first reported to measure thermodynamic stability shifts of purified proteins in 2008(43). It was expanded to a large scale proteomics technique in 2010 with a proof-of-principle study that measured the direct and indirect binding partners of CsA in yeast(9). In this study, two known targets were identified as well as eight novel binding partners. The SPROX technique was further applied to identify yeast cell lysate interactions with a known promiscuous ligand NAD^+ and the small molecule resveratrol. The NAD^+ experiment identified 11 protein hits. The hits were enriched for known binding partners of NAD^+, dehydrogenases (7 of the 11 hits were annotated as such). Furthermore, a K_d was measured for alcohol dehydrogenase that agrees with literature values validating the ability of SPROX to identify and quantify affinities of binding interactions(19). In the resveratrol experiment 7 total proteins were identified as hits and one of the seven was a known direct binder. Further proof-of-principle SPROX studies focused on identifying the CsA-Cyclophilin A interaction and ATP binding proteins by expanding the quantitation to SILAC labeled cells(20). Interactions with ATP were also studied with the iTRAQ-SPROX technique, 28 total protein targets were identified. Of the 28 hits, 9 novel ATP binding proteins that were identified via the SILAC-SPROX technique were confirmed and 14 hits had previously been annotated as ATP binding proteins(21). A further expansion of the technique was the development of the so-called hybrid-SPROX protocol(44). This

combines the methionine oxidation of the SPROX technique with a tryptophan modification. This increased the proteomic coverage of the technique as now any peptide containing a methionine or a tryptophan can report back on the thermodynamic stability of the protein.

The SPROX technique has been used as a proteome level screen for both identifying novel ligand-binding partners and characterizing disease states. The technique was used to identify proteins with altered stability in the presence and absence of the natural product, anti-cancer agent, Manassantin A(36). This was conducted by growing MDA-MB-231 cells in hypoxic conditions and then incubate cell lysates were incubated with or without the small molecule. Two hits, filamin A and elongation factor 1α, from iTRAQ-SPROX were confirmed via the SILAC-Pulse Proteolysis technique. The SPROX technique was also used to identify binding interactions between the natural product Geldanamycin and Hsp90(22). This study was conducted by incubating MCF-7 human cell lysate with or without geldanamycin. Geldanamycin is a natural product known to inhibit Hsp90 but the binding affinity remains unclear. Through this work the iTRAQ-SPROX and Hybrid-SPROX techniques were able to identify domain specific Hsp90 stability changes upon incubation with geldanamycin. Only peptides identified in the N-terminal ATP binding domain were shown to have thermodynamic stability changes upon incubation with geldanamycin. Furthermore, a slow and fast binding constant were measured that are consistent with

literature. These were measured by allowing the geldanamycin to incubate with the cell lysate for either 30 minutes (fast binding) or 24 hours (slow binding constant).

The SPROX technique has also been used to study and characterize disease state differences in protein thermodynamic stability. SPROX successfully differentiated three breast cancer cell lines with different levels of invasiveness (MCF7, MDA-MB-231 and MCF-10A). Protein hits were identified in all comparisons and a number of the proteins have been previously linked to cancer through catalytic activity of post-translational modifications. Interestingly, it was possible to identify specific proteins that are of importance in the MCF7 type cancer progress, biomarkers that are broadly related to breast cancer and those specific to the MDA-MB-231 type. This study utilized SILAC labeling and was able to concurrently gather protein expression level data with the protein thermodynamic stability measurements(37). The Hybrid-SPROX technique was used to study the dust mite proteome and identified that allergenic proteins are both more abundant and more thermodynamically stable than other proteins in the proteome(38). The SPROX technique has recently been used to characterize the aging disease state in mouse brain proteins which will be discussed in more detail in Chapter 3. The SPROX technique has also been used to study targeted proteomics with light and heavy labeling of unoxidized methionine residues(45). Through this new labeling technique it is possible to track the protein folding stability of a single methionine containing peptide of interest. Such targeted analysis is of interest for future diagnostic

work due to its ability to ensure data is gathered on the specific peptide that is known to exhibit disease behavior.

1.3.3 Using SPROX to study Disease States

The experiments described in this dissertation were designed to investigate the ability of the SPROX technique to characterize mouse models of disease. This is an important step in the development of SPROX because it opens the door for higher order biological systems to be studied. Furthermore, it gets the technique one step closer to being clinically relevant in human tissues. The SPROX technique has been used previously to differentiate breast cancer cell lines(37). Taking the SPROX technique into mouse models will allow for the global study of biological systems that are more closely related to humans than the previous cell line studies. Furthermore, the studies of the rodent models described here provide, for the first time, an understanding of the biological variability of the protein stability measurements determined by SPROX. Understanding the extent of biological variability is important for future steps into clinical usage.

1.4 Overview of Mouse Disease Models

1.4.1 Normal Aging

One biological system studied in this thesis is the normal aging process of mouse brains. The mice in this study were a base strain of mice (C57BL/6) that did not have genetic alterations. As the life expectancy of humans continues to increase the number

of people affected by age-related disorders also increases. Aging is often described as a breakdown of cellular function and has been tied to oxidative stress(46-48), deamidation(49) and ubiquitination(50-53). However, researchers are still struggling to fully characterize and understand the biological process of aging and links between different age-related disorders. Through studying aging it is possible to identify areas of interest for anti-aging drug development and commonalities between many diseases that share aging as a risk factor.

Several large-scale gene and protein expression level studies have been conducted in rodents and nematodes to better understand the molecular basis of aging(5, 54, 55). Of particular significance to the current work is that two rodent studies identified relatively few age-related differences in gene and protein expression levels(5, 55); perhaps because changes in protein abundance are not always directly tied to changes in protein function. In contrast, the link between protein folding stability and function is more direct(56, 57). Changes in protein folding stability can occur as a result of several biologically significant phenomena such as the mutation, modification, and misfolding of proteins. These phenomena are commonly associated with aging(46-53, 58-61). Indeed, the folding properties of a number of proteins with importance in the aging process and in age-related diseases have been investigated(62-71). However, these investigations have largely involved the targeted analysis of specific purified protein constructs. The global analysis of protein folding and stability in aging and age-related

diseases has the potential to produce a more complete understanding of the functionally relevant proteins and pathways involved in this biological process. Protein folding stability is a biophysical property that can be modulated with small molecule drugs. For example, pharmacological chaperones have been targeted to proteins that play pathogenic roles in various protein misfolding diseases(72-77). Therefore, it is possible that proteins with age-related destabilizations may be useful therapeutic targets to treat the adverse effects of aging with pharmacological chaperones.

1.4.2 Parkinson's Disease

Two of the mouse models in this thesis are related to Parkinson's Disease (PD). PD is a progressive neurodegenerative disorder that was first identified in 1817(78). The progression and presentation of PD is highly complex and still not fully understood even after 200 years of study. With current diagnostic tools up to 70% of final degradation has occurred upon the time of phenotypic presentation of PD and typical diagnosis(79). Neuronal degradation and death cannot be reversed. Therefore, the earlier a patient can be accurately diagnosed with PD the more effective treatments can be. The identification biomarkers and understanding of the disease progression has the potential to alter the way PD is diagnosed and treated.

Parkinson's Disease presents through progressive loss of dopaminergic neurons, accumulation of Lewy Bodies and tremors. The first protein that was linked to PD development is α-synuclein(80) and since has been studied to elucidate its biological

properties and links to PD development. Throughout these studies it was identified as the major component of Lewy Bodies(81) and a number of animal models of the disease have been created based on mutations in α-synuclein(82). The protein α-synuclein is encoded for by the gene SNCA and is a 140 amino acid natively unfolded protein. The protein folds into α-helices with a random coil tail in the presence of lipid membranes (**Figure 2A**)(83). A recent effort determined a 3D structure of α-synuclein fibrils that confirms the generation of β-sheets (**Figure 2B**)(84). The true neurotoxic effects of α-synuclein are unknown. However, many consider the process of aggregation and eventual Lewy Body formation to be major players in the disease progression. Three point mutations of α-synuclein have been linked to PD progression—A30P, E46K and A53T—and all three affect the formation of the characteristic fibrils found in PD brains. Both the A30P and A53T mutations induce more protofibril formation than the wildtype while E46K causes less protofibril formation(85, 86). Furthermore, A53T forms more fully mature fibrils than the other versions of the protein(85). Even though α-synuclein has a strong genetic and phenotypic link to PD pathogenesis a complete understanding of the cellular mechanisms of PD is still unknown.

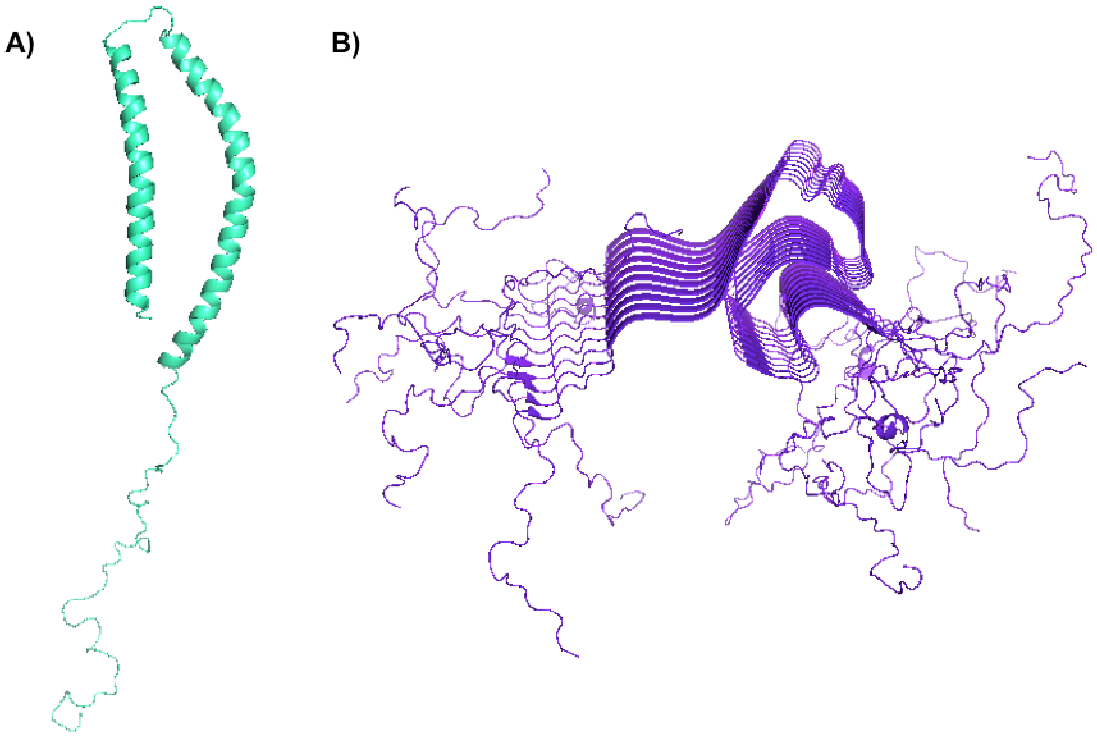

Figure 2: Crystal structures of the α-synuclein protein isolated A) in the presence of a membrane (PDB:1XQ8) B) as the characteristic fibrils seen in Lewy Bodies (PDB:2N0A)

Another protein of interest in the development of PD is leuceine rich repeat kinase 2 (LRRK2). Mutations in LRRK2 are implicated in 7% of familial cases of PD and <1% of all sporadic cases making LRRK2 a well-known molecular player in the progression of PD(87). LRRK2 is a large (~286kDa) multi-domain serine/threonine kinase that typically exists as a dimer and can be found in both the membrane and the cytosol(88-90). The LRRK2 protein is made up of four major domains: a Ras of complex protein (ROC)/GTPase domain, a C-terminal of ROC (COR) domain, a kinase domain and a number of scaffolding domains. The major familial mutations (G2019S, I2020T,

R1441G/C/H, N1437H and Y1699C) occur in the ROC/GTPase, COR and kinase domains as shown in **Figure 3.**

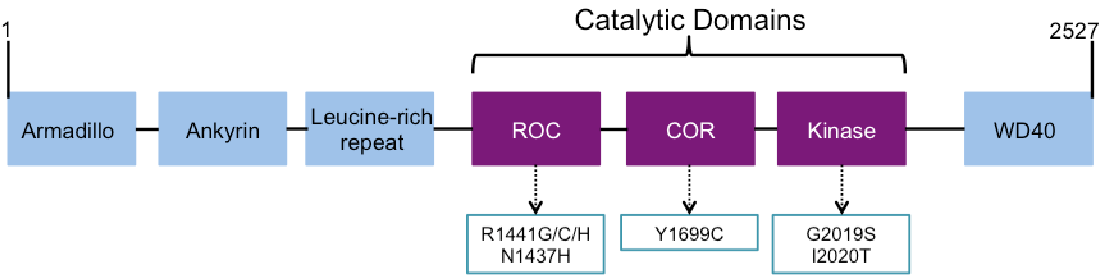

Figure 3: Schematic of the LRRK2 domain structure. Parkinson's Disease related familial mutations are indicated in boxes under their respective domains.

The G2019S mutation is the most common in familial cases and has been observed in some sporadic cases(91). It has been shown to significantly increase the kinase activity of LRRK2(92). Mutations in the ROC/GTPase domain have been shown to alter the ability of the GTPase domain to fold and function properly(93-95). The kinase domain of LRRK2 autophosphorylates the protein. This autophosphorylation is likely important for the downstream effects of LRRK2(88, 96). Autophosphorylation typically occurs in the ROC domain(97) indicating phosphorylation of specific amino acids could be required for GTPase function and interruption of this modification could lead to disease progression. Understanding which protein interactions are altered due to a loss of GTPase function could provide insight into the protein pathways important in PD. These proteins and pathways impacted by the mutation in the ROC domain have the potential to act as drug targets (i.e. rescuing a mutation specific loss of

thermodynamic stability) or biomarkers due to the similarities in symptoms seen between genetic LRRK2 PD and sporadic PD. Previous studies of the importance of LRRK2 pathogenic mutations on cellular stability and LRRK2 function have identified a number of potential biological pathways and protein-protein interactions that may play a role in disease progression (e.g. vesicular trafficking(98), membrane association(99), GTPase function(100)). However, there are still many questions about the role of LRRK2 in PD. The proteins identified with differential thermodynamic stability due to α-synuclein and LRRK2 could prove to be useful biomarkers of PD. Furthermore, these proteins will provide a deeper understanding of the pathways and proteins involved in disease progression.

1.5 Focus of this dissertation

Current approaches to study disease states focus on quantifying differences in protein or gene expression levels. While this provides useful information, expression levels are not directly tied to functional differences. Therefore, a more relevant and/or complementary avenue to characterizing disease states is the use of thermodynamic stability measurements. These measurements are of interest because they identify a distinct biophysical property of the protein that may be altered in the disease state. If such a protein hit has been previously annotated in an expression level study the new biophysical information about stability adds to the disease related understanding of the

protein. If the protein is a novel discovery it indicates a biophysical link, and probes a region of the proteome that previously was not associated with the disease.

The focus of this dissertation is the application of the SPROX technique to mouse models of disease. This thesis describes the first use of proteome-wide thermodynamic stability measurements in rodent models. The move into mouse models is an important step in identifying the compatibility of these techniques with highly complex biological systems. The compatibility of SPROX with higher orders of complexity is a promising step towards measuring stabilities in human clinical samples. The work in this thesis is conducted on proteins derived from mouse brain tissue lysates.

The work in Chapter 2 of this dissertation described the introduction of the SPROX technique into mice with an experiment that was designed to closely mimic previous ligand binding experiments. In this work a FVB/NJ mouse model with overexpressed LRRK2 protein (wildtype and mutated) was used to identify protein-protein interactions of the LRRK2 protein and the effect of a disease related mutation on these interactions. The work in Chapter 3 is focused on the application of the SPROX to a mouse model of normal aging. This study compared the thermodynamic stability of proteins from young and old mouse brains to capture changes associated with the natural aging process. Chapter 4 described work conducted on a mouse model of Parkinson's Disease progression using C57BL/6 mice genetically altered to overexpress human α-synuclein with the disease mutation A53T. This study compared

thermodynamic stability over the progression of Parkinson's Disease to identify future biomarkers or drug targets.

2.Identifying protein interactions of the LRRK2 protein in mouse brains

2.1 Introduction

Even though a number of protein mutations associated with Parkinson's Disease (PD) have been identified, many of the molecular details of the disease remain unknown. This has made both the diagnosis of the disease and the development of drug therapies especially challenging. Therefore, it is of great interest to continue characterizing the molecular basis of PD. The goal of the work described in this chapter was to better understand the role of a mutation in the protein leucine-rich repeat kinase 2 (LRRK2) that has been implicated in familial and sporadic PD.

The work described here utilized the iTRAQ-SPROX technique to identify thermodynamic stability differences in mouse brain proteins that are induced by the overexpression of wildtype LRRK2 or the overexpression of R1441G mutated LRRK2. This was a discovery effort on two fronts: 1) to identify the sensitivity of the SPROX technique to characterize protein stability differences induced by a single point mutation and 2) to identify protein-protein interactions of LRRK2 and the impact the R1441G mutation has on those interactions. The iTRAQ-SPROX technique was originally developed to study thermodynamic stability changes induced by protein-ligand interactions(9). Stability changes in such studies are probed by incubating a protein sample in the presence and absence of a ligand. The thermodynamic stabilities are quantified in both samples and proteins are considered hits if the ligand incubation

causes a measureable shift in stability. Typically, these studies are conducted with vast excess of ligand concentration (100-1000 μM) to probe a large range of binding affinities. The experiment described here was designed to expand the use of the iTRAQ-SPROX technique into mouse models where the overexpression of the LRRK2 protein (either wildtype or R1441G mutated) acts as the 'ligand'.

Identifying these binding partners could give insight into specific proteins and pathways to be utilized as biomarkers of PD or potential drug targets to treat PD. The three mouse models studied here included: a control mouse, a mouse that had the wild-type LRRK2 protein overexpressed by 5- to 10-fold and a mouse that had the LRRK2 protein with the R1441G mutation overexpressed by 5- to 10-fold(101). Two mice were used in each cohort and the brain tissue lysates for each mouse in this study were subjected to two iTRAQ-SPROX experiments. In this study, three comparisons were conducted: control vs. overexpressed wildtype LRRK2, control vs. overexpressed LRRK2(R1441G) and overexpressed wildtype LRRK2 vs. overexpressed LRRK2(R1441G). In each of the three comparisons over 660 peptides from over 380 proteins were quantitatively characterized. Very few hits were identified in the comparisons. In fact the hit rate (1-2%) was in range of the false positive rate of the SPROX technique(102). Even with the small hit rate, four proteins of interest (myelin based protein, dihydropyrimidinase-related protein 2, eukaryotic translation initiation

factor 4A2, Rap1 GTP-GDP dissociation stimulator 1) were identified that indicate protein-protein interactions with LRRK2.

2.2 Experimental Procedures

2.2.1 Mouse Euthanasia and Tissue Lysis

The mice used in this study were purchased from The Jackson Laboratory and euthanized by cervical dislocation upon arrival at Duke University. All mice were three month old females. The control, overexpressed and overexpressed-mutated strains were FVBNJ, FVB/N-Tg(LRRK2)1Cjli/J and FVB/N-Tg(LRRK2*R1441G)134Cjli/J respectively. Immediately following euthanasia the brains were removed and kept at -20°C until the cell lysis was performed. Immediately prior to cell lysis brains were cut into pieces with a straight razor placed in a Lysing Matrix A tube (MP Biomedicals) with 400 μL of 20mM phosphate buffer (pH 7.4) and 4 μL of 100X protease inhibitor cocktail (pepstatin A (0.2 mM), leupeptin (0.4 mM), E-64 (0.3 nM), bestatin (1 mM), and AEBSF (20 mM) protease (all from ThermoFisher Scientific, Waltham, MA)) and lysed via MP Fast-Prep 24 Tissue Homogenizer. The lysis involved 20 seconds of homogenization at 4m/s followed by 5 minutes on ice and 20 seconds of homogenization at 4m/s. The lysate was centrifuged at 4°C and 14,000 rcf for 90 minutes. The supernatant was removed and kept at -20°C until iTRAQ-SPROX analysis.

2.2.2 iTRAQ-SPROX Protocol

Immediately prior to iTRAQ-SPROX analysis a Bradford Assay was used to quantify the protein concentration of the lysates. Lysates were diluted to 5mg/mL and an aliquot of 20 μL of lysate (100 μg of total protein) was distributed into a series of 8 GdmCl-containing SPROX buffers comprised of 20 mM phosphate buffer (pH 7.4) and increasing concentrations of GdmCl). Each tube contained 25 μL of SPROX buffer. Samples were then incubated at room temperature for 1 hour. After incubation, 5 μL of 30% H_2O_2 (v/v) was added and allowed to react for 3 minutes before being quenched by a 300 mM L-Methionine solution. The final concentration of GdmCl in the reaction buffers for the two iTRAQ-SPROX experiments performed on each mouse brain lysate are shown in **Table 2**. Both of the iTRAQ-SPROX experiments on each mouse were conducted using identical iTRAQ-SPROX protocols except that the two experiments employed slightly different final denaturant concentrations.

Table 2: GdmCl denaturant conditions used for the A and B experiments of each mouse brain tissue lysate.

		Final denaturant concentrations [GdmCl] (M)							
Experiment	**A**	0.6	1.1	1.2	1.6	1.8	2.0	2.5	3.0
	B	0.8	1.1	1.2	1.4	1.6	1.8	2.0	2.5

2.2.3 Proteomic Sample Preparation

The proteins in each SPROX buffer were precipitated with the addition of 200 μL of 1 g/mL tricholoroacetic acid (TCA) on ice overnight. Precipitated proteins were

pelleted by centrifugation at 8,000 rcf and 4°C for 30 minutes. Pellets were decanted and washed 3 times with 300 μL of ice cold ethanol. Samples were placed at room temperature in a fume hood for 30 minutes to allow all residual ethanol to evaporate.

Protein pellets were dissolved with 0.1% SDS in 30 μL of 0.5 M TEAB buffer. The dissolution was aided by vortexing for 10 minutes, heating at 60°C with shaking for 10 minutes and sonicating for 10 minutes. After dissolution, disulfide bonds were reduced by reacting the protein samples with 5mM TCEP for 1 hour at 60°C with shaking. The now exposed cysteine residues were modified with 10mM MMTS for 10 minutes at room temperature. The proteins were then digested with 1μg of trypsin over night at 37°C with shaking. Samples were labeled with 0.5 unit of iTRAQ reagent dissolved in 50 μL of isopropanol. In each experiment the protein samples from the SPROX buffers with increasing GdmCl concentrations were reacted with iTRAQ tags 113, 114, 115, 116, 117, 118, 119 and 121 respectively. The iTRAQ labeling reaction was conducted at room temperature for 2 hours. A 55 μL aliquot of the labeled samples from the two experiments were combined. Aliquots (120 μL each) from the combined samples from each experiment were removed and desalted via a C18 resin clean up (The Nest Group). These were the so-called 'non-enriched' samples. Aliquots (240 μL each) from the combined samples from each experiment were also removed and enriched for methionine residue containing peptides using a Pi^{3TM} Methionine Reagent according to

the manufacturer instructions (The Nest Group). These were the so-called 'enriched' samples.

2.2.4 LC-MS/MS Analyses

All samples were analyzed on a Orbitrap Elite ETD mass spectrometer with an EASY-nLC system (ThermoFIscher Scientific Inc.). The trapping column used in these experiments was a 100 μm x 2 cm Integrafrit column (New Objective) that was packed with 200 Å Magic C18 AQ 5 μm material from Michrom. The column in these runs was a 75 μm x 25 cm PicoFrit column (New Objective) packed with 100 Å Magic C18 AQ 5 μm material from Michrom. A flow rate of 400 nL/min was used for all runs. The chromatography gradient was as follows: 5% to 7% solvent B over 2 minutes, 7% to 35% solvent B over 90 minutes, 35% to 50% solvent B over 1 minute, 50% solvent B for 9 minutes, 50% to 95% solvent B over 1 minute and 95% solvent B for the final 8 minutes. Solvent B is 0.1% Formic Acid in ACN. The sample was trapped on a column (Symmetry C18 300 mm x 180 μm) for 3 minutes at 5 μL/min 0.1% formic acid in water. The sample was then separated using the following gradient: 3% to 30% acetonitrile with 0.1% formic acid over 90 minutes. A resolution of 15,000 was used for product ion scans and collected for the top 10 most intense peaks for a specific precursor scan (resolution of 60,000). An intensity threshold of 5,000 was used. Dynamic exclusion was set at 1 scan in a 0.75 minute window for a given m/z ratio. The scan range for the precursor scan was 400-1,800 m/z with an isolation width of 1.2 m/z. A product ion scan

range of 100-2,000 m/z was used. Collision induced dissociation (CID) was conducted with HCD and a normalized collision energy of 40% and activation time of 0.1ms.

Peak lists were extracted from the LC-MS/MS data and were searched against the 59, 534 proteins in the IPI *Mus musculus* database version 3.79, released on 1/18/2011 and downloaded from ftp://ftp.ebi.ac.uk/pub/databases/IPI/last_release/old/MOUSE/ using Proteome Discoverer (Version 1.4.1.14). Cysteine residue modification by MMTS and N-termini and lysine residues modified by iTRAQ 8-plex were fixed modifications in the search. Oxidized methionine residues and deamidation on asparagine and glutamine were variable modifications in the search. Up to two missed tryptic cleavages after R and K were allowed. The parameters included a 10 ppm mass tolerance window for precursor masses and 0.8 Da for fragment mass tolerance. Only peptide spectra with FDR <5% and iTRAQ reporter ion intensities that summed to >1000 were used in subsequent analyses of the data.

The LC-MS/MS analyses of the iTRAQ-SPROX samples analyzed here included 2 replicate LC-MS/MS runs of each methionine-containing peptide enriched sample and 1 LC-MS/MS run of each non-enriched sample generated from each brain tissue cell lysate.

2.2.5 Data Analysis

The data was normalized as previously described in reference(42). Briefly, the 8 iTRAQ reporter ion intensities generated in each product ion mass spectra were

averaged and the raw intensity of each reporter ion in the product ion mass spectrum was divided by the average to generate so-called N1-normalized values. All the N1 values for non-methionine containing peptides were averaged for each reporter ion. Summarized in **Table 3** are the set of 8 average values (so-called N2 normalization factors) that were generated in each SPROX analysis.

Table 3: Summary of the N2 normalization factors and standard deviations calculated for all iTRAQ-SPROX experiments

Model	Mouse	Exp		113	114	115	116	117	118	119	121
Control	1	A	N2	0.79	1.1	0.93	1.0	0.98	0.93	1.1	1.2
			SD	0.15	0.18	0.13	0.17	0.14	0.15	0.14	0.21
		B	N2	0.97	0.95	1.1	1.1	1.0	0.91	0.97	1.1
			SD	0.15	0.19	0.16	0.16	0.13	0.14	0.14	0.24
	2	A	N2	0.60	0.95	1.1	1.1	1.1	0.80	1.3	1.0
			SD	0.14	0.16	0.14	0.14	0.13	0.14	0.14	0.25
		B	N2	0.98	1.0	0.57	0.76	1.5	0.81	1.3	1.1
			SD	0.18	0.24	0.15	0.17	0.19	0.18	0.19	0.19
Wildtype LRRK2	1	A	N2	1.0	0.87	0.88	0.96	0.94	0.95	1.1	1.2
			SD	0.19	0.17	0.15	0.16	0.14	0.16	0.16	0.22
		B	N2	0.84	0.92	0.97	1.0	1.1	0.87	1.0	1.3
			SD	0.17	0.20	0.14	0.17	0.15	0.14	0.14	0.23
	2	A	N2	1.1	0.90	0.92	0.91	1.1	1.0	1.2	0.86
			SD	0.17	0.15	0.16	0.14	0.16	0.17	0.15	0.24
		B	N2	1.3	1.0	0.79	1.1	0.94	0.69	0.98	1.1
			SD	0.24	0.19	0.14	0.20	0.20	0.16	0.15	0.24
LRRK2 (R1441G)	1	A	N2	1.1	0.18	1.0	1.1	1.2	0.87	1.3	1.3
			SD	0.16	0.24	0.16	0.16	0.15	0.16	0.18	0.21
		B	N2	1.0	1.0	0.90	1.2	0.98	0.84	0.92	1.2
			SD	0.16	0.20	0.14	0.16	0.16	0.15	0.15	0.25
	2	A	N2	1.0	0.24	1.0	1.2	1.1	1.1	1.9	1.3
			SD	0.23	0.29	0.21	0.21	0.20	0.21	0.20	0.41
		B	N2	1.1	1.0	1.0	0.98	0.56	1.0	1.0	1.1
			SD	0.19	0.18	0.16	0.17	0.15	0.16	0.15	0.21

Ultimately, the N1-normalized values generated for the methionine containing peptides were divided by the corresponding N2 normalization factor to determine the final N2-normalized reporter ion intensity. The chemical denaturation data sets were fitted to a four parameter sigmoidal equation, equation 1, using a JAVA-based program (developed in house) that utilized the Nelder and Mead Simplex method for regression analysis(103).

$$y = A + \frac{(B - A)}{1 + e^{-\frac{C_{1/2} - x}{b}}} \qquad \text{Equation (1)}$$

In equation 1, A is the pre-transition baseline, B is the post-transition baseline, $C_{1/2}$ is the transition midpoint and b is a measure of the steepness of the transition. This program fits each set of data nine times, once with all eight points and then eight times systematically ignoring one point. The fit with the highest R^2 value was chosen as the final output. Subsequent analyses of the data only utilized the chemical denaturation data sets that were determined to be high quality ($R^2 \geq 0.8$) and were generated from product ion mass spectra with low isolation interference (≤ 30%). If a peptide was identified multiple times within the same iTRAQ-SPROX experiment the N2-normalized iTRAQ reporter ion intensities from the high quality data were averaged together to generate one set of iTRAQ reporter ion intensities at the 8 denaturant concentrations and the averaged data was fit to equation 1 as described above to extract a single $C_{1/2}$ value per experiment.

2.2.6 Hit Identification

A Student's two-tailed t-test was used to identify significant differences between the assigned $C_{1/2}$ values for a given peptide in the comparative analyses performed here. Three different analyses were conducted to identify protein-protein interactions involving wildtype LRRK2 and the PD related mutant R1441G: one in which the control was compared to the overexpressed wildtype LRRK2 to elucidate proteins with altered stability due to the overexpression of LRRK2, one in which the control was compared to the overexpressed LRRK2(R1441G) to elucidate proteins with altered stability due to the overexpression of the mutated LRRK2 and one in which the overexpressed wildtype LRRK2 was compared to the LRRK2(R1441G) to elucidate proteins with altered stability due to the disease related mutation R1441G. Additional comparative analyses were also conducted to compare the stabilities of proteins within each cohort to assess biological variability. A $\Delta C_{1/2}$ value was determined to be significant if the determined t-test p-value was < 0.05.

2.2.7 Quantitation of Thermodyanmic Stability Changes

The transition midpoint shifts of the hit peptides were used to calculate free energy ($\Delta\Delta G$) changes according to equation 2.

$$\Delta\Delta G = - m \times \Delta C_{1/2} \qquad \text{Equation (2)}$$

In equation 2, $\Delta\Delta G$ is the change in free energy, m is $\delta\Delta G/\delta\Delta C_{1/2}$, and $\Delta C_{1/2}$ is the transition midpoint shift. An m-value of 2.6 kcal $mol^{-1}M^{-1}$ for GdmCl was used for all

proteins. This *m*-value was estimated based upon the average protein domain size of 100 amino acids and the average contribution of 0.026 kcal mol^{-1} M^{-1} per amino acid to the *m*-value of the protein as determined in reference(104).

2.3 Results

2.3.1 Experimental Design

The goal of this work was two-fold: i) to identify protein-protein binding interactions involving LRRK2; and ii) to identify those protein-protein binding interactions involving LRRK2 that are affected by the R1441G mutation. The mouse models of PD employed in this work included: control FVB/NJ mice, FVB/NJ mice overexpressing wildtype LRRK2 and FVB/NJ mice overexpressing LRRK2 (R1441G). Two iTRAQ-SPROX experiments were performed on brain tissue cell lysates from each mouse in this study (**Figure 4**).

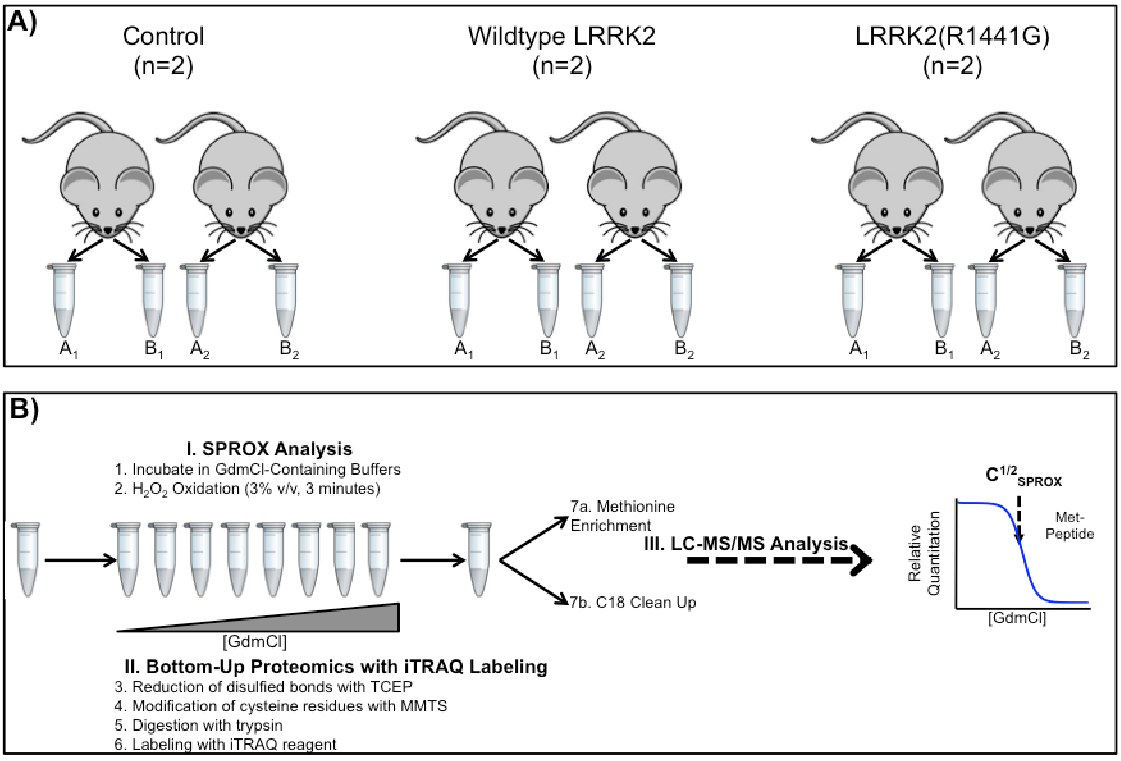

Figure 4: Schematic representation of the experimental workflow used in this work. (A) Description of the mouse models used in this work. (B) Detailed description of the iTRAQ-SPROX protocol used for each experiment.

Ultimately, four sets of thermodynamic stability measurements were generated for the mice in each cohort; and the Student's two-tailed t-test was used to identify peptides with significantly different stability within and between the cohorts to characterize the biological variability and induced thermodynamic stability differences respectively. The thermodynamic stability data generated for the brain tissue cell lysate in each cohort were used to conduct three comparative analyses. In one comparison, which was designed to identify potential LRRK2 protein-protein interactions, proteins that showed differential thermodynamic stability due to the overexpression of LRRK2

(Control vs. Wildtype LRRK2) were identified. In a second comparison, which was designed to identify potential LRRK2-R1441G protein-protein interactions, proteins that showed differential thermodynamic stability due to the overexpression of the R1441G-LRRK2 (Control vs. LRRK2(R1441G)) were identified. In a third comparison, which was designed to identify mutation induced protein-protein interaction differences, proteins that showed differential stability due to the R1441G mutation (Wildtype LRRK2 vs LRRK2(R1441G)) were identified. Comparative analyses were also conducted to assess the biological variability of the $C_{1/2}$ values by comparing the peptide stability measurements between the two mice within a cohort.

2.3.2 Overall Proteomic Coverage

In the work described here, 12 total iTRAQ-SPROX experiments were conducted with proteomic coverage averaging 825 unique peptide identifications from ~470 unique proteins per experiment (**Table 4**). For a peptide to be included in the coverage it must contain a wildtype methionine residue and generate high quality chemical denaturation data (FDR <5%, $R^2 \geq 0.8$ and isolation interference ≤30%) in the quantitative proteomics readout.

Table 4: Summary of the proteomic data obtained in each iTRAQ-SPROX experiment. Peptides included in this table are those identified with high quality chemical denaturation data and are reported as unique peptides (proteins).

Model	Mouse	Experiment	Assayed Peptides (Proteins)
Control	1	A	434 (297)
		B	1424 (737)
	2	A	423 (275)
		B	1177 (636)
Wildtype LRRK2	1	A	316 (217)
		B	1256 (659)
	2	A	583 (358)
		B	914 (534)
LRRK2 (R1441G)	1	A	764 (471)
		B	1043 (601)
	2	A	312 (217)
		B	1259 (659)

2.3.3 Comparative Analyses

To compare the biological variability of the iTRAQ-SPROX methodology the A and B datasets within a mouse were combined to generate one set for each mouse. These combined data sets were then compared within a mouse model to identify peptides and proteins with differential thermodynamic stabilities between mice of the same state. Using a Student's two-tailed t-test it was possible to generate chemical denaturation data for 135-172 unique peptides from 98-124 unique proteins. To be considered in the t-test analysis the peptide must have been assayed with high quality data in at least two experiments. In these comparisons that means the peptide must be seen in both experiments within a mouse. Due to this restriction, only a small

percentage of peptides were able to be included in the analysis. Several hit peptides and proteins were identified in each comparison with the peptide hit rate of ~1-2% (**Table 5, Figure 5**) similar to the documented false positive rate of the SPROX technique(102). It is noteworthy that the hits identified in the comparative analyses summarized in **Table 5** were all unique, and the peptide and proteins hits in **Table 5** did not appear as hits in the between cohort comparisons (**Tables 8-10**).

Table 5: Total proteomic coverage, assayed peptides and proteins in the t-test and number of hits identified via the t-test from comparisons of biological variability. Peptides included in this table are those identified with high quality chemical denaturation data and are reported as unique peptides (proteins).

Mouse	Proteomic Coverage Peptides (Proteins)	Assayed Peptides (Proteins)	Hits Peptides (Proteins)
Control 1	1546 (842)	172 (124)	2 (2)
Control 2	1300 (712)		
Wildtype LRRK2 1	1384 (718)	135 (98)	3 (3)
Wildtype LRRK2 2	1170 (662)		
LRRK2(R1441G) 1	1362 (782)	159 (116)	4 (4)
LRRK2(R1441G) 2	1329 (719)		

For the three comparative analyses involving the Control, Wildtype LRRK2 and LRRK2(R1441G) mouse models the assayed peptides and proteins from the two mice studied in each model were combined to create a single Control, Wildtype LRRK2 and LRRK2(R1441G) dataset. In the combined data sets the number of unique peptides range from 1629-1876 and the number of unique proteins range from 908-1048 (**Table 6**).

Table 6: Summary of the proteomic data combined within a biological state. Peptides included in this table are those identified with high quality chemical denaturation data and are reported as unique peptides (proteins).

Biological State	Total Proteomic Coverage Peptides (Proteins)
Control	1876 (1048)
Wildtype LRRK2	1629 (908)
LRRK2 (R1441G)	1749 (998)

As explained above, in order to be assayed in the t-test a peptide must have at least two high quality chemical denaturation curves in each dataset being compared. From these t-test comparisons between 12 and 17 peptides were identified with differential thermodynamic stability behavior (**Table 7, Figure 6**). This corresponded to a hit rate of 1-2% in all comparisons.

Table 7: Summary of the proteomic data used to identify protein folding and stability differences between comparative analyses of the mouse models. Peptides included in this table are those identified with high quality chemical denaturation data and are reported as unique peptides (proteins).

Comparison	Assayed in t-Test Peptides (Proteins)	Hits Peptides (Proteins)
Control vs. Wildtype LRRK2	669 (385)	12 (12)
Control vs. LRRK2(R1441G)	742 (431)	17 (17)
Wildtype LRRK2 vs. LRRK2(R1441G)	693 (405)	16 (15)

The hit peptides and proteins identified in these comparisons are summarized in **Tables 8-10**. In general the stabilizations/destabilizations ranged from absolute values of 0.01-0.86 M GdmCl with 75% of the $\Delta C_{1/2}$ values having an absolute value ≥0.2 M GdmCl. The distributions of destabilization/stabilizations were roughly equal in all three comparisons.

Table 8: Hit peptides identified from the Control vs. Wildtype LRRK2 Comparison. Bolded peptides were identified as hits in more than one comparison. A ($^{\theta}$) indicates the peptide was also identified as a hit in the Control vs. LRRK2(R1441G) comparison. A ($^{+}$) indicates the peptide was also identified as a hit in the Wildtype LRRK2 vs LRRK2(R1441G). A (§) indicates the peptide was identified as a hit in all three comparisons. The $\Delta C_{1/2}$ value reported was determined by subtracting Wildtype LRRK2 $C_{1/2}$ measurement from the Control $C_{1/2}$ measurement.

Comparison	Sequence	Gene ID	$\Delta C_{1/2}$ [GdmCl]	$\Delta\Delta G$ kcal/mol	p-value
Control vs. Wildtype LRRK2	AVLVDLEPGTMDSVR	Tubb2c	-0.28	0.73	0.033
	GLTPTGMLPSGVLSGGK	Ppp3ca	-0.35	0.90	0.042
	ISAYMK	Gstm1	0.22	-0.57	0.029
	LFTTMELMR	Psmd12	-0.24	0.62	0.020
	LWTVPTNMPSK	Omg	-0.45	1.18	0.045
	MLVVGGIDR	Kars	0.24	-0.64	0.043
	NQVAMNPTNTVFDAK$^{\theta}$	**Hspa8**	**-0.43**	**1.12**	**0.046**
	SEMPPVQFK^{+}	**Rap1gds1**	**0.67**	**-1.73**	**0.004**
	SIPMTVDFIR	Hprt1	0.20	-0.52	0.043
	VFDMLNR^{+}	**Eif4a2**	**0.29**	**-0.74**	**0.005**
	YFDSFGDLSSASAIMGNPK	Hbb-b2	-0.32	0.82	0.001
	YLATASTMDHAR§	**Mbp**	**-0.43**	**1.12**	**0.022**

Table 9: Hit peptides identified from the Control vs. LRRK2(R1441G) comparison. Bolded peptides were identified as hits in more than one comparison. A (*) indicates the peptide was also identified as a hit in the Wildtype LRRK2 vs. LRRK2(R1441G) comparison. A ($^{\theta}$) indicates the peptide was also identified as a hit in the Control vs. Wildtype LRRK2 comparison. A (§) indicates the peptide was identified as a hit in all three comparisons. The $\Delta C_{1/2}$ value reported was determined by subtracting LRRK2 (R1441G) $C_{1/2}$ measurement from the Control $C_{1/2}$ measurement.

Comparison	Sequence	Gene ID	$\Delta C_{1/2}$ [GdmCl]	$\Delta\Delta G$ kcal/mol	p-value
Control vs. LRRK2 (R1441G)	AFVHWYVGEGMEEGEFSEAR	Tuba4a	-0.24	0.62	0.037
	AQMIEK	Spna2	0.01	-0.03	0.002
	EMLSSTTYPVVVK	Syn1	-0.61	1.58	0.016
	FQMPDQGMTSADDFFQGTK*	**Dpysl2**	**-0.74**	**1.92**	**0.010**
	GVAPLWMR	Slc25a3	0.21	-0.55	0.044
	MVSADAYK	Cnp	0.26	-0.67	0.033
	NLDPEQMSQVLDAMFEK	Prkar2b	-0.20	0.53	0.032
	NLKPIKPMQFLGDEETVR	Pgam1	0.07	-0.18	0.048
	NQVAMNPTNTVFDAK$^{\theta}$	**Hspa8**	**-0.46**	**1.19**	**0.039**
	QDLPNAMNAAEITDK	Arf2	-0.08	0.22	0.050
	QGHIYMEMNFTNK	Ap2b1	-0.17	0.44	0.045
	RLDSGSASMAK	Acadl	-0.46	1.21	0.005
	VVDLMAYMASK	Gm2574	0.08	-0.21	0.043
	WIVPGGGMEPEEEPSVAAVR	Nudt3	0.17	-0.45	0.024
	WMIPPEAK	Idh3a	0.31	-0.81	0.017
	YHTSQSGDEMTSLSEYVSR	Hsp90ab1	0.20	-0.53	0.022
	YLATASTMDHAR§	**Mbp**	**-0.10**	**0.27**	**0.021**

Table 10: Hit peptides from the Wildtype LRRK2 vs. LRRK2(R1441G) comparison. Bolded peptides were identified as hits in more than one comparison. A (*) indicates the peptide was also identified as a hit in the Control vs. LRRK2(R1441G) comparison. A (†) indicates the peptide was also identified as a hit in the Control vs. Wildtype LRRK2 comparison. A (§) indicates the peptide was identified as a hit in all three comparisons. The $\Delta C_{1/2}$ value reported was determined by subtracting LRRK2(R1441G) $C_{1/2}$ measurement from the Wildtype LRRK2 $C_{1/2}$ measurement.

Comparison	Sequence	Gene ID	$\Delta C_{1/2}$ [GdmCl]	$\Delta\Delta G$ kcal/mol	p-value
Wildtype LRRK2 vs. LRRK2 (R1441G)	AILVDLEPGTMDSVR	Tubb2b	0.25	-0.66	0.021
	AIPMYK	Atp6b1e1	-0.86	2.24	0.002
	AKAEEMLSK	Grb2	0.06	-0.16	0.003
	DSTLIMQLLR	Ywhae	-0.47	1.23	0.003
	EGVMFQIEQATK	Epdr1	-0.32	0.84	0.020
	EIVSGMK	Arhgdia	-0.19	0.50	0.027
	FQMPDQGMTSADDFFQGTK*	**Dpysl2**	**-0.63**	**1.65**	**0.021**
	GAAGALMVYDITR	Rab14	-0.40	1.04	0.012
	IPAMTIAK	Hspd1	-0.63	1.63	0.010
	ISEQFTAMFR	Tubb2b	-0.33	0.86	0.018
	MNLGVGAYR	Got2	-0.04	0.11	0.021
	QMEQISQFLK	Tagln3	0.19	-0.49	0.010
	SEMPPVQFK†	**Rap1gds1**	**-0.50**	**1.29**	**0.041**
	SLMDEVVK	Pgk1	0.39	-1.02	0.044
	VFDMLNR†	**Eif4a2**	**-0.38**	**0.99**	**0.008**
	YLATASTMDHAR§	**Mbp**	**0.33**	**-0.85**	**0.018**

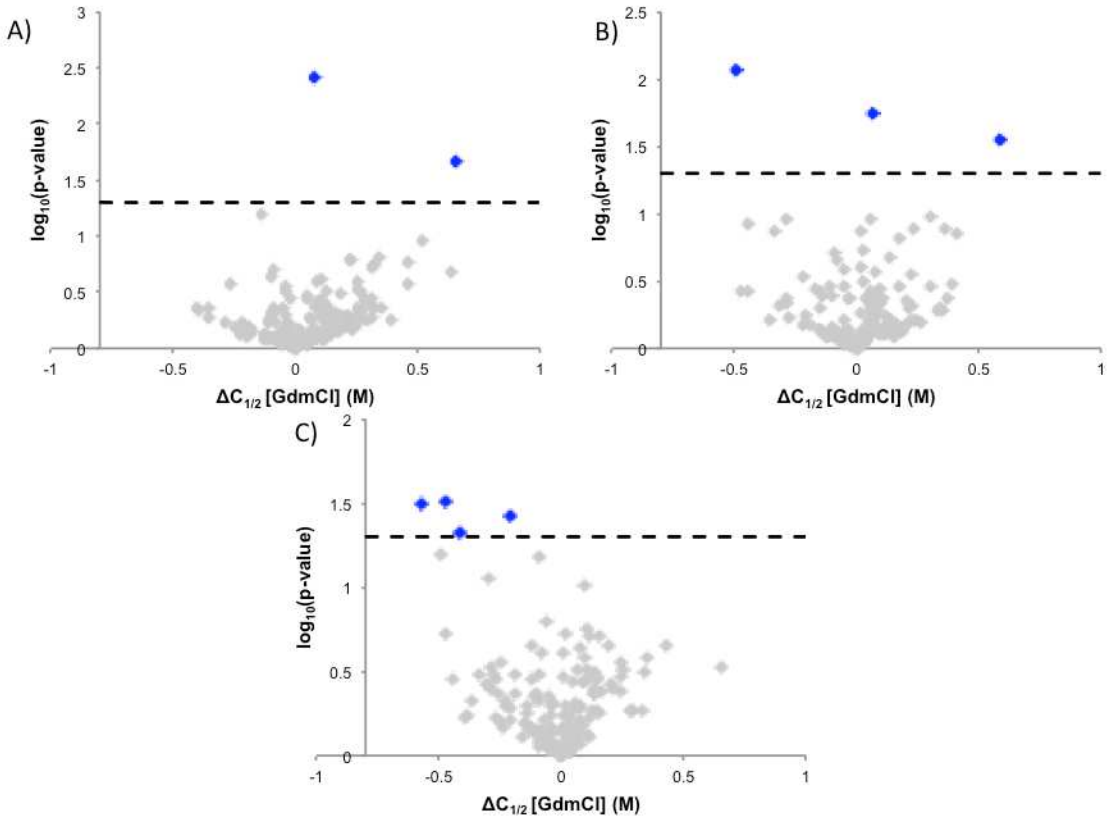

Figure 5: Volcano plots showing the statistical significance of the $\Delta C_{1/2}$ values generated for the peptides in the three comparisons. All $\Delta C_{1/2}$ values were determined by subtracting the $C_{1/2}$ value of the second mouse from the $C_{1/2}$ value of the first mouse. The reported *p* value was calculated from a Student's two-tailed t test. Hit peptide identifications are shown in blue, non-hit peptides are shown in grey. The dotted line indicates the *p* value cutoff that was used to identify hits (<0.05). (A) Control Mouse 1 vs. Control Mouse 2 comparison, (B) Wildtype LRRK2 Mouse 1 vs. Wildtype LRRK2 Mouse 2 comparison, (C) LRRK2(R1441G) Mouse 1 vs. LRRK2(R1441G) Mouse 2 comparison

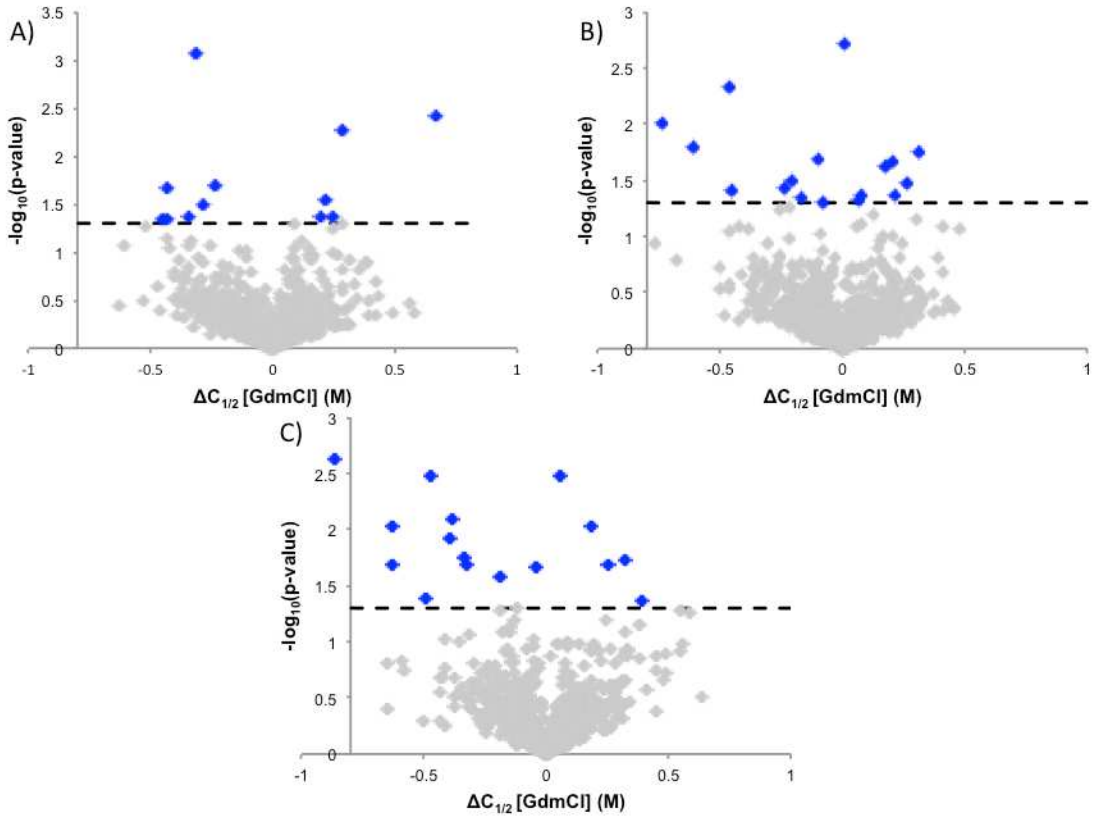

Figure 6: Volcano plots showing the statistical significance of the $\Delta C_{1/2}$ values generated for the peptides in the three comparisons. All $\Delta C_{1/2}$ values were determined by subtracting the $C_{1/2}$ value of the second state from the $C_{1/2}$ value of the first state. The reported *p* value was calculated from a Student's two-tailed t test. Hit peptide identifications are shown in blue, non-hit peptides are shown in grey. The dotted line indicates the *p* value cutoff that was used to identify hits (<0.05). (A) Control vs. Wildtype LRRK2 comparison, (B) Control vs. LRRK2(R1441G) comparison, (C) Wildtype LRRK2 vs. LRRK2(R1441G) comparison

2.4 Discussion

2.4.1 Peptide Hit Rate

A peptide hit rate of 1-2% was measured in the comparative analyses involving the mouse models with different overexpressed versions of the LRRK2 protein. This rate is lower than that observed in recent work utilizing the iTRAQ-SPROX protocol to study mouse models of aging (see Chapter 3 and reference (1)). The peptide hit rate observed here is on the order of that previously reported for the false positive rate of the iTRAQ-SPROX experiment(102). In fact, the peptide hit rates observed in the comparative analyses involving the mouse models with different overexpressed proteins was similar to that observed in the biological replicates. This study was designed as a biological model of a ligand binding experiment where the overexpressed LRRK2 and LRRK2(R1441G) act as the 'ligand' in the system. Previous protein ligand binding studies using iTRAQ-SPROX have involved the use of ligand concentrations in the 100-1000 μM range. The use of such high ligand concentrations, which are in vast excess of the concentration of any given potential protein target, are attractive in SPROX experiments as they maximize the sensitivity of the assay by increasing the magnitude of $\Delta\Delta G_f$ (as measured by $C_{1/2}$ value shifts) for a given protein target (see equation 3).

$$K_d = \frac{[L]}{e^{\frac{-\Delta\Delta G_f}{nRT}} - 1} \qquad \text{Equation (3)}$$

While the LRRK2 and LRRK2(R1441G) 'ligands' in the iTRAQ-SPROX experiments in this work were overexpressed in the mouse models by 5-10 fold they

were likely not in large excess of many potential target proteins in the brain lysates. Therefore, this limits the magnitude of the $C_{1/2}$ value shifts that could be observed. This may explain why so few protein hits were observed in the comparative analyses described here.

The low hit rate observed here makes it especially challenging to differentiate the true positives from the false positives. Given the apparent randomness of false positives, peptide hits that appeared due to consistencies in midpoint assignments in two mice in each state and those identified in multiple comparisons are likely to be true positives and are of the most interest. The identification in multiple comparisons allows for a characterization of the peptide thermodynamic stability in all three mouse models used in this study. This gives a better understand of the mutation related behavior of the protein and thus these peptides are of the most compelling. In total 39 unique peptides were identified as hits in three comparisons. Of the 39 peptide hits 32 were identified in at least two mice in each model being compared. This provides more confidence that the difference measured is due to consistency within biological state rather than from just one mouse. A Venn diagram showing the overlap of the peptide and protein hits in the three different comparative analyses performed here is shown in **Figure 7**.

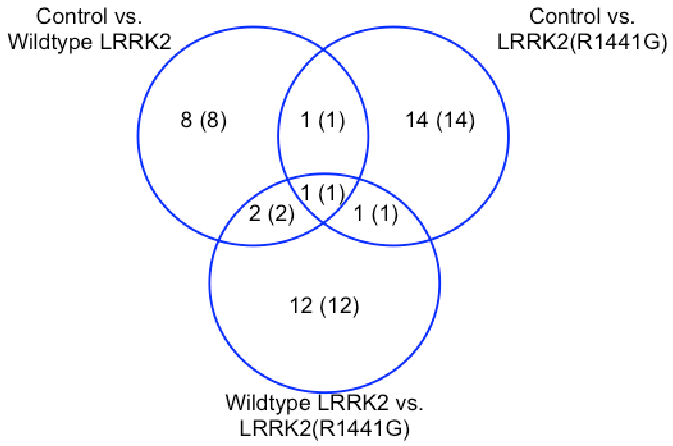

Figure 7: Venn diagram showing the overlap of peptide and protein hits between the three comparative analyses. Numbers reported are of peptides (proteins).

As shown in the venn diagram in **Figure 7**, one peptide from one protein (myelin basic protein) was identified as a hit in all three comparisons. There is also one overlapping hit protein (heat shock cognate 71 kDa) between the Control vs. Wildtype LRRK2 and the Control vs. LRRK2(R1441G) comparisons. This protein appears to have a stability difference induced by the overexpression of LRRK2, indicating that it is a target of LRRK2. The one overlapping protein between the Control vs. LRRK2(R1441G) and Wildtype LRRK2 vs. LRRK2(R1441G) (dihydropyrimidinase-related protein 2) appears to be a protein that has a mutation-induced protein thermodynamic stability differences. The two overlapping proteins between the Control vs. Wildtype LRRK2 and the Wildtype LRRK2 vs. LRRK2(R1441G) (eukaryotic translation initiation factor 4A2 and Rap1 GTP-GDP dissociation stimulation 1) appear to be proteins that have

consistencies in the Control and LRRK2(R1441G) cohorts and a difference induced by the Wildtype LRRK2 overexpression. All but one of the five overlapping hits (heat shock cognate 71 kDa) were identified in multiple mice within a cohort. The remaining four proteins (myelin basic protein, dihydropyrimidinase-related protein 2, eukaryotic translation initiation factor 4A2 and Rap1 GDP-GTP dissociation stimulation 1) represent the peptides of the most interest as disease specific protein interactors from this study

2.4.2 Biological Significance of Hits

One goal of this work was to identify proteins with thermodynamic stability differences induced by the R1441G mutation on LRRK2 protein. Four proteins—dihydropyrimidinase-related protein 2, eukaryotic translation initiator factor 4A2, Rap1 GTP-GDP dissociation stimulator 1 and myelin basic protein—were identified as being those of the most interest due to the identification of consistent $C_{1/2}$ values in multiple mice within a model and appearance as hits in multiple comparisons (**Figure 8**). Furthermore, 10 of the 11 $C_{1/2}$ shifts are >0.3 M and in the upper 50% of $\Delta C_{1/2}$ magnitudes. Therefore, these four proteins are those that are most likely to provide insight into the biological interactions of wildtype LRRK2 and the effect that R1441G mutation has on the LRRK2 interactions.

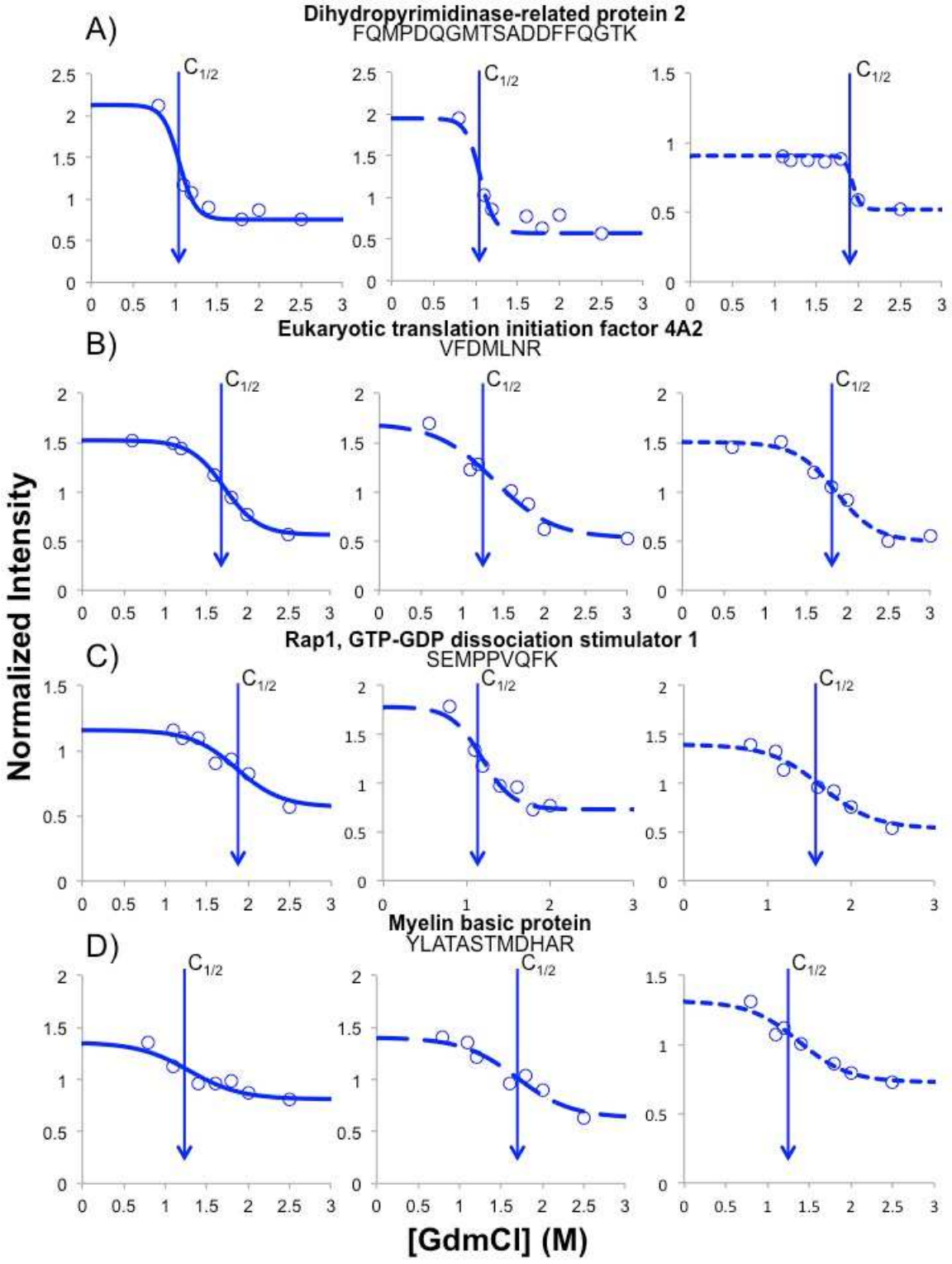
A)
Dihydropyrimidinase-related protein 2
FQMPDQGMTSADDFFQGTK
B)
Eukaryotic translation initiation factor 4A2
VFDMLNR
C)
Rap1, GTP-GDP dissociation stimulator 1
SEMPPVQFK
D)
Myelin basic protein
YLATASTMDHAR
C1/2
Normalized Intensity
[GdmCl] (M)

Figure 8: Representative iTRAQ-SPROX data for the four strongest hit peptides. Shown are the chemical denaturation data sets and corresponding fitted curve obtained for the peptides. The solid line is from the control dataset, the long dashed line is from the Wildtype LRRK2 dataset and the short dashed line is from the LRRK2(R1441G) dataset. The data shown here represent the averaged data generated from all product ion spectra gathered for the peptide within one experiment. The curve represents the best fit of the data points as determined by eq 1. The vertical arrows indicate the assigned $C_{1/2}$ values. A) *Dihydropyrimidinase-related protein 2*—Control: 1.0 M, Wildtype LRRK2: 1.1 M, R1441G(LRRK2): 1.9 M, B) *Eukaryotic translation initiation factor 4A2*—Control: 1.7 M, Wildtype LRRK2: 1.4 M, R1441G(LRRK2): 1.9 M, C) *Rap1*—Control: 1.9 M, Wildtype LRRK2: 1.2 M, R1441G(LRRK2): 1.6 M, D) *Myelin basic protein*—Control: 1.3 M, Wildtype LRRK2: 1.7 M, R1441G(LRRK2): 1.4 M.

The peptide FQMPDQGMTSADDFFQGTK (**Figure 8A)** was identified as a hit in the two comparisons Control vs. LRRK2(R1441G) and Wildtype LRRK2 vs. LRRK2(R1441G) and is from the protein Dihydropyrimidinase-related protein 2 (Dpysl2). The thermodynamic stability difference shows a stabilization due to the R1441G mutation on LRRK2. This protein hit has been linked to the development of Alzheimer's Disease (AD) via the post translational mutation of oxidation(105). Two closely related proteins (Dpysl3 and Dpysl5) were identified as hits in the previous study on thermodynamic stability differences in aging mouse brain proteins(1) (Chapter 3). It is interesting to note that both AD and PD share aging as the major risk factor for development of the disease. Furthermore, the protein Dpsyl2 is known to be important for neuronal growth and development(106). Seeing this protein in multiple neurodegenerative disorder and normal aging studies may indicate that it is an

important player in age related neurodegeneration that leads to higher susceptibility for disease progression.

The peptides VFDMLNR and SEMPPVQFK from the proteins eukaryotic translation initiation factor 4A2 (Eifa2) and Rap1, GTP-GDP dissociation stimulator 1 (Rap1gds1), respectively, were identified as hits in both the Control vs. Wildtype LRRK2 and the Wildtype LRRK2 vs. LRRK2(R1441G) comparisons. As shown in **Figure 8B and C**, both of the peptides show a decreased thermodynamic stability in the wildtype LRRK2 and then a recovered thermodynamic stability in the LRRK2(R1441G) to the stability observed in control mice. One explanation for this trend in stabilities is that the overexpression of LRRK2 affects the function of the proteins either via a direct interaction with LRRK2 or an indirect interaction. The addition of the R1441G mutation then interrupted the affected LRRK2 interaction. The protein Rap1gds1 is a member of the small GTP-binding protein class that mediates various cellular functions including vesicle trafficking (Rab proteins) and cytoskeletal organization (Rho proteins)(107). The protein Rap1gds1 is a member of a class of GTPase/GDP dissociation stimulator (GDS) proteins that are known to stimulate the exchange of GDP/GTP in a way that inhibits binding of the small G protein to membranes and therefore, reduces the ability of the G protein to function appropriately. The protein Eifa2 has not been previously linked to LRRK2. This work identifies it as having a novel interaction with LRRK2 which may

indicate a new pathway that is important in the progression of PD and LRRK2 interactions.

The peptide YLATASTMDHAR from Myelin basic protein (Mbp) was identified as a hit in all three comparisons. As shown in **Figure 8D**, the peptide shows a trend of an increased thermodynamic stability in the wildtype LRRK2 and then a return to the initial thermodynamic stability in the LRRK2(R1441G) system. While this was identified as a hit between the Control and the LRRK2(R1441G) it was with a very small $\Delta C_{1/2}$ of 0.1M. Therefore, the true trend is in the increased stability in the wildtype LRRK2. This protein is of particular interest because MBP is well documented as being phosphorylated by LRRK2, even so far as to be used as the kinase substituent in a protocol to measure the in vitro activity of LRRK2(108). As mentioned previously, it is likely that the increased expression of LRRK2 would increase the activity of LRRK2 and thus may increase the quantity of MBP phosphorylation. This could be measured by an increase in the thermodynamic stability. However, upon the R1441G mutation the stability returns to the initial value, perhaps indicating a decrease in phosphorylation. LRRK2 is well known to autophosphorylate and most sites of autophosphorylation occur in the GTPase domain where the R1441G mutation occurs(109). It is possible that the addition of the R1441G mutation impedes the ability of the LRRK2 to autophosphorylate and impacts the downstream kinase activity of LRRK2.

2.5 Conclusion

The iTRAQ-SPROX experiments described here were designed to determine the ability of the technique to characterize proteins with differential thermodynamic stability measurements due to overexpression of the LRRK2 protein and the impact of a point mutation on the LRRK2 protein interactions. This experiment was designed to mimic a more traditional iTRAQ-SPROX experiment to study ligand-binding interactions with the overexpressed LRRK2 protein acting as the 'ligand'. The hit rate in the comparative analyses was low, between 1-2%. Even so, four proteins were identified as the most likely to be true positives due to their consistent $C_{1/2}$ behavior in multiple mice within a model and appearance as hits in multiple comparisons. Three of the four proteins have been previously linked to Parkinson's Disease, Alzheimer's Disease, aging and the phosphorylation of LRRK2. These known connections further support the idea that the four strongest hits showing disease mutation related stability differences are true positives. However, future studies must be conducted to confirm the wildtype LRRK2 and R1441G induced stability differences measured in this work and eliminate the question of false positives. These connections and their corresponding thermodynamic stability differences provide interesting starting points for future drug development and further characterization of LRRK2 protein interactions to better understand the development of Parkinson's Disease.

3. Discovery of Age-Related Protein Folding Stability Differences in the Mouse Brain Proteome

The work described in this chapter comes largely from a paper titled "Discovery of Age-Related Protein Folding Stability Differences in the Mouse Brain Proteome"(1).

3.1 Introduction

Aging is phenotypically categorized by a loss of cellular function or an increase in cellular degeneration. Certain biological pathways (e.g. oxidative stress, deamidation, ubiquitination) are known to be critically important in aging(46-53). Age-related changes in the function of some proteins in these pathways have also been documented(48, 59-61, 110). However, the molecular level understanding of this important biological process is incomplete. Such an understanding is not only of fundamental importance, but it also serves as a starting point for finding connections between seemingly disparate diseases that share age as a major risk factor (e.g., cancer, neurodegenerative disorders).

This work was designed as the first example of the iTRAQ-SPROX technique to characterize different biological states of mouse brain proteomes. Previous work, as described in Chapter 2, identified that the iTRAQ-SPROX technique is able to measure thermodynamic stabilities on hundreds of proteins from a mouse brain but identified only a small number of thermodynamic stability shifts due to a single point mutation. This study seeks to expand the types of mouse models studied by the iTRAQ-SPROX

experiment, identify specific proteins and pathways impacted by aging as well as quantify global differences between the young and old state.

Described here is the use of SPROX to profile the thermodynamic stability of proteins in mouse tissue lysates from the brains of young and old mice, aged 6- and 18-months, respectively. The thermodynamic stabilities of over 800 proteins in brain tissue cell lysates (n=7 for young and n=9 for old) were profiled to determine age-related thermodynamic stability differences. A total of 83 protein hits with age-related differences were identified. The protein hits identified included many that have known functions in, and connections to, biological pathways previously linked to aging. This not only substantiates the results reported here, but it also establishes a biophysical link between these proteins and aging. This link suggests that pharmacological chaperones designed to rescue the stability of one or more of the protein hits identified here could potentially be used to combat the adverse affects of aging and age-related diseases.

3.2 Experimental

3.2.1 Mouse Tissue Lysis

The 6-month old female mice (C57BL/6) were purchased from Jackson Laboratory (Mouse 1-7). The 18-month old female mice (C57BL/6) (Mouse 8-16) were obtained from the NIH National Institute on Aging (NIA) aging mouse colony. Mice were euthanized by cervical dislocation, and the brains used for these studies were

harvested immediately and kept at -20°C until tissue cell lysates were prepared. Lysates were prepared exactly as described in Chapter 2.2.1.

3.2.2 iTRAQ-SPROX Analysis

iTRAQ-SPROX analyses were performed on the brain tissue cell lysates according to previously established protocols(42). Briefly, ~100 μg of total protein from each lysate was distributed into a series of 8 GdmCl-containing SPROX buffers comprised of 20 mM phosphate buffer, pH 7.4, and increasing concentrations of GdmCl. A concentrated solution of hydrogen peroxide was added into each protein-containing buffer to selectively oxidize solvent exposed methionine residues in each denaturant-containing SPROX buffer. The final GdmCl concentrations in SPROX buffers were 0.8, 1.1, 1.2, 1.4, 1.6, 1.8, 2.0, and 2.5 M. The final hydrogen peroxide concentration (3% v/v) and reaction time (3 min) was the same in each SPROX buffer. The oxidation reaction in each SPROX buffer was quenched with L-methionine, and the protein precipitated with trichloroacetic acid.

3.2.3 Proteomic Sample Preparation

The protein pellets from each denaturant-containing buffer were submitted to a standard quantitative, bottom-up proteomics workflow using iTRAQ reagents for quantitation as described above in Chapter 2.2.3. The protein samples from the 0.8, 1.1, 1.2, 1.4, 1.6, 1.8, 2.0, 2.5 M denaturant concentrations were labeled with the 113, 114, 115, 116, 117, 118, 119, and 121 iTRAQ reagents, respectively. The iTRAQ labeled samples

were combined and an aliquot of 120 μL was desalted with a C18 column (Nest Group, Southborough, MA) according to the manufacturer's protocol, and 240 μL was enriched for methionine-containing peptides using a Pi^{3} ™-Methionine Reagent kit (Nest Group, Southborough, MA) according to the manufacturer's protocol.

3.2.4 LC-MS/MS Analyses

All samples were analyzed on a Thermo Scientific Q-Exactive Plus high-resolution mass spectrometer with a nanoAcquity UPLC system (Waters Corp, Milford, MA). This instrument also utilized a nano-electrospray ionization source. Sample was trapped on a column (Symmetry C18 300 mm x 180 μm) for 3 minutes at 5 μL/min 0.1% formic acid in water. The sample was then separated using the following gradient: 3% to 30% acetonitrile with 0.1% formic acid over 90 minutes. The column used for separation was 75 μm x 250 mm packed with 1.7 μm Acquity HSST3 C18 stationary phase (Waters Corp). The flow rate used was 0.4 μL/min at 55°C. This mass spectrometer used a full MS scan from *m/z* 375-1600 with a target AGC value of 1 x 10^{6} ions in profile mode and a resolution of 70,000 (at *m/z* 200) for data dependent acquisition. This was followed by 20 MS/MS scans at a resolution of 17,500 at *m/z* of 200 in centroid mode with an AGC target value of 1 x 10^{5}. The MS/MS scans also had a normalized collision energy of 30 V and a maximum fill time of 60 msec. Dynamic exclusion of 30 seconds was used to reduce MS/MS oversampling.

Peak lists were extracted from the LC-MS/MS data and were searched against the 24,855 proteins in the SwissProt *Mus musculus* database version 2016-04-13, downloaded on 05/17/16 using Proteome Discoverer (Version 2.1.0.81). Cysteine residue modification by MMTS was a fixed modification in the search. N-termini and lysine residues modified by iTRAQ 8-plex and oxidized methionine residues and deamidation on asparagine and glutamine were variable modifications in the search. Up to three missed tryptic cleavages after R and K were allowed. The parameters included a 10 ppm mass tolerance window for precursor masses and 0.02 Da for fragment mass tolerance. Only peptide spectra with FDR <1% and iTRAQ reporter ion intensities that summed to >1000 were used in subsequent analyses of the data.

The LC-MS/MS analyses of the iTRAQ-SPROX samples analyzed here included 2 replicate LC-MS/MS runs of each methionine-containing peptide enriched sample and 1 LC-MS/MS run of each non-enriched sample generated for each brain. The number of replicates was chosen to maximize peptide and protein coverage.

3.2.5 Data Analysis

The data was normalized as previously described in reference(42) and Chapter 2.2.5. The N2 normalization factors determined through this process are shown below in **Table 11**. The chemical denaturation data sets were fitted to a four parameter sigmoidal equation, equation 1, using a JAVA-based program (developed in house) that is described in more details in Chapter 2.2.5.

Table 11: Table of the N2-normalization factors determined in each iTRAQ-SPROX experiment. In this table N2 is the normalization factor and SD is the standard deviation of the factor. The concentrations are in molarity of GdmCl.

Age	Mouse		0.8 M	1.1 M	1.2 M	1.4 M	1.6 M	1.8 M	2.0 M	2.5 M
Young (6 Month)	1	**N2**	1.03	0.95	0.77	0.87	0.98	1.17	1.04	1.18
		SD	0.17	0.13	0.12	0.12	0.13	0.14	0.20	0.18
	2	**N2**	0.80	0.97	1.19	1.24	0.87	0.86	1.07	1.00
		SD	0.17	0.15	0.16	0.15	0.14	0.11	0.23	0.18
	3	**N2**	0.79	1.20	0.96	0.96	1.01	1.04	1.00	1.03
		SD	0.17	0.14	0.17	0.12	0.11	0.15	0.14	0.13
	4	**N2**	0.94	1.07	0.94	1.01	1.08	1.06	0.93	0.98
		SD	0.14	0.12	0.22	0.10	0.13	0.15	0.13	0.13
	5	**N2**	1.05	0.75	0.86	0.99	1.06	1.20	0.93	1.16
		SD	0.17	0.15	0.10	0.09	0.20	0.15	0.13	0.14
	6	**N2**	0.79	0.78	0.78	1.13	0.86	1.02	1.35	1.29
		SD	0.13	0.14	0.30	0.13	0.17	0.11	0.30	0.20
	7	**N2**	0.98	0.93	0.86	1.29	1.04	1.07	0.90	0.91
		SD	0.15	0.12	0.36	0.31	0.12	0.12	0.13	0.17
Old (18 Month)	8	**N2**	1.14	0.84	0.92	0.89	1.15	1.04	0.99	1.03
		SD	0.17	0.15	0.14	0.14	0.16	0.15	0.14	0.16
	9	**N2**	0.91	0.96	0.89	1.06	1.09	1.01	1.02	1.05
		SD	0.12	0.12	0.10	0.10	0.10	0.10	0.10	0.12
	10	**N2**	1.17	1.21	0.80	0.87	1.12	1.10	0.80	0.93
		SD	0.17	0.13	0.10	0.09	0.09	0.10	0.15	0.12
	11	**N2**	1.03	1.09	0.99	0.89	1.21	0.86	0.83	1.09
		SD	0.12	0.10	0.11	0.12	0.09	0.10	0.15	0.11
	12	**N2**	1.11	1.07	0.74	1.02	1.04	1.15	0.93	0.93
		SD	0.19	0.13	0.39	0.12	0.13	0.17	0.17	0.13
	13	**N2**	0.90	0.99	0.92	0.99	1.10	0.99	1.00	1.11
		SD	0.14	0.12	0.12	0.12	0.11	0.11	0.14	0.16
	14	**N2**	0.94	1.09	0.78	1.09	0.90	1.01	1.01	1.18
		SD	0.15	0.12	0.36	0.12	0.14	0.13	0.28	0.20
	15	**N2**	0.99	0.90	0.87	1.07	0.96	1.03	0.91	1.29
		SD	0.15	0.13	0.23	0.15	0.19	0.13	0.13	0.26
	16	**N2**	0.97	1.04	1.00	1.05	1.04	0.86	0.94	1.10
		SD	0.16	0.15	0.16	0.12	0.12	0.12	0.15	0.23

Subsequent analyses of the data only utilized the chemical denaturation data sets that were determined to be high quality ($R^2 \geq 0.8$) and were generated from product ion mass spectra with low isolation interference (≤ 30%). If a peptide was identified multiple times within the same mouse the N2-normalized iTRAQ reporter ion intensities from the high quality data were averaged together to generate one set of iTRAQ reporter ion intensities at the 8 denaturant concentrations and the averaged data was fit to equation 1 as described above to extract a single $C^{1/2}$ value used for the mouse.

3.2.6 Hit Identification

A Student's two-tailed t-test was used to identify significant differences between the assigned $C^{1/2}$ values in the young and old mice. A value was determined to be significant if the determined t-test p-value was < 0.05.

3.2.7 Quantitation of Thermodynamic Stability Differences

The transition midpoint shifts of the hit peptides were used to calculate free energy ($\Delta\Delta G$) changes according to equation 2 and described previously in Chapter 2.2.7.

$$\Delta\Delta G = - m \times \Delta C_{1/2} \qquad \text{Equation (2)}$$

In equation 2, $\Delta\Delta G$ is the change in free energy, m is $\delta\Delta G/\delta\Delta C_{1/2}$, and $\Delta C_{1/2}$ is the transition midpoint shift.

3.3 Results

3.3.1 Experimental Design

The experimental workflow outlined in **Figure 9** was used to characterize the chemical denaturant-induced equilibrium unfolding properties of the proteins in organ tissue cell lysates from a total of 16 mice (n=7 for 6 month age point, n=9 for 18 month age point). The iTRAQ-SPROX technique used to generate the chemical denaturation data sets in this work utilizes the chemical denaturant dependence of a methionine oxidation reaction with H_2O_2 to report on the thermodynamic stability of proteins. Oxidative stress has long been known to be an aging factor(111). Therefore, it is possible that some background oxidation may exist in the samples prior to the H_2O_2 treatment in SPROX. However, such background oxidation will not be denaturant dependent, and thus not compromise the chemical denaturation data generated in SPROX experiment. Furthermore, only those denaturation curves from wild-type methionine residues were considered for this work.

The SPROX technique relies on the detection and quantitation of methionine-containing peptides in the bottom-up proteomics readout to report on the folding stability of the protein folding domains to which they map. Therefore, the proteomic coverage in iTRAQ-SPROX experiments is restricted to those proteins that can be identified with methionine-containing peptides. The frequency of methionine residues in protein sequences is relatively low, ~2.5%.

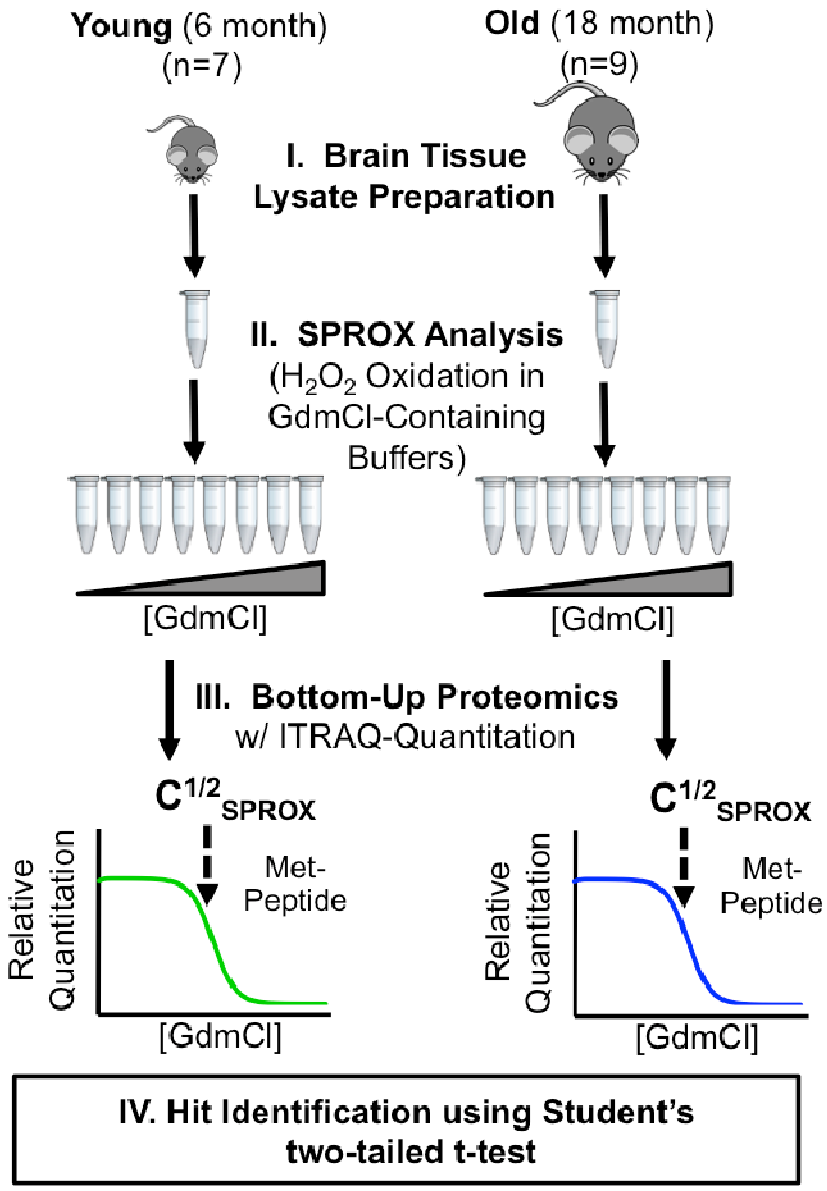

Figure 9: Schematic representation of the experimental workflow used in this work.

However, based on this frequency, a typical protein contains a number of methionine residues. In theory, one methionine-containing peptide probe can report on age-related thermodynamic stability differences occurring anywhere in the protein folding domain to which the peptide probe maps. Thus, the cause of the stability change (e.g., mutation, post-translational modification, and/or altered binding interaction) need not directly involve the methionine-containing peptide probe for the stability change to be successfully detected in the iTRAQ-SPROX experiment.

3.3.2 Proteomic Coverage

The proteomic coverage in the iTRAQ-SPROX experiments conducted on the sixteen mice brain samples averaged about 1200 methionine-containing peptides from about 675 proteins per mouse. The exact coverage obtained for each mouse is summarized in **Table 12**. To be included in the peptide coverage reported in **Table 12**, a methionine-containing peptide must have been identified with Isolation Interference ≤ 30% and the chemical denaturation curve fitted to equation 1 with an $R^2 \geq 0.8$.

In total, the young mouse data set (mice 1 to 7) was comprised of 3260 unique peptide identifications from 1448 proteins and the old mouse data set (mice 8 to 16) was comprised of 3394 unique peptide identifications from 1506 proteins (**Table 13**). The Student's two-tailed t-test requires that a peptide be identified in at least two mice in each age group. Overall, 1630 unique peptides from 809 proteins were assayed in the t-test analysis and used for further age-related difference analyses.

Table 12: Summary of the proteomic data obtained in the iTRAQ-SPROX experiments on each mouse brain tissue lysate. Numbers reported are of unique peptide and (protein) identifications.

Mouse Age	Mouse Identifier	Assayed Peptides (Proteins)
Young (6 months)	1	1342 (753)
	2	1660 (897)
	3	586 (381)
	4	1315 (752)
	5	1595 (835)
	6	670 (426)
	7	1559 (838)
Old (18 months)	8	1593 (887)
	9	1245 (721)
	10	1861 (982)
	11	857 (516)
	12	340 (232)
	13	832 (496)
	14	1617 (855)
	15	829 (538)
	16	1252 (674)

Table 13: Summary of the proteomic data in the iTRAQ-SPROX experiments used to determine age-related protein folding and stability differences. Numbers reported are of unique peptides and (protein) identifications.

Mouse Age	Assayed Peptides (Proteins)	Included in t.Test Peptides (Proteins)	Hit Peptides (Proteins)
Young (6 months)	3260 (1448)	1630 (809)	89 (83)
Old (18 months)	3394 (1506)		

3.3.3 Biological Variability

The experiments described here are the first instance in which the iTRAQ-SPROX methodology was used to study the thermodynamic stability of proteins from a rodent model of disease. Previous SPROX experiments have been conducted on yeast and human cell lines(34-42). The increase in biological relevancy that comes with a rodent model also increases the potential for biological variability. The averages and standard deviations of the $C_{1/2}$ values assigned for a given methionine-containing peptide within the old and young mouse age group samples were considered in order to assess the biological variability of the $C_{1/2}$ value measurements. The distributions of the standard deviations associated with the $C_{1/2}$ value assignments for a given methioinine-containing peptide in the old and young mice samples were similar **(Figure 10)**.

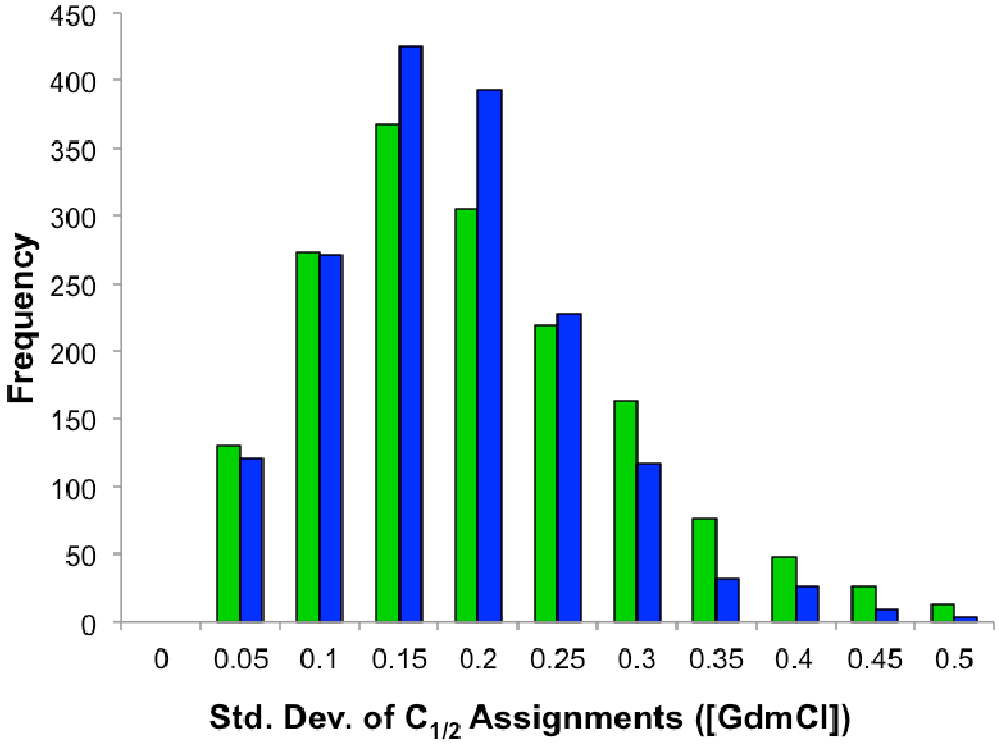

Figure 10: Frequency distribution of standard deviations associated with the $C_{1/2}$ values determined for the assayed peptides in the different young (green) and old (blue) mice. Each bar represents the number of total peptides within each standard deviation bin. The high limit of each bin is listed on the x-axis.

The median value in both cases was 0.15 M GdmCl, which was also very close to the pooled standard deviation (s_{pooled}) of 0.18 M GdmCl calculated using all the peptide $C_{1/2}$ values in the young and old data sets. These values are consistent with that expected based on the denaturant concentration spacing of the data points in the experiment, which was 0.2 M GdmCl for the majority of the denaturant curve. The $C_{1/2}$ assignments in this experiment were consistent between mice to less than the spacing between data

points. Thus, it appears that any biological variability in the $C_{1/2}$ values reported here is generally small and within the technical error of the measurement.

3.3.4 Age Related Thermodynamic Stability Differences

A Student's two-tailed t-test was used to identify age-related thermodynamic stability differences that were consistent within an age group and different between young and old mice. To be considered in this analysis a peptide had to be identified in at least two mice in each age group (four mice total). In total this analysis included 1630 peptides from 807 proteins, and it identified 89 peptides from 83 proteins as hits. All peptide hits can be found in Appendix A. Data representative of a non-hit peptide identification and a hit peptide identification is shown in **Figure 11.** A volcano plot showing the distribution of $\Delta C_{1/2}$ values and associated p-values **(Figure 12)** reveals that the protein hits were largely destabilized in the old mouse brain. In fact, over 90% of the 89 peptide hits were the result of a protein destabilization in the old mouse brain. This is particularly remarkable given that the differentially stabilized protein hits previously identified in an earlier disease state analysis involving cell culture models of breast cancer was almost equally split between stabilizations and destabilizations(41). The $\Delta C_{1/2}$ values associated with these destabilizations ranged from 0.1 to 0.7 M, which correspond to destabilizations on the order of 0.3 to 1.8 kcal/mol. Two-thirds of the $\Delta C_{1/2}$ values were in the range of 0.2 to 0.4 M, corresponding to destabilizations of 0.5 to 1.0 kcal/mol.

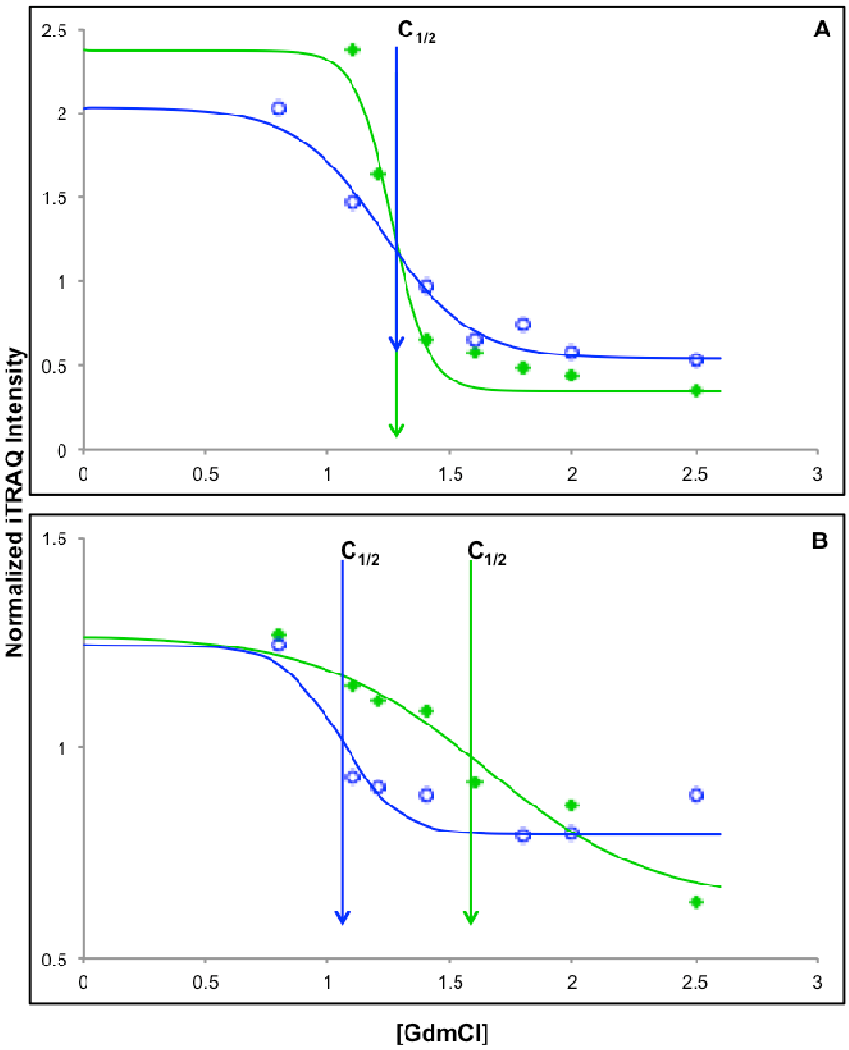

Figure 11: Representative iTRAQ-SPROX data for non-hit and hit peptides. The data shown in (A) and (B) represent the average data generated from all the product ion spectra generated for each peptide within the stated mouse experiment. The solid curve represents the best fit of the data to equation 1. The vertical arrows indicate the $C_{1/2}$ value of each curve. (A) non-hit peptide AGAGSATLSMAYAGAR from the protein malate dehydrogenase when it was analyzed in young mouse 3 (green filled diamonds and green curve) and in old mouse 14 (blue open circles and blue curve) (B) hit peptide SVMDQANLQR from the protein heat shock 70 kDa 4L when it was analyzed in young mouse 2 (green filled diamonds and green curve) and in old mouse 16 (blue open circles and blue curve).

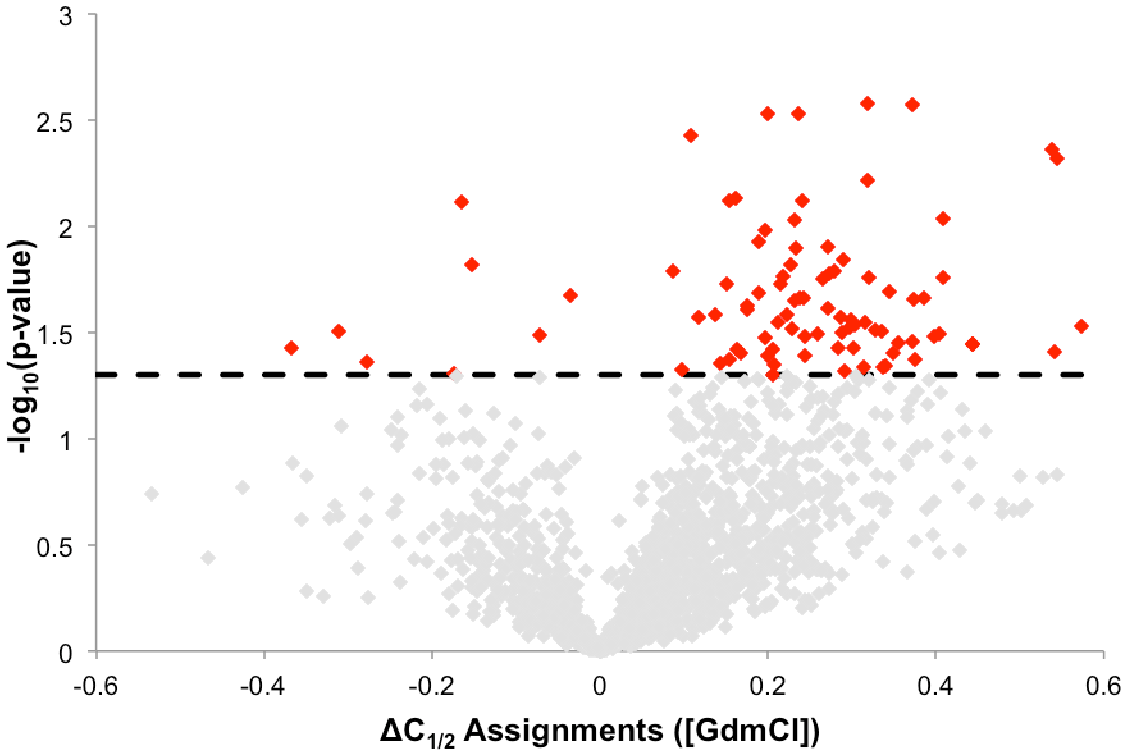

Figure 12: Volcano plot showing the statistical significance of the $\Delta C_{1/2}$ values generated for the peptides in the young versus old mice comparison. The $\Delta C_{1/2}$ values were determined by subtracting the old mouse $C_{1/2}$ value from the young mouse $C_{1/2}$ value. A positive $\Delta C_{1/2}$ indicates a peptide that is more stable in the young mice than the old mice. The reported p-value was determined from a Student's two-tailed t-test performed on the young and old mouse data sets. Non-hit peptide identifications are shown in grey. Hit peptide identifications are shown in red. The dotted line indicates the p-value cutoff (< 0.05) used to identify hits.

3.4 Discussion

3.4.1 Classification of Age Related Protein Hits

The age-related thermodynamic stability changes detected here were generally small and indicated destabilizations in the old mice. This is in contrast to an earlier study of the thermodynamic stability changes of proteins in cell culture models of breast

cancer in which the changes were not only larger (from 1.7 to 6 kcal/mol) but also equally distributed between stabilizing and destabilizing(41). A number of different biologically significant phenomena (e.g., point mutations and post-translational modifications) can change the folding stability of a protein. Therefore, the exact cause of the thermodynamic stability changes observed here can not be determined from the data collected in this work. However, one explanation for the destabilizations is that they result from age-related post-translational modifications (PTM) (e.g., protein carbonylation events that are known to occur during aging) of the protein hits or of other proteins that interact with the protein hits. Such PTMs have been theorized to destabilize proteins(112). Indeed, a significant fraction of the peptide hits (32 of 89) map to proteins known to have post-translational modifications, specifically carbonylation or oxidation, related to aging or a neurodegenerative disease with aging as a risk factor (**Table 14)**. However, we note that the detailed molecular basis for the detected stability changes in hit peptides (proteins) cannot be directly determined from the data generated here.

Table 14: Summary of the hit proteins and corresponding classification. The (+) indicates that the information in these columns is from the reference(113). A (*) indicates that the protein identified as a hit was a different isoform, subunit or closely related protein to the protein linked to aging or age-related diseases. The number inside of the box corresponds to the reference for the experimental connection.

Gene	Homeostasis /Metabolism+	Aging /Mortality+	Oxidation /Carbonylation	Connections to Aging or Disease
Aak1				
Aars				
Acat1			(114)	
Acot1				
Actb			(115)	
Actr10				
Add2				
Aldh1a1				
Aldh1a7				(116)
Aldh2				(117)
Aldh7a1				
Ap2a1			(115)*	(118)
Ap2b1			(115)*	
Appl1				(119)*
Atp1a3			(120)*	(121)
Atp5b			(122)	(123)
Atp6v0a1			(120)*	
Atp6v1e1			(120)*	
Ca2			(124)	(125)*
Cct3				(126)*
Cd81				
Clpp				(127)
Cltc				(128)
Cntn1				
Cops6				
Crmp1			(129)*	(105)*
Cul3				(130)
Dnm1			(129)	(131)
Dpysl3			(129)*	(105)*
Dpysl5			(129)*	(105)*
Dync1h1				(132)*
Eef1a1			(133)*	(134)

Fabp7				
Gad1				(135)
Gda				(116)
Ggact				
Gls				(121)
Got1			(114)	
Gpx1			(136)	(137)
Gstm7			(138)*	
Hbb-b1			(120)	(134)
Hint1				
Hnrnpd				
Hnrnpll				
Hspa4			(120)*	(139)
Hspa4l			(120)*	(139)
Hspd1			(122)	(140)
Ivd				
Lancl1				(141)
Ldhb			(142)	
Lypla2				
Map1b				
Map2				(143)
Mark3				
Matr3				(144)
Myg1				
Nisch				
Nsf			(120)	(145)
Pde1b				
Pfkm				
Pkm			(142)	(146)
Ppfia3				
Psmd14				
Pygb				(147)
Rdx				(148)
Rhoa				(61)*
Snap25				(149)
Srm				
Stip1				(150)
Stub1				(151)
Stxbp1			(124)	(152)
Tnnc2				

Tnr				
Tuba3a			(122)*	
Tubb2a			(122)*	
Uba2				
Ube2i				(153)
Ubfb1				(154)
Ubqln1				(155)
Ubqln2				(156)
Usp14			(133)	(157)
Vamp1				(158)

It has been shown that brain proteins have lifetimes that average about 9 days, with a larger majority of brain proteins having lifetimes between 1 and 100 days(159). An analysis of the turnover rates available for 51 of the 89 brain protein hits identified here revealed a distribution that was shifted toward longer lived proteins when compared to all the brain proteins assayed in this work and all of the proteins characterized in reference(159) (**Figure 13**).

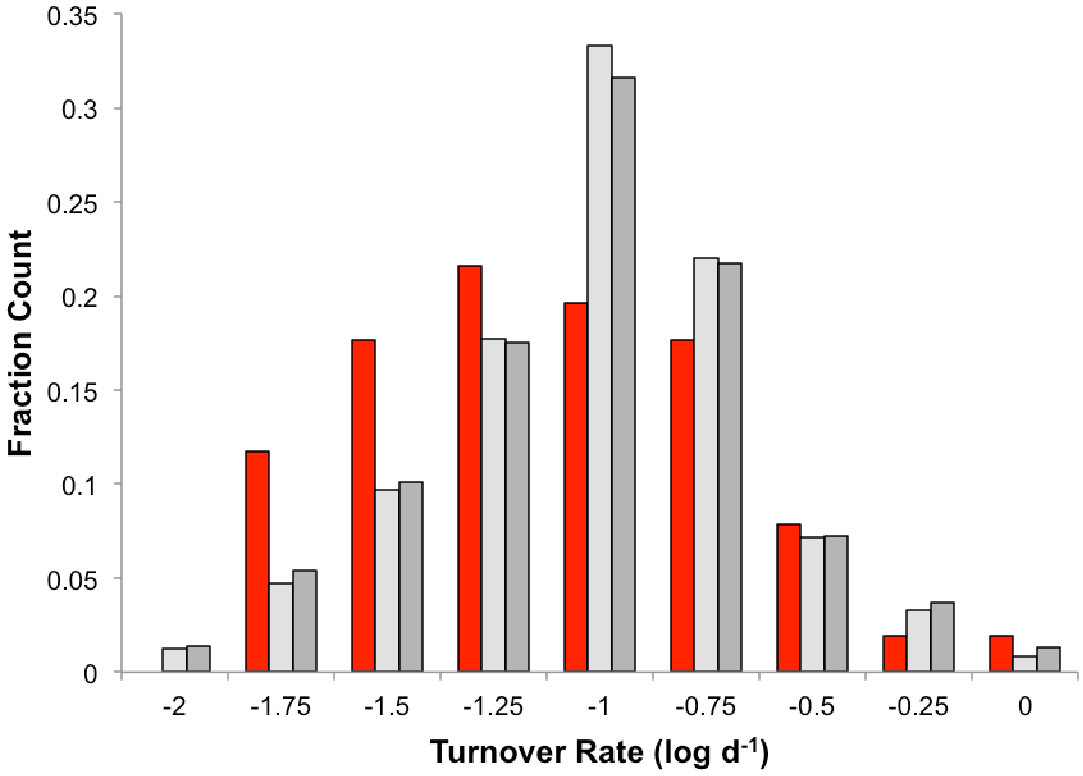

Figure 13: Bar graph showing the distribution of protein turnover rates previously measured for 51 of the brain protein hits identified here (red shaded bars), for 486 of the brain assayed proteins identified in this work (light grey shaded bars) and for all of the 1007 brain proteins analyzed in reference(159) (dark grey shaded bars). Each bar represents the fraction of the total protein population within each rate bin. The high limit of each bin is listed on the x-axis.

A Student's two-tailed t-test between the turnover rates for the hit proteins determined in this work and all turnover rates for the 1007 proteins assayed by Price et. Al. indicated a p-value of 0.07. The turnover rates used to construct the distributions were those measured in relatively young (~4 month old) mice(159). Protein turnover rates may be age-dependent and different proteins may have different age-dependencies

to their turnover rates. A longer-lived protein has more time in the organism before being turned over and therefore more time to experience an aberrant PTM or protein-protein interaction that could lead to its inability to function properly or be degraded appropriately. For example, proteins that accumulate aberrant and destabilizing post-translational modifications may overburden and escape the proteostasis network and biological pathways that regulate their synthesis and degradation.

It has been well documented that there is an increase in oxidation with aging. However the exact impact oxidation has on aging cells is still not well-understood. Recently it was theorized that highly charged proteins may be more susceptible to age dependent oxidation and thus a change in stability and functionality(112). The addition of an oxidation event on the side chain of a protein has the potential to destabilize that protein and cause functional deficits throughout the organism. In order to explore this potential connection further, net charges for all 809 proteins that were assayed in this work were calculated as described previously(112). A global trend in our hits to be more or less enriched in highly charged proteins was not observed. However, there were a small number of our hits that have high charge to length ratio, which makes a compelling argument for the age-dependent thermodynamic stability loss of those proteins being due to age-related oxidations.

The phenotypic effects of the hit proteins identified here were also investigated. The Mouse Genome Database(113) was used to identify if a protein has been linked to

one of two specific phenotypes of particular interest to the study of aging: homeostasis/metabolism and mortality/aging. A total of 33 of the 83 protein hits identified in this work induced an alteration in the homeostasis/metabolism phenotype (**Table 14)**. An even larger fraction of the protein hits (41 of the 83) were implicated in a mortality/aging phenotype (**Table 14)**. These enrichments provide support for the use of this experimental setup for determining proteins with age-related functionality differences. The work here suggests a biophysical mechanism for why the known proteins are important in aging and added a list of novel age-related proteins for future study.

3.4.2 Correlations Between Different Stability and Altered Functions

In total 58 of the 83 protein hits have been previously associated with aging or age-related neurodegenerative diseases **(Table 14)**. For example, gene-knockout studies in mice have shown that dynamin 1 is important in memory development(160) and a knock-out of the stress induced-phosphoprotein 1 gene in nematode shortened the lifespan by 40%(150). Our results suggest that the important age-related functions of dynamin 1 and stress-induced-phosphoprotein 1 may be compromised in old mice because the proteins are destabilized.

Stress-induced phosphoprotein 1 has been shown to coordinate the functional interaction between HSP70 and HSP90(161) two well known chaperone proteins necessary to aid in the proper folding of proteins. It is also interesting to note that there

are 6 other protein hits that are heat shock proteins or associated with the functionality of heat shock proteins (Clpp, Stub1, Hspa4, Hspa4L, Hspd1, Cct3). Furthermore, experiments conducted in *C. elegans* have indicated an increase in organism longevity upon overexpression of chaperone proteins(162, 163). Even more relevant to the work shown here, a study of an Hsp70 chaperone protein (Stub1), a protein hit in this work, indicated that lower levels of this protein decreased the longevity of a mouse model(164). These studies and our protein hits together could be an interesting insight into the down stream effects caused by an age-related loss of functionality in the identified protein hits. Our work suggests that the specific age-related functions of these proteins may be compromised with age due to a loss of thermodynamic stability.

The protein hits involved in the ubiquitin proteasome pathway are also of interest due to the importance of the proteasome in the progression of aging. The ubiquitin proteasome pathway is the major mode of protein degradation in the cell and has been shown to have a decrease in activity with aging leading to a loss of cellular proteostasis and increase in aggregation and dysfunction(165). Ten of the protein hits described here (Ubfd1, Psdm14, Usp14, Ubqln2, Cops6, Cul3, Uba2, Ubei2, Stub1, Cct3) are annotated with association to the ubiquitin or proteasome pathways. These proteins are involved in many different stages of the proteasome pathway. A small change in the protein thermodynamic stability, and thus functionality, at any point could lead to a breakdown of the pathway.

Our results suggest that altered thermodynamic stability may be a biophysical reason for the loss of functionality of these proteins in aging systems. Furthermore, this provides validity to the use of thermodynamic stability measurements to capture age-related changes in the proteome. Although small, the stability differences detected here still have the potential to impair the ability of cells to function properly (i.e., through affecting the degradation of improperly folded proteins via the ubiquitin pathway or through affecting the ability for proteins to properly fold via chaperones) and lead to poor conditions for cell homeostasis.

3.5 Conclusion

This study is the first proteome-wide screen of the effect of aging on protein thermodynamic stability. Identified here were 89 peptide probes from 83 proteins that that were differentially stabilized in the old and young mice populations. The protein hit rate observed here, ~12%, is significantly higher than that previously reported for age-related protein expression level changes (<1%) in a similar mouse model of aging(5). Our results suggest that thermodynamic stability measurements may provide a better means than protein expression levels to study the effects of aging. The thermodynamic stability differences detected in the protein hits provide an important first step in understanding the role that proteins play in the progression of aging. The age-related thermodynamic stability changes detected here were generally small and destabilizing in old mice. This has important implications for the development of longevity drugs.

For example, small molecule ligands that stabilize protein folds (i.e., pharmacological chaperones) could be pursued to rescue a loss of protein thermodynamic stability and treat the adverse effects of aging. Such an approach has shown promise for the treatment of specific protein misfolding diseases. Because aging is such a complex process, it is likely that the use of pharmacological chaperones to reverse or slow such aging process will require the targeting of multiple proteins. This work helps identify some such proteins that may be useful targets for such a strategy.

4. A Study of Protein Folding Stability Differences Caused by Parkinson's Disease Progression in Mice

4.1 Introduction

The presentation of Parkinson's Disease (PD) has been phenotypically described for centuries (bradykinesia, tremors and muscle rigidity). The protein α-synuclein was first tied to the disease twenty years ago through genetic mutations in early onset patients(80). Furthermore, the protein has been shown to be a major component of the Lewy body fibrils characteristic of the disease(81). Even with advances in the study of the disease, such as the discovery of PD related proteins, a detailed molecular level understanding of the disease is lacking. There is also still no cure. Therefore, it is of great interest to characterize the disease progression to help identify new disease-related proteins and pathways to aid in drug discovery and biomarker identification.

The work described here utilizes thermodynamic stability measurements of proteins via the iTRAQ-SPROX technique to identify specific proteins and pathways that play a role in the progression of PD in mouse models. The mouse model used in this work was one in which the human α-synuclein protein with an A53T mutation was overexpressed at roughly 6-fold over that of the endogenous mouse α-synuclein protein. This PD mouse model spontaneously presents with the symptoms of PD between 9-16 months of age with a mean age of onset of 13 months(166). The goal of this work was to generate thermodynamic stability profiles for brain derived proteins from this mouse model at 1 and 6 months when the mice were pre-symptomatic and at a third time point

when the mice first presented symptoms. The identification of proteins with altered thermodynamic stabilities during the progression of the disease is expected to elucidate specific pathways and downstream effects of the formation of abnormal α-synuclein fibrils and aggregation that are related to the stability difference. These proteins have the potential to be future drug targets and/or biomarkers to aid physicians in accurate early diagnosis. For example, proteins that are thermodynamically affected in both the middle and symptomatic time point have the potential to act as biomarkers of early stages of the disease.

As part of this work brain tissue cell lysates from each mouse within a time point (1 Month: n=4, 6 Month: n=4, Symptomatic: n=3) were subjected to an iTRAQ-SPROX analysis. Ultimately, three comparisons were conducted between the three cohorts: 1 Month vs. 6 Months, 1 Month vs. Symptomatic and 6 Months vs. Symptomatic. In these comparisons ~400 unique proteins were assayed using ~800 peptide probes. In total 244 peptides from 184 proteins were identified as hits. Of these 244 peptides, a subset of 52 peptides from 48 proteins were determined to be especially significant due to consistent identification with hit behavior in multiple comparisons and large thermodynamic stability shifts. Identification within multiple comparisons allows for a characterization of the thermodynamic stability trends across the disease progression time points. More than sixty percent of these especially significant proteins have been previously connected to PD in animal models via altered protein expression levels in animal models

of PD. The work described here identifies an important PD-related biophysical property of these proteins that can be exploited in future efforts to treat and diagnose Parkinson's Disease.

4.2 Experimental

4.2.1 Mouse Euthanasia and Tissue Lysis

The mice used in this study were purchased from The Jackson Laboratory and euthanized by cervical dislocation at Duke University. All mice were females with the α-synuclein A53T mutation (strain: B6.Cg-Tg(Prnp-SNCA*A53T)23Mkle/J). Mice were euthanized either at 1 month of age, 6 months of age or upon becoming symptomatic. The mice became symptomatic at 10.5 months (Mouse 1), 15 months (Mouse 2) and 16 months (Mouse 3). Mice were determined to be symptomatic upon indicating signs previously determined(166) such as: tremors, lack of righting response and difficulty walking due to tremors. Immediately following euthanasia the brains were removed and kept at -20°C until the cell lysis was performed as previously described in Chapter 2.2.1.

4.2.2 iTRAQ-SPROX Protocol

Immediately prior to iTRAQ-SPROX analysis a Bradford Assay was used to quantify the protein concentration of the lysates. Lysates were diluted to 5mg/mL for iTRAQ-SPROX analysis. The iTRAQ-SPROX experiments were conducted as previously

described in Chapter 2.2.2. The final concentration of GdmCl in the reaction buffers for all mouse experiments are 0.8 M, 1.1 M, 1.2 M, 1.4 M, 1.6 M, 1.8 M, 2.0 M, and 2.5 M.

4.2.3 Proteomic Sample Preparation

Protein samples were then processed through standard bottom-up proteomics methods as described in Chapter 2.2.3. Once the protein samples had been digested to peptides they were labeled with iTRAQ. In each of the 1 Month old experiments the protein samples from the SPROX buffers with increasing GdmCl concentrations were reacted with iTRAQ tags 114, 115, 116, 117, 118, 119, 121 and 113 respectively. In mouse 1 and 2 of the 6 Months cohort the protein samples from the SPROX buffers with increasing GdmCl concentrations were reacted with iTRAQ tags 113, 114, 115, 116, 117, 118, 119, and 121 respectively. In mouse 3 and 4 of the 6 Months old experiments the protein samples from the SPROX buffers with increasing GdmCl concentrations were reacted with iTRAQ tags 121, 119, 113, 114, 115, 116, 117, and 118 respectively. In each of the Symptomatic experiments the protein samples from the SPROX buffers with increasing GdmCl concentrations were reacted with iTRAQ tags 113, 114, 115, 116, 117, 118, 119, and 121 respectively. The iTRAQ labeling reaction was conducted at room temperature for 2 hours. Samples were combined within an experiment and aliquots (120 μL each) from the combined samples were removed and desalted via a C18 resin clean up (The Nest Group). These were the 'non-enriched' samples. Further aliquots were removed (240 μL each) from the combined samples enriched for methionine

residue containing peptides using a Pi^{3TM} Methionine Reagent according to the manufacturer instructions (The Nest Group). These were the 'enriched' samples.

4.2.4 LC-MS/MS Analyses

All samples were analyzed on a Orbitrap Fusion mass spectrometer with an EASY-nLC 1000 system (ThermoFIscher Scientific Inc.). The trapping column used in these experiments was a 100 μm x 2 cm Integrafrit column (New Objective) that was packed with 200 Å Magic C18 AQ 5 μm material from Michrom. The column in these runs was a 75 μm x 25 cm PicoFrit column (New Objective) packed with 100 Å Magic C18 AQ 5 μm material from Michrom. A flow rate of 300 nL/min was used for all runs. For the following chromatographic information Solvent B is 0.1% Formic Acid in ACN. The chromatography gradient for 1 Month and 6 Month non-enriched and 01 and 02 enriched samples was as follows: 3% to 6% solvent B over 2 minutes, 6% to 33% solvent B over 92 minutes, 33% to 50% solvent B over 7 minutes, 50% solvent B for 5 minutes, 50% to 90% solvent B over 3 minutes and 95% solvent B for the final 8 minutes. The chromatography gradient for all symptomatic samples and for all enriched 03 and 04 samples for the 1 Month and 6 Month time points was as follows: 3% to 7% solvent B over 2 minutes, 7% to 33% solvent B over 92 minutes, 33% to 50% solvent B over 8 minutes, 50% solvent B for 5 minutes, 50% to 90% solvent B over 3 minutes and 95% solvent B for the final 8 minutes. The LC-MS/MS data were collected in a data dependent MS/MS mode using a m/z range of 350-1500. Resolution of the instrument was set to

120,000. Cycles were 3 seconds long, the most abundant ions from the precursor scan were selected for MS/MS analysis and selected ions were dynamically excluded for 30 seconds. Collision induced dissociation (CID) was conducted with HCD and a normalized collision energy of 40% analyzed via Orbitrap with a resolution of 15,000.

Peak lists were extracted from the LC-MS/MS data and were searched against the 24,855 proteins in the SwissProt *Mus musculus* database version 2016-04-13, downloaded on 05/17/16 using Proteome Discoverer (Version 2.1.0.81). Cysteine residue modification by MMTS and N-termini and lysine residues modified by iTRAQ 8-plex were fixed modifications in the search. Oxidized methionine residues and deamidation on asparagine and glutamine and arginine were variable modifications in the search. Up to two missed tryptic cleavages after R and K were allowed. The parameters included a 10 ppm mass tolerance window for precursor masses and 0.6 Da for fragment mass tolerance. Only peptide spectra with FDR <1% and iTRAQ reporter ion intensities that summed to >1000 were used in subsequent analyses of the data.

The LC-MS/MS analyses of the iTRAQ-SPROX samples analyzed here included 4 replicate LC-MS/MS runs of each methionine-containing peptide enriched sample and 1 LC-MS/MS run of each non-enriched sample generated from each brain tissue cell lysate.

4.2.5 Data Analysis

The data was normalized as previously described in reference(42) (see also Chapter 2.2.5). Summarized in **Table 15** are the set of 8 average values (N2 normalization factors) that were generated in each SPROX analysis.

Table 15:N2 normalization factors and standard deviations determined for the iTRAQ-SPROX experiments described in this work.

Time point	Mouse		113	114	115	116	117	118	119	121
1 Month	1	**N2**	0.83	0.91	0.94	1.16	1.23	1.08	0.90	0.95
		SD	0.21	0.18	0.14	0.17	0.15	0.15	0.19	0.21
	2	**N2**	0.85	0.92	0.93	1.19	1.02	1.09	0.96	1.04
		SD	0.26	0.19	0.14	0.17	0.16	0.13	0.21	0.23
	3	**N2**	0.49	0.52	0.46	0.68	0.66	0.58	0.51	0.61
		SD	0.12	0.10	0.08	0.08	0.07	0.07	0.10	0.13
	4	**N2**	0.88	0.57	1.09	1.07	1.02	1.20	1.06	1.10
		SD	0.22	0.15	0.17	0.12	0.12	0.14	0.20	0.22
6 Month	1	**N2**	0.58	0.97	1.22	1.10	1.32	0.99	0.69	1.13
		SD	0.25	0.19	0.18	0.18	0.16	0.23	0.17	0.20
	2	**N2**	1.01	0.97	1.13	1.12	0.70	0.85	0.97	1.25
		SD	0.24	0.20	0.18	0.17	0.13	0.15	0.21	0.25
	3	**N2**	1.34	1.08	0.79	1.24	1.44	1.35	0.40	0.36
		SD	0.30	0.20	0.19	0.17	0.17	0.19	0.14	0.14
	4	**N2**	1.13	1.44	0.37	1.28	0.42	1.30	1.16	0.91
		SD	0.26	0.28	0.26	0.21	0.16	0.22	0.25	0.23
Symptomatic	1	**N2**	0.88	0.96	0.82	1.09	1.07	1.10	0.95	1.12
		SD	0.16	0.14	0.13	0.12	0.11	0.10	0.14	0.11
	2	**N2**	0.58	0.65	0.71	1.26	1.10	1.06	1.13	1.50
		SD	0.26	0.22	0.44	0.17	0.13	0.12	0.20	0.28
	3	**N2**	0.98	1.14	0.80	1.10	0.97	1.05	0.99	0.97
		SD	0.10	0.12	0.16	0.09	0.10	0.11	0.13	0.10

Ultimately, the N1-normalized values generated for the methionine containing peptides were divided by the corresponding N2 normalization factor to determine the final N2-normalized reporter ion intensity. The chemical denaturation data sets were fitted to a four parameter sigmoidal equation, equation 1, using a JAVA-based program (developed in house) that utilized the Nelder and Mead Simplex method for regression analysis (103). More details on the fitting can be found in Chapter 2.2.5.

4.2.6 Hit Identification

A Student's two-tailed t-test was used to identify significant differences between the assigned $C_{1/2}$ values for a given peptide in the comparative analyses performed here. In order to study the Parkinson's disease progression in the mouse models the three sets of data were compared to each other in the following ways: 1 Month vs. 6 Months, 1 Month vs. Symptomatic and 6 Months vs. Symptomatic. A $\Delta C_{1/2}$ value was determined to be significant if the determined t-test p-value was < 0.05.

4.3 Results

4.3.1 Experimental Design

The experiments described here were designed to identify protein folding stability differences that resulted from PD progression induced by the α-synuclein mutation A53T in mouse brain samples. Mice were sacrificed at three time points including at 1 Month old to provide a baseline reading of protein thermodynamic stability, at 6 Months old to act as a roughly half-way point to disease presentation and

at 10-16 Months old, the age which each mouse because symptomatic. Each of these time points contained multiple mice (1 Month n=4, 6 Months n=4, Symptomatic n=3) and 1 iTRAQ-SPROX experiment was conducted on the brain tissue cell lysate from each mouse (**Figure 14**).

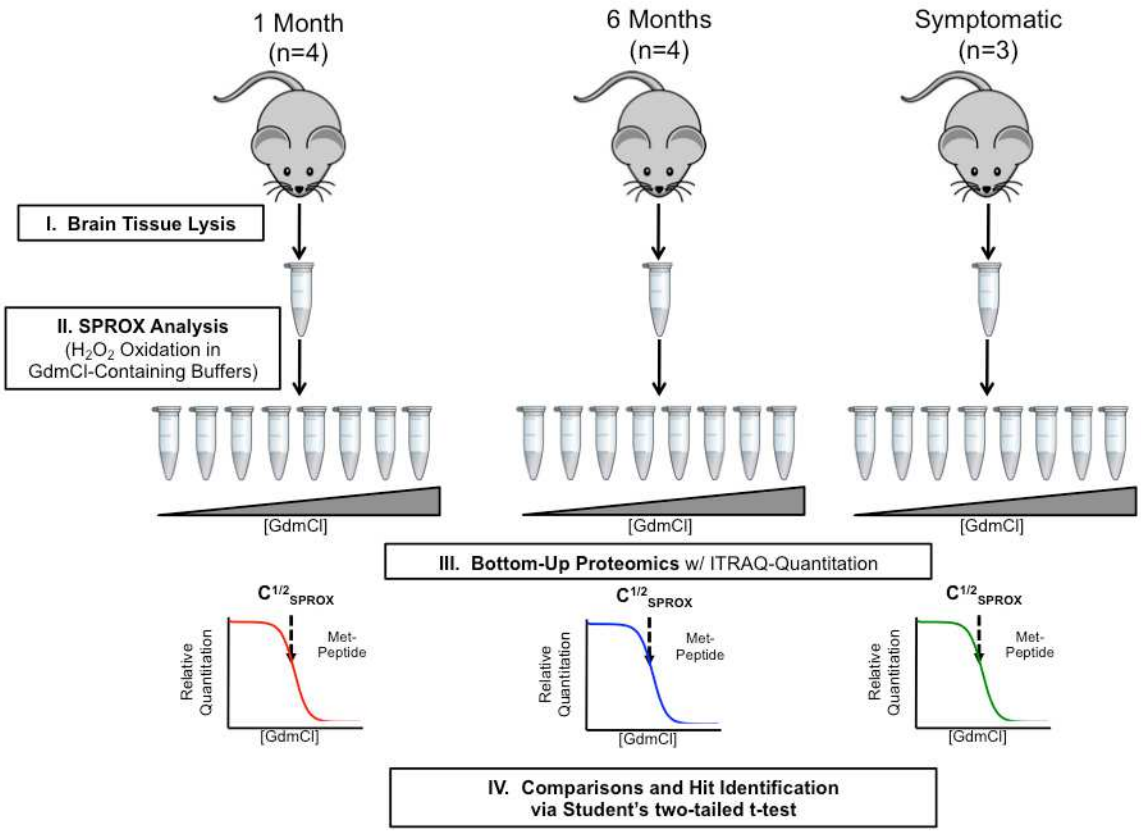

Figure 14: Schematic describing the experimental protocol utilized in this work to study the protein thermodynamic stabilities via iTRAQ-SPROX

The thermodynamic stability measurements generated in the iTRAQ-SPROX experiments were used in three comparative analyses to identify proteins with disease-related thermodynamic stability changes. The Student's two-tailed t-test was used to

identify peptides with significantly different $C_{1/2}$ midpoint values in each comparison. The first comparison, 1 Month vs. 6 Months, was conducted in order to identify the extent of protein stability differences with a pre-symptomatic onset. This comparison is particularly important because the vast majority of neurodegeneration in human PD occurs before patients present with symptoms. The differentially stabilized protein hits identified in the 1 Month vs 6 Months comparison could be utilized as early biomarkers of the disease. The second comparison, 1 Month vs. Symptomatic, was conducted to identify the extent of protein stability differences upon symptomatic presentation. Symptomatic mice have presented the phenotype of PD; therefore protein hits in this comparison are likely to be directly linked to disease progression. Such protein hits are expected to provide information about the specific proteins/pathways affected in PD. The third comparison, 6 Months vs. Symptomatic, was conducted to consider proteins and peptides that have altered stability in the later stages of disease progression. These proteins likely describe pathways that are involved in phenotypic presentation and are potentially useful as drug targets for treating patients who have already presented with PD.

4.3.2 Proteomic Coverage

A total of 11 iTRAQ-SPROX experiments were conducted as part of this work. Each analysis generated high quality chemical denaturation data (Isolation Interference

≤30%, FDR < 1%) for between 300 and 900 proteins using between 400 and 1900 methionine-containing peptide probes (**Table 16**).

Table 16: Summary of the proteomic data obtained in each iTRAQ-SPROX experiment. Numbers of peptides (proteins) with high quality denaturant data are shown below.

	Assayed Peptides (Proteins)				
Time Point	**Mouse 1**	**Mouse 2**	**Mouse 3**	**Mouse 4**	**Combined**
1 Month	1590 (755)	1562 (736)	1906 (917)	1650 (816)	2828 (1178)
6 Months	413 (268)	1170 (638)	1239 (642)	640 (362)	1893 (870)
Symptomatic	1382 (701)	903 (466)	1701 (827)		2345 (999)

4.3.3 Comparative Analyses

4.3.3.1 Comparisons Between Different PD Progression Time Points

To compare the thermodynamic stability of proteins at different stages of PD progression data from the successfully identified peptides from the different mice within a time point were combined to create one data set for each time point. These datasets were then compared using the Student's two-tailed t-test to identify peptides with significantly different $C_{1/2}$ values at the different time points (**Table 17).** In order to be included in the comparative analysis a peptide must have been identified with high quality data in at least two mice from each time point. The three comparisons involved between 678-953 unique peptides from 375-485 unique proteins. In the 1 Month vs. 6 Months and 1 Month vs. Symptomatic comparisons over 100 peptides from 100 proteins were identified as hits. The 6 Month vs. Symptomatic comparison generated 35 unique peptide hits from 35 proteins were identified as hits (**Table 17, Figure 15**). This

corresponds to a hit rate of 16% for 1 Month vs. 6 Months, 11% for 1 Month vs. Symptomatic and 5% for 6 Months vs. Symptomatic. Full lists of peptides identified as hits in the three comparisons can be found in Appendix A.

Table 17: Summary of the proteomic data and hits obtained in each comparative analysis between PD progression time points. Numbers are shown of unique peptides and (proteins).

Comparison	Assayed Peptides (Proteins)	Hit Peptides (Proteins)
1 Month vs. 6 Month	832 (443)	137 (113)
1 Month vs. Symptomatic	953 (485)	113 (108)
6 Month vs. Symptomatic	678 (375)	35 (35)

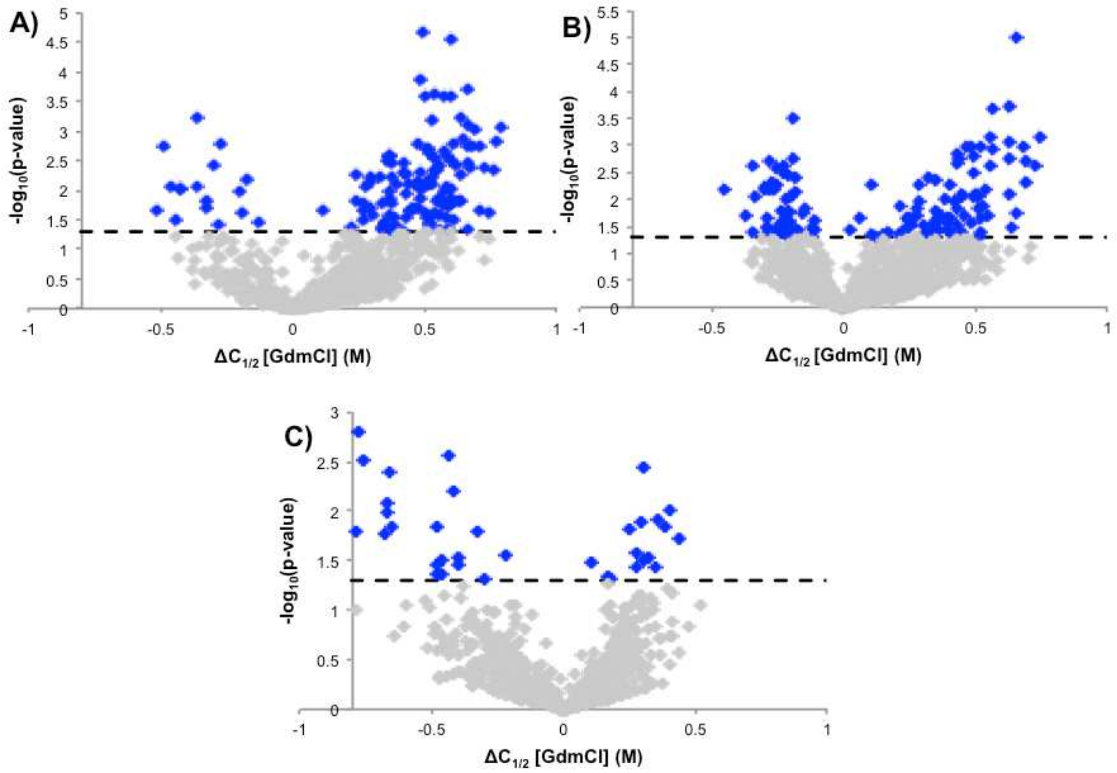

Figure 15: Volcano plots showing the thermodynamic stability measurements and hits identified in the three comparisons described here: A) 1 Month vs. 6 Months, B) 1 Month vs. Symptomatic, C) 6 Months vs. Symptomatic. All $\Delta C_{1/2}$ values were calculated by subtracting the later time point from the earlier time point (i.e. 1 month-6 months). Therefore, a positive $\Delta C_{1/2}$ indicates a decrease in stability with disease progression. The dotted line indicates the p-value cutoff used to determine hit peptides. The grey diamonds are representative of a non-hit peptide and the blue diamonds are representative of hit peptides.

4.3.3.2 Comparisons Between Normal Aging and PD Progression

Two additional comparisons were conducted using data previously generated on control mice at normally aged 6 months and at 18 months ((1)Chapter 3). The hits in these comparative analyses included proteins that are disease specific at the same age

(6months control vs. 6 months disease related) and those proteins that are symptomatic specific (18 months vs. symptomatic). These datasets were compared via the Student two-tailed t-test and hits were determined as described above. In these two comparisons 676 and 919 unique peptides from 381 and 488 unique proteins were assayed and 73 and 71 peptides from 69 and 64 proteins were identified as hits (**Table 18, Figure 16**). Full lists of peptides identified as hits in the two comparisons can be found in Appendix A.

Table 18: Summary of the proteomic data and hits obtained in each comparative analysis. Numbers reported are of unique peptides and (proteins) used in the analyses.

Comparisons	Assayed Peptides (Proteins)	Hit Peptides (Proteins)
6 Month Control vs 6 Month Disease	676 (381)	73 (69)
18 Month vs. Symptomatic	919 (488)	71 (64)

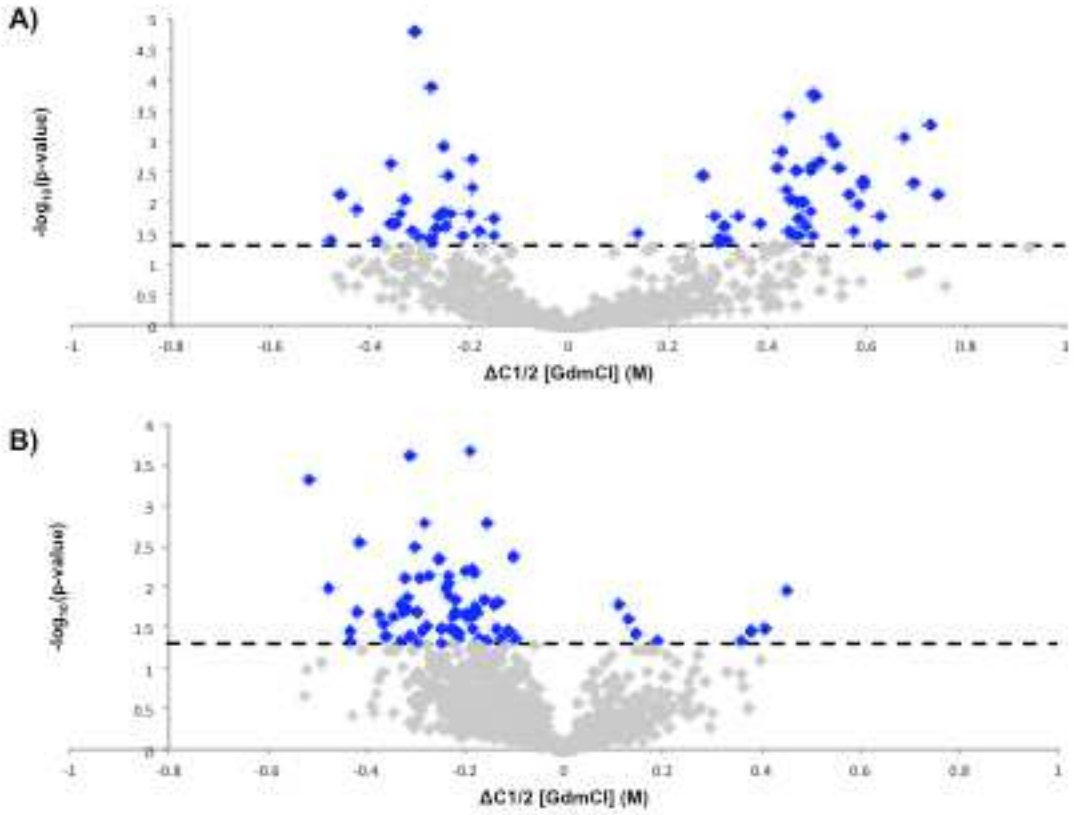

Figure 16: Volcano plots showing the thermodynamic stability measurements and hits identified in the two comparisons described here: A) 6 Month Control vs. 6 Months PD, B) 18 Months Control vs. Symptomatic. All $\Delta C_{1/2}$ values were calculated by subtracting the PD state from the control state (i.e. 6 Month Control – 6 Months PD). A positive $\Delta C_{1/2}$ value indicates a higher stability in the control state. The dotted line indicates the p-value cutoff used to determine hit peptides. The grey diamonds indicate non-hit peptides and the blue diamonds indicate hit peptides.

4.4 Discussion

4.4.1 Biological Variability

The standard deviations of the $C_{1/2}$ value measurements were considered to assess the biological variability of the chemical denaturation curves generated on the proteins derived from the mouse brain samples (**Figure 17**). Peptides that were assayed

in at least two mice within a time point were included in this assessment. The frequency distribution of the standard deviations for the 1 Month is centered around 0.15 M, a value which is similar to that previously observed for the biological variability of the chemical denaturation curves generated on the proteins derived from normally aged mouse brain samples (**Figure 17B**).

The 6 month and symptomatic time points have much broader distributions of $C_{1/2}$ standard deviations than the 1 month time point. This broadening of the distribution is likely due to the heterogeneity of disease progression in the mouse models. This is highlighted by the wide range of ages (10.5 months-16 months old) at which the mice became symptomatic. The 6 month time point was chosen to represent a pre-symptomatic 'middle' time point of the disease based on the average age of disease phenotypic presentation. However, since PD development is clearly different from one mouse to the next, it is not surprising that this time point has the most biological variability. The symptomatic samples show a greater spread of standard deviations than the 1 Month, but less than the 6 month, further supporting the theory of disease heterogeneity.

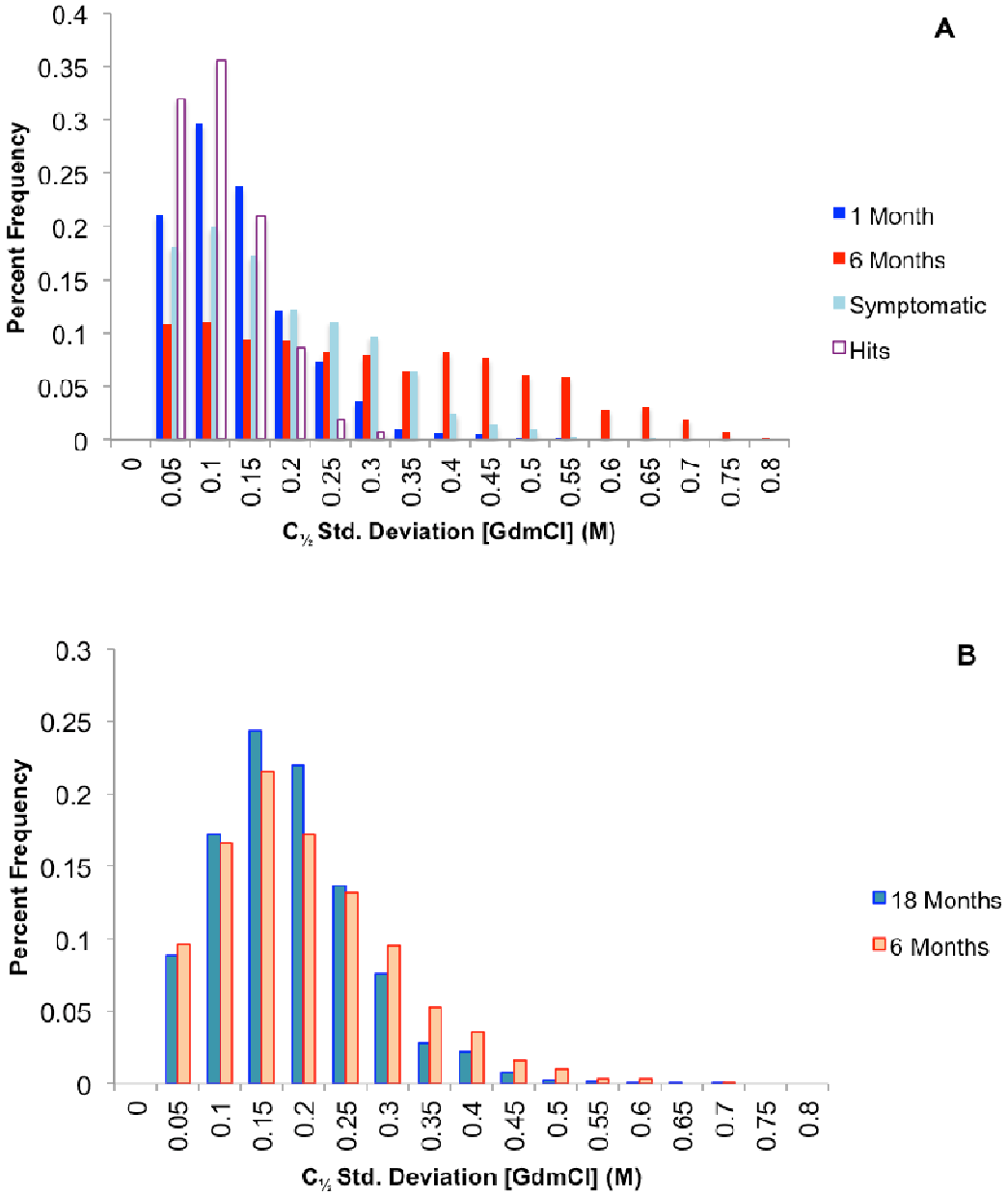

Figure 17: Percent frequency distribution of standard deviations associated with (A) $C_{1/2}$ values determined for the assayed peptides in the different time points studied in this work (B) $C_{1/2}$ values determined for the assayed peptides in the aging study (Chapter 3). Also shown is the percent frequency distribution of the standard deviations of all hit peptides. Each bar represents the percent of the total peptides in that state that have a standard deviation within the bin. The x-axis indicates the high limit of each bin.

4.4.2 Overlap between Normal Aging and PD Progression Comparisons

The chemical denaturation data generated on the PD mouse models was compared to the chemical denaturation data gathered on the normal mouse model of aging investigated in Chapter 3. These comparisons were used to determine: 1) if the thermodynamic stabilities of the PD mouse derived samples were different from those in the normally aged mouse model, 2) if the hits identified in the PD model analysis were disease specific or age-related stability differences. The 6 Month and 18 Month control datasets used in these comparisons were from previously published work(1), which is also described in Chapter 3 of this thesis. These mice were the same base strain (C57BL/6) as the PD mouse model used in this study. In both the 6 Month control vs. 6 Month PD and 18 Month Control vs. Symptomatic PD comparisons (shown in **Figure 16, Table 18)** over 70 peptide hits were identified resulting in peptide hit rates of 8-11%. These hit rates are above the estimated 1-2% false positive rate of the iTRAQ-SPROX technique(102) and indicate that there is indeed a measurable difference in thermodynamic stabilities of the control mice from the Parkinson's Disease state mice.

The comparison of the 6 Month control and 6 Month PD states not show a clear trend in stabilization or destabilization hits. However, the 18 Month vs Symptomatic comparison indicated a trend toward higher thermodynamic stability of the Symptomatic hits. Interestingly, the previous comparative analyses performed on normally aged mice revealed a clear trend of decrease stability with age. All the

symptomatic PD mice were sacrificed at younger ages (10.5 to 16 months) than the 18 month old mice in the aging study. Thus, the trend of higher stability of the hits in the symptomatic mice vs. the normally aged 18 month old mice may be due to the effects of aging. To this point, 10 of the 71 hits identified here were among the 89 hits identified in the previous study of the normally aged mice (**Table 19).** All 10 indicated a higher stability in the PD symptomatic mice compared to the 18 Month control. Of the remaining 61 peptide hits, 86% of which are the result of a lower stability measurement in the 18 Month mice, 45 were assayed in the previous study of normal aging and not found to be differentially stabilized with age. Therefore, these 43 protein hits are likely due to PD related stability changes either directly or indirectly induced by the generation of fibrils from the A53T α-synuclein mutant.

Table 19: Summary of the peptides identified as hits in both the 18 Month vs PD Symptomatic comparison and the normal aging comparison. 18 Month and PD Symptomatic columns report the average $C_{1/2}$ value for the peptide from multiple mice within the biological states.

Peptide Sequence	Protein	18 Month $C_{1/2}$ Value (Std. Dev)	Symptomatic PD $C_{1/2}$ Value (Std. Dev)
ALMEEFFR	Q01065	1.42 (0.16)	1.73 (0.11)
ASPDLVPMGEWTAR	P17426-2	1.50 (0.15)	1.63 (0.02)
LLLATMEALNGGK	P24549	1.38 (0.06)	1.66 (0.03)
LPAYLTIQMVR	Q9JMA1	1.59 (0.21)	1.95 (0.02)
MAGNEYVGFSNATFQSER	D3Z7P3-2	1.30 (0.21)	1.59 (0.09)
MDSTEPPYSQK	P10126	1.20 (0.11)	1.43 (0.03)
NFTTEQVTAMLLSK	Q61316	1.39 (0.10)	1.55 (0.04)
QSTEPSIVMPSIGLSAEPPAPK	P20357	1.35 (0.08)	1.47 (0.01)
VLVVDQLSMR	O08599	1.40 (0.10)	1.62 (0.09)
VMLDHSHGLAAFR	Q923B0-1	1.33 (0.10)	1.57 (0.07)

4.4.3 Disease Progression Comparisons and Trends

The thermodynamic stability differences observed in this work showed that the most dramatic differences were seen when comparing the 1 Month PD mice to either the 6 Month PD mice or the Symptomatic PD mice. The peptide hit rates in these comparisons were relatively high (11-16%) compared to the previously reported hit rate of 5% in the normally–aged mouse brain study (Chapter 3). This suggests that the disease progression induced by the A53T mutation is likely causing a larger disturbance to the proteome than was observed in the case of normal aging.

This work was designed to study the progression of the A53T α-synuclein induced PD mouse model and identify proteins with potential for use as biomarkers and drug targets. In total there were 244 unique peptide hits from 184 unique proteins. Of these peptide hits 52 were identified in multiple comparisons and will be discussed below as those of particular interest. The peptide hits identified in only one comparison likely contain a subset of disease relevant hits. However, some of these hits were only assayed in one comparison because the peptide was not identified in the third time point. Other peptides were not hits in multiple PD time point comparisons because the biological variability of the $C_{1/2}$ value measurement was too large in one time point for an accurate comparison to be made. These peptides may be of true biological interest but there was too much variability in the current measurement to be certain and thus they were not used for further characterization.

A subset of 52 peptides from 48 proteins were identified as hits in multiple comparisons (**Figure 18**) and are of particular interest. Each peptide in this subset was assayed with consistent $C_{1/2}$ assignments within all three time points, suggesting that these hits are not biologically variable. These hit peptides (see **Tables 21-24)** were then placed in one of four disease progression categories: 1) consistent thermodynamic stability shifts in the 6 Month and Symptomatic states when compared to the 1 Month state (Early) (**Figure 19, Table 21)**, 2) consistent stability shifts that appear in only the Symptomatic state (Late), **(Figure 20, Table 22)**, 3) a gradual trend in thermodynamic stability shifts that progresses through all states (Gradual), (**Figure 21,Table 23)**, 4) no consistent disease progression thermodynamic stability behavior (No trend), **(Figure 22, Table 24)**. Within these categories, stability measurements were determined to be the same between two states if they were measured with $\Delta C_{1/2}$ values ≤0.2 M. This was determined as a cutoff because 90% of the total hits identified in the three comparisons have a $\Delta C_{1/2}$ >0.2 M. The number of peptide hits in each category are summarized in **Table 20**. Interesting, nearly all 29 of the hit proteins in early, late and gradual trend categories showed PD related destabilizations.

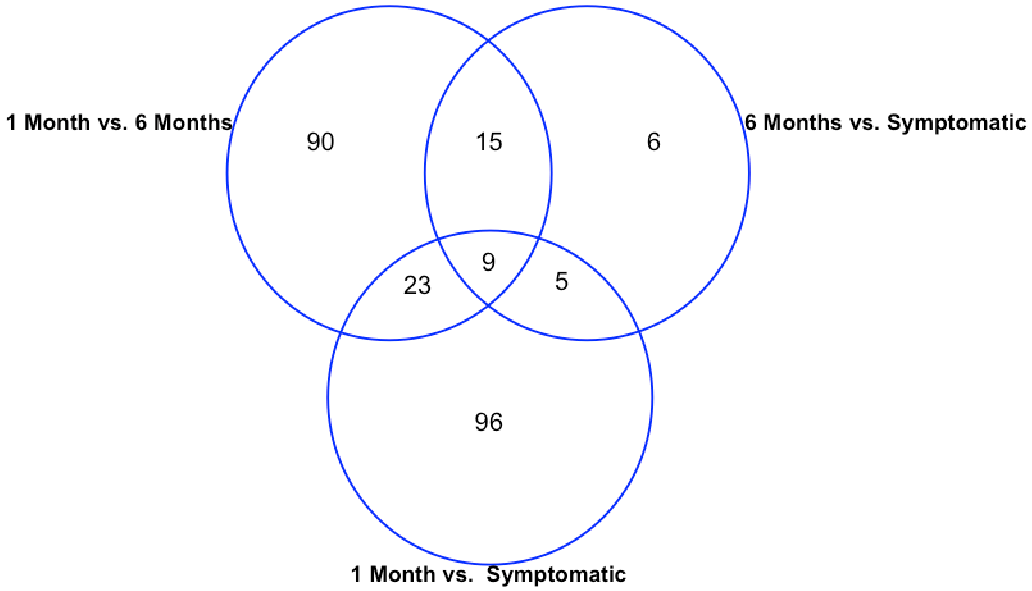

Figure 18: A venn diagram showing the peptide overlap between the three comparative analyses.

Table 20: Breakdown of the 52 peptides identified as the most interesting hits in this work by disease trend behavior. Destabilization with disease progression was determined based on the overall trend from 1 Month to Symptomatic and was unable to be determined for the no trend peptides. Specific literature connections are cited in subsequent tables 21-24.

Trend	Hits Peptide (Protein)	PD Literature Connection Peptide (Protein)	Destabilization with Disease Progression
Early	22 (19)	16 (13)	90%
Late	5 (5)	4 (4)	100%
Gradual	5 (5)	4 (4)	100%
No trend	20 (20)	12 (12)	

4.4.4 Disease Progression Trends

4.4.4.1 Biomarker Discovery (Early Trend)

The peptides that are most promising for use as potential biomarkers of PD are those with a thermodynamic stability difference in the 6 Month time point that is consistent with the Symptomatic state (**Table 21)**. The hit protein, phosphoglycerate mutase, is an example of such a potential biomarker (**Figure 19)**. This is the largest group of the four trends with 22 peptides from 19 proteins. Furthermore, 90% of these hits show decreased thermodynamic stability of the 6 Months and Symptomatic cohorts compared to the 1 Month mice. A previous study indicated a trend in decreasing thermodynamic stability with aging in mouse brains(1) and it is striking to see this trend again in a disease state closely related to the natural aging process. Discovering biomarkers of PD that indicate a pre-symptomatic stability difference that remains consistent in the symptomatic state have the greatest potential for use as a diagnostic tool. Eventually, this may lead to a protein thermodynamic stability screen that is applicable to human cerebrospinal fluid at a pre-symptomatic disease state. Diagnosing PD is still very difficult and relies on the presentation of symptoms that occur at a very late stage of disease progression. If an earlier diagnosis could be made patients could begin treatment earlier and prevent progress of the disease.

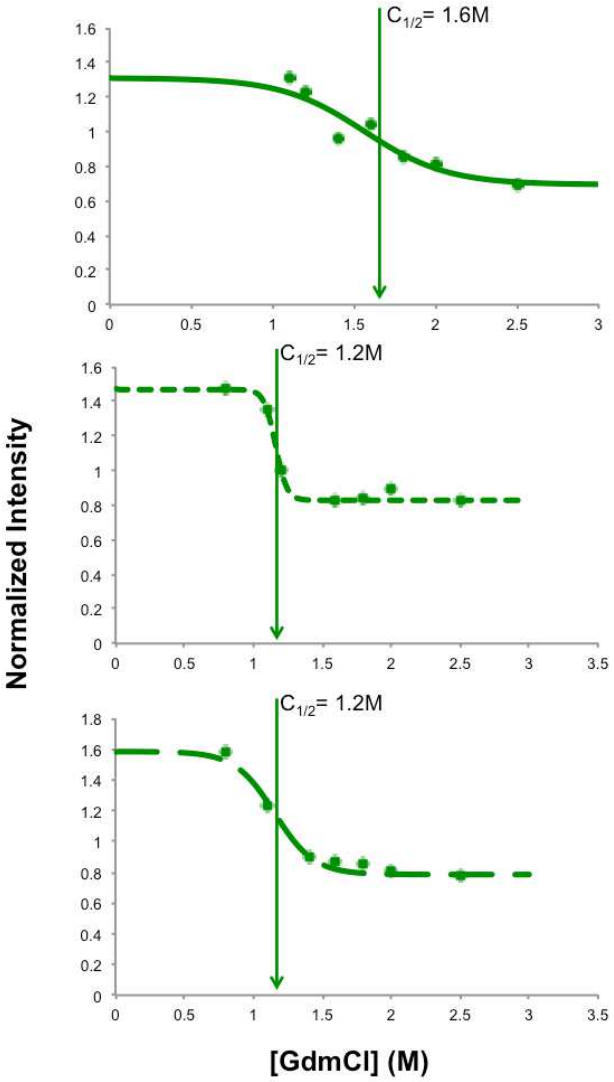

Figure 19: iTRAQ-SPROX data for the peptide AMEAVAAQGK from the protein phosphoglycerate mutase that was identified as a hit in the 1 Month v 6 Month and 1 Month v Symptomatic comparisons and indicate an early onset trend. Shown are the chemical denaturant data sets and fitted curves obtained on this peptide in Mouse 3 of the 1 Month time point (solid line), Mouse 4 of 6 Month time point (short dash) and Mouse 3 of the Symptomatic time point (long dash). The data shown are the average data generated from all product ion spectra gathered within that mouse, the solid line is the best fit of the data according to eq 2 and the vertical arrows indicate the assigned $C_{1/2}$ value of each curve.

Table 21: Peptide hits that were identified with a behavior indicative of Early Biomarkers (1 Month is different from the consistent 6 Month and Symptomatic). References indicate specific proteins that have been previously annotated as related to PD through protein expression level studies. Proteins with a * indicate that the protein expression level difference was measured on an isoform or closely related protein to the protein identified in this work.

Sequence	Protein	1 Month $C_{1/2}$ Value (Std. Dev)	6 Month $C_{1/2}$ Value (Std. Dev)	Symptomatic $C_{1/2}$ Value (Std. Dev)
AMEAVAAQGK	Q9DBJ1[a,b]	1.69 (0.10)	1.08 (0.12)	1.26 (0.09)
EGMNIVEAMER	P17742[a]	1.57 (0.12)	1.12 (0.17)	1.02 (0.01)
EHMQPTHPIR	P68510[a,c,d*]	1.61 (0.10)	1.25 (0.04)	1.08 (0.02)
FIPQMTAGK	P51174[c]	1.67 (0.11)	1.15 (0.04)	1.31 (0.09)
GMTPGEAEIHFLENAK	Q9Z2H5-3	1.62 (0.09)	1.33 (0.08)	1.22 (0.14)
LDLIAQQMMPEVR	P50518[a]	1.71 (0.08)	1.23 (0.06)	1.43 (0.03)
LDNLMLELDGTENK	P17183[a,c]	1.74 (0.11)	1.36 (0.15)	1.29 (0.20)
MSVIWDK	O08553[a,c]	1.64 (0.10)	1.27 (0.08)	1.32 (0.04)
MTLSDPSEMDELMSEEAYEK	Q91WK5	1.50 (0.15)	1.93 (0.01)	1.75 (0.07)
MVPDFYVDSIADLLPALQG	Q8CHP8	1.79 (0.23)	1.08 (0.16)	1.26 (0.14)
NMEEEVAITR	Q60597-4	1.71 (0.17)	1.04 (0.09)	1.20 (0.25)
NSLESYAFNMK	P63017[c]	1.63 (0.05)	1.19 (0.16)	1.08 (0.07)
RDHFEEAMR	Q01853	1.55 (0.17)	1.03 (0.04)	1.10 (0.06)
RFDEILEASDGIMVAR	P52480[a,c,d]	1.74 (0.20)	1.21 (0.11)	1.05 (0.03)
SITDIINIGIGGSDLGPLMVTEALKPYSK	P06745	1.63 (0.10)	1.39 (0.04)	1.23 (0.10)
SLGMAVEDLVAAK	O54983	1.65 (0.04)	1.26 (0.06)	1.44 (0.05)
SYDVPPPPMEPDHPFYSNISK	Q9DBJ1[a,b]	1.76 (0.16)	1.10 (0.11)	1.04 (0.02)
VDIEFDYDGPLMK	P61922[a,c]	1.72 (0.22)	1.09 (0.12)	1.27 (0.12)
VIHDNFGIVEGLMTTVHAITATQK	P16858[a,c]	1.56 (0.11)	1.34 (0.13)	1.34 (0.10)
VIPELNGKLTGMAFR	P16858[a,c]	1.69 (0.16)	1.08 (0.10)	1.19 (0.10)
YDDMASAMK	P68510[a,c,d*]	1.65 (0.11)	1.01 (0.0001)	1.02 (0.03)
YLGAEYMQSVGNMR	Q921I1[f]	1.34 (0.68)	1.71 (0.02)	1.60 (0.02)

a: references(167), b: reference(168), c: reference(169), d: reference(170), e: reference(171), f: reference(172)

4.4.4.2 Late Stage Protein Differences

The second disease trend of interest is late stage development of the disease (i.e. phenotypic presentation). These proteins show a difference in thermodynamic stability

in the Symptomatic time point when compared to the 1 Month and 6 Months time points (**Table 22)**. Synapsin 2 is an example of such a hit (**Figure 20)**. All five of these proteins show a destabilization trend over the course of disease progression. The proteins identified in this group are important for the characterization and understanding of the final, symptomatic stage of the disease. These proteins are likely to be of interest for the development of therapeutic agents. For example, it is possible that pharmacological chaperons targeted to these proteins may rescue protein folding stability and restore functionality.

Table 22: Peptide hits that were identified with a behavior indicative of Late onset/phenotypic presentation (Symptomatic is different from the consistent 1 Month and 6 Months). References indicate specific proteins that have been previously annotated as related to PD through protein expression level studies. Proteins with a * indicate that the protein expression level difference was measured on an isoform or closely related protein to the protein identified in this work.

Sequence	Protein	1 Month $C_{1/2}$ Value (Std. Dev)	6 Month $C_{1/2}$ Value (Std. Dev)	Symptomatic $C_{1/2}$ Value (Std. Dev)
DLVPHYYVESIADLMEGLED	P60487	1.38 (0.03)	1.45 (0.16)	1.17 (0.06)
MIEEAGAIISTR	Q91V12-3[a]	1.53 (0.10)	1.56 (0.13)	1.21 (0.14)
MNQLLSR	Q64332[b]	1.64 (0.03)	1.62 (0.05)	1.32 (0.06)
MVVEFR	P51863[b*]	1.51 (0.05)	1.61 (0.08)	1.20 (0.06)
SLDLVTMK	Q8CHH9-2[a,b*]	1.54 (0.08)	1.47 (0.02)	1.20 (0.09)

a: reference(169), b: reference(167),

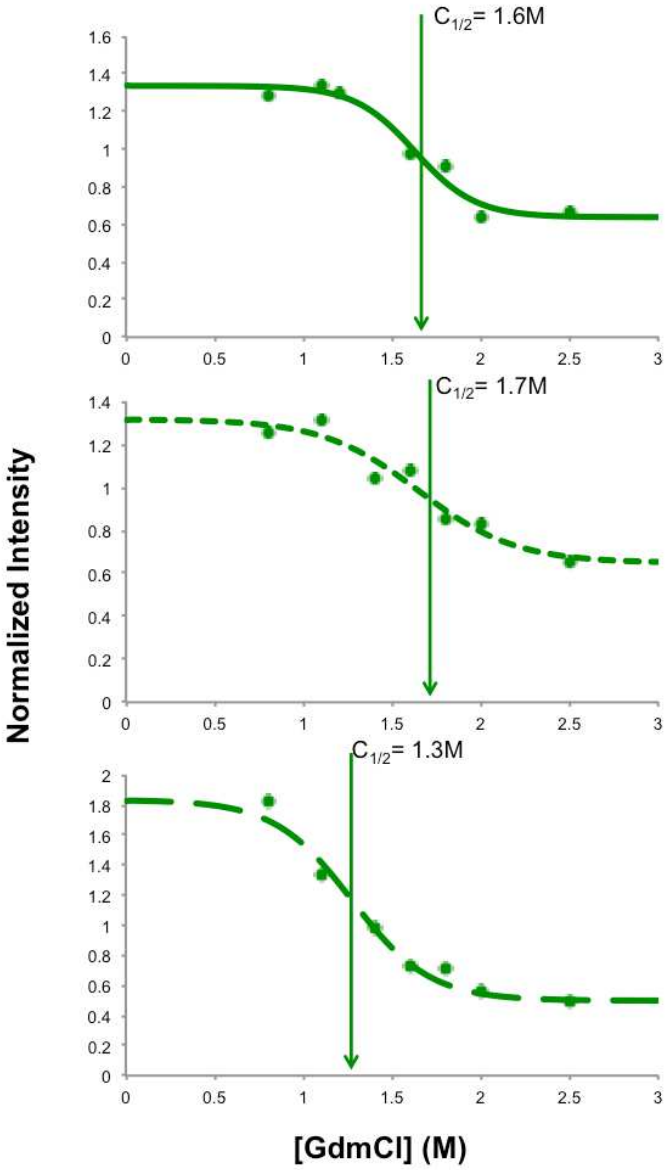

Figure 20: iTRAQ-SPROX data for the peptide MNQLLSR from the protein synapsin 2 that was identified as a hit in the 6 Month v Symptomatic and 1 Month v Symptomatic comparisons and indicate a late onset trend. Shown are the chemical denaturant data sets and fitted curves obtained on this peptide in Mouse 4 of the 1 Month time point (solid line) Mouse 4 of 6 Month time point (short dash) and Mouse 1 of the Symptomatic time point (long dash). The data shown are the average data generated from all product ion spectra gathered within that mouse, the solid line is the best fit of the data according to eq 2 and the vertical arrows indicate the assigned $C_{1/2}$ value of each curve.

4.4.4.3 Gradual Difference in Stability

A trend of interest is peptides that indicate consistently decreasing thermodynamic stability from 1 Month to 6 Months to Symptomatic (**Table 23)**. A peptide from the protein putative adenosylhomocysteinase 2 is one example of this trend (**Figure 21**). These proteins are of interest because they appear to gradually be destabilized throughout the progression of the disease. They may provide an interesting insight into pathways and proteins that play a role in all stages of the disease. For example, the 5 proteins identified in this category have the potential to be used as biomarker due to a consistent trend in thermodynamic stability differences that appears before symptoms. They also have the potential to be drugable targets for future therapeutics due to their gradual destabilization and functional decline throughout disease progression.

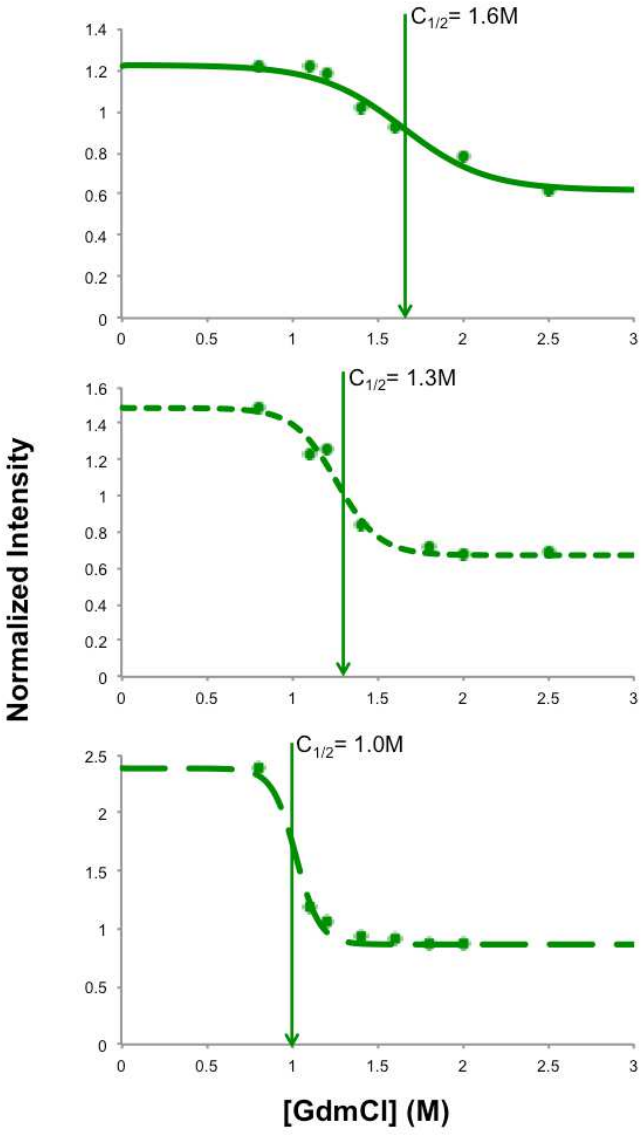

Figure 21: iTRAQ-SPROX data for the peptide EIEIAEQDMSALISLR from the protein putative adenosylhomocysteinase 2 that was identified as a hit in the 1 Month v 6 months and 1 Month v Symptomatic comparisons and indicates an gradual difference in thermodynamic stability over disease progression. Shown are the chemical denaturant data sets and fitted curves obtained on this peptide in Mouse 2 of the 1 Month time point (solid line Mouse 4 of the 6 Month time point (short dash) and Mouse 3 of the Symptomatic time point (long dash). The data shown are the average data generated from all product ion spectra gathered within that mouse, the solid line is the best fit of the data according to eq 2 and the vertical arrows indicate the assigned $C_{1/2}$ value of each curve.

Table 23: Peptide hits that were identified with the gradual thermodynamic stability differences throughout PD progression. References indicate specific proteins that have been previously annotated as related to PD through protein expression level studies. Proteins with a * indicate that the protein expression level difference was measured on an isoform or closely related protein to the protein identified in this work.

Sequence	Protein	1 Month $C_{1/2}$ Value (Std. Dev)	6 Month $C_{1/2}$ Value (Std. Dev)	Symptomatic $C_{1/2}$ Value (Std. Dev)
EIEIAEQDMSALISLR	Q80SW1[a*]	1.69 (0.15)	1.31 (0.19)	1.06 (0.06)
LIGNMALLPLR	Q9JM76[b]	1.70 (0.09)	1.43 (0.13)	1.14 (0.06)
NLKPIKPMQFLGDEETVR	Q9DBJ1[b,c]	1.72 (0.12)	1.32 (0.06)	1.04 (0.03)
SANEFSETESMLK	P24527	1.58 (0.11)	1.31 (0.07)	1.08 (0.03)
TLNFNEEGDAEEAMVDNWRPAQPLK	P00920[d,e]	1.68 (0.03)	1.34 (0.21)	1.05 (0.05)

a: reference (173), b: reference(167), c: reference(168), d: reference(169), e:reference (174)

4.4.4.4 No Trend in Stability Differences

A final category of hits was identified that showed no clear disease progression trend. These peptides indicate a thermodynamic stability shift in the 6 Month time point but a reversion of the stability in the symptomatic state (**Table 24)**. The protein fumarate hydratase is one example of this behavior (**Figure 22**). The proteins in this category are difficult to place in a disease progression context. Due to the reversion of stability, these proteins may not be good choices as biomarkers. It would be difficult to discern if a patient did not show the anticipated thermodynamic stability due to a lack of the disease or progression beyond the middle stage of disease progression.

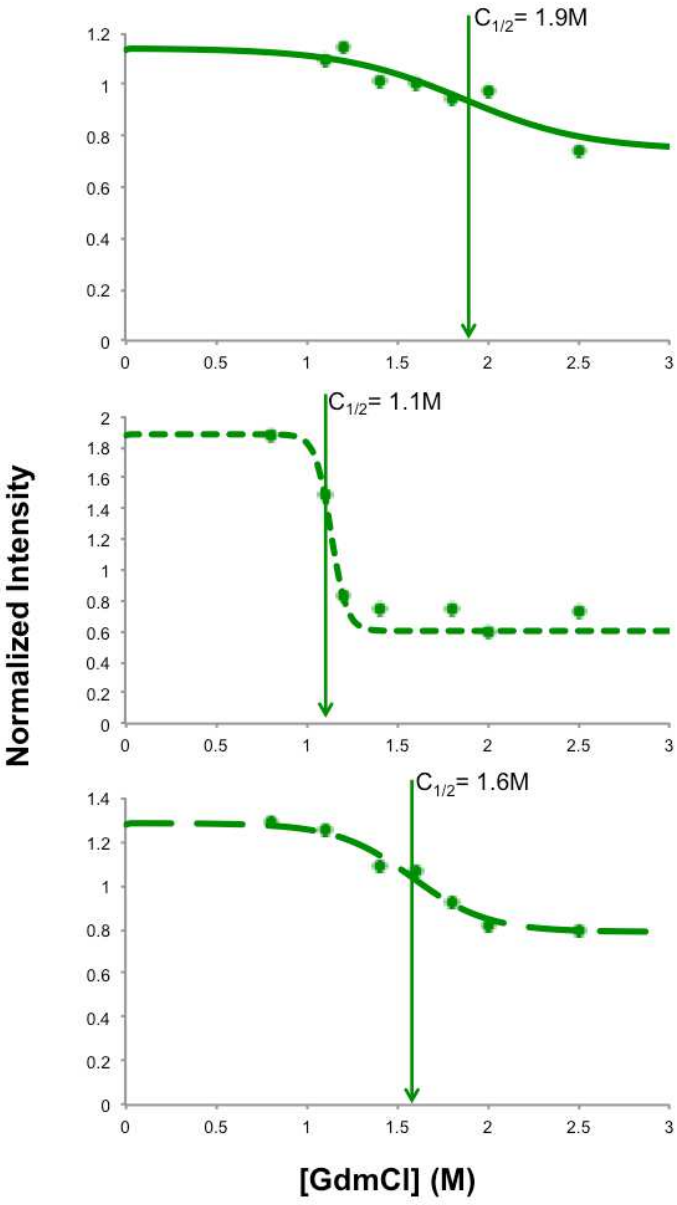

Figure 22: iTRAQ-SPROX data for the peptide SGLGELILPENEPGSSIMPGK from the protein fumarate hydratase that was identified as a hit in all three comparisons. Shown are the chemical denaturant data sets and fitted curves obtained on this peptide in Mouse 2 of the 1 Month time point (solid line Mouse 4 of 6 Month time point (short dash) and Mouse 2 of the Symptomatic time point (long dash). The data shown are the average data generated from all product ion spectra gathered within that mouse, the solid line is the best fit of the data according to eq 2 and the vertical arrows indicate the assigned $C_{1/2}$ value of each curve.

Table 24: Peptide hits that were identified with no consistent trend behavior. References indicate specific proteins that have been previously annotated as related to PD through protein expression level studies. Proteins with a * indicate that the protein expression level difference was measured on an isoform or closely related protein to the protein identified in this work.

Sequence	Protein	1 Month $C_{1/2}$ Value (Std. Dev)	6 Month $C_{1/2}$ Value (Std. Dev)	Symptomatic $C_{1/2}$ Value (Std. Dev)
AALAGGTTMIIDHVVPEPGSSLLTSFEK	P97427[a,b*]	1.67 (0.07)	1.17 (0.02)	1.39 (0.07)
AGLELSPEMK	P12658[c]	1.65 (0.05)	1.07 (0.08)	1.85 (0.05)
AHSSMVGVNLPQK	P09411[a]	1.47 (0.10)	1.10 (0.05)	1.77 (0.03)
ALPDMEVVGLNFSSATTPELLLK	Q9JHU4	1.61 (0.16)	1.04 (0.10)	1.71 (0.13)
EAEAQAAMEANSEGSLTRPK	P63040[b]	1.57 (0.14)	1.06 (0.08)	1.54 (0.11)
ELIPNIPFQMLLR	Q05920	1.58 (0.04)	1.25 (0.04)	1.64 (0.07)
LVPDMIPEVVSEQVSSYLSK	Q9D1A2[d*]	1.32 (0.05)	1.59 (0.08)	1.29 (0.07)
MAGSAFDFENMKR	P50396	1.41 (0.12)	1.84 (0.07)	1.40 (0.13)
MAVTFIGNSTAIQELFK	P99024[b*]	1.70 (0.04)	1.21 (0.01)	1.89 (0.04)
MESPIPILPLPTPDAETEK	Q9Z2Q6[a,b*]	1.74 (0.26)	1.10 (0.04)	1.54 (0.06)
MKPLVVFVLGGPGAGK	Q9DBP5	1.68 (0.03)	1.12 (0.05)	1.60 (0.19)
MPLFEHYTR	Q9CPY7-1	1.58 (0.11)	1.11 (0.04)	1.77 (0.11)
MSATFIGNSTAIQELFK	Q7TMM9[b*]	1.63 (0.08)	1.30 (0.15)	1.69 (0.07)
SGLGELILPENEPGSSIMPGK	P97807-1	1.86 (0.05)	1.10 (0.05)	1.51 (0.07)
SVPMSTVFYPSDGVATEK	P40142[b]	1.68 (0.06)	1.08 (0.03)	1.55 (0.18)
TDLVPAFQNLMK	Q76MZ3	1.60 (0.09)	1.30 (0.04)	1.63 (0.04)
TPVGFIGLGNMGNPMAK	Q99L13	1.47 (0.12)	1.97 (0.04)	1.61 (0.09)
TQGPYDVVVLPGGNLGAQNLSESPMVK	Q99LX0[e]	1.79 (0.13)	1.10 (0.04)	1.56 (0.16)
TVGMLSNMISFYDMAR	P50516-1[b*]	1.50 (0.06)	1.78 (0.17)	1.47 (0.11)
VETGVLKPGMVVTFAPVNVTTEVK	P10126[c]	1.62 (0.06)	1.05 (0.002	1.53 (0.18)

a: reference(169), b: reference(167), c: reference(173), d: reference(175), e: reference(170)

4.4.5 Characterization of Disease Progression Hits

4.4.5.1 Age-Related Hit Overlap

One explanation for the continued trend in destabilizations with disease progression is that the A53T mutation induced PD state is simply speeding up processes that are naturally occurring with age. To consider this, the 48 hit proteins in the subset

of 52 peptides that were identified as hits in multiple comparisons (**Figure 18**) were compared to the hit peptides previously identified in a normal aging study. Interestingly, only one of the peptide hits in the PD progression studies overlapped with natural aging progression. This peptide (TLNFNEEGDAEEAMVDNWRPAQPLK) from the protein carbonic anhydrase 2 gradually decreased stability with the progression of PD. It was assayed as a hit in the natural aging progression study (Chapter 3) with an increase in thermodynamic stability in the old mice. The stability shift in the aging study was very small ($\Delta C_{1/2}$ = -0.07 M, Appendix A) so it is possible this was a false positive in the aging study. The overall trend of a lack of shared thermodynamic stability shifts between the aging study and the PD study indicates the hits in this work are in fact PD progression specific rather than linked to general aging. There are a two reasons to explain why there is minimal overlap of peptide hits between these comparisons: 1) the oldest PD progression mice are not as old as the aged mice, 2) the PD mice have a genetically induced disease progression that is drastically affecting cellular homeostasis. It is highly possible that the mice in PD progression are too young to indicate the natural aging thermodynamic stability shifts (i.e. the 10.5 month old mouse is closer in age to the 6 month time point than the 18 month). Furthermore, the induced disease progression may be disruptive to the natural aging process and thus peptides identified with shifts in either comparison will not overlap. However, it is intriguing that the PD related protein hits and the normal aging related protein hits both

trend toward thermodynamic destabilizations with disease and normal aging progression, respectively.

The overlap of disease progression hits and hits in the 6 month control vs. the 6 month PD comparison was also examined. There are 17 peptides from the subset of 52 peptides that were identified as hits in multiple comparisons (**Figure 18**) that are also hits in the 6 month control vs. the 6 month PD comparison (**Table 25**). It is not surprising that a large fraction, ~65%, of these 17 peptides are in the No Trend category, as the 6 Month time point is the outlier in that category. The other peptides that show overlap between the two comparative analyses indicate that the thermodynamic stability observed in the 6 Month PD state is altered from the age-matched normal mouse. These differences are likely disease progression related.

Table 25: Summary of the peptides identified as hits in both the PD progression analyses and the 6 month control vs 6 Month PD analysis. 6 Month Control and 6 Month PD columns report the average $C_{1/2}$ value for the mice within the biological states.

Sequence	6 Month Control $C_{1/2}$ Value (Std. Dev)	6 Month PD $C_{1/2}$ Value (Std. Dev)	Trend
AGLELSPEMK	1.74 (0.10)	1.07 (0.08)	No Trend
AHSSMVGVNLPQK	1.57 (0.11)	1.10 (0.05)	No Trend
AMEAVAAQGK	1.52 (0.30)	1.08 (0.12)	Early
EAEAQAAMEANSEGSLTRPK	1.63 (0.21)	1.06 (0.08)	No Trend
EHMQPTHPIR	1.10 (0.08)	1.25 (0.04)	Early
MAGSAFDFENMKR	1.49 (0.11)	1.84 (0.07)	No Trend
MAVTFIGNSTAIQELFK	1.73 (0.18)	1.21 (0.01)	No Trend
MNQLLSR	1.33 (0.26)	1.62 (0.05)	Late
MSATFIGNSTAIQELFK	1.60 (0.14)	1.30 (0.15)	No Trend
MTLSDPSEMDELMSEEAYEK	1.47 (0.21)	1.93 (0.01)	Early
MVVEFR	1.35 (0.15)	1.61 (0.08)	Late
SGLGELILPENEPGSSIMPGK	1.54 (0.22)	1.10 (0.05)	No Trend
SLDLVTMK	1.16 (0.08)	1.47 (0.02)	Late
SVPMSTVFYPSDGVATEK	1.54 (0.28)	1.08 (0.03)	No Trend
TPVGFIGLGNMGNPMAK	1.60 (0.08)	1.97 (0.04)	No Trend
TQGPYDVVVLPGGNLGAQNLSESPMVK	1.54 (0.14)	1.10 (0.04)	No Trend
VETGVLKPGMVVTFAPVNVTTEVK	1.54 (0.16)	1.05 (0.002)	No Trend

4.4.5.2 Overlap with Protein Expression Level Studies

The 52 peptides identified in multiple comparisons correspond to 48 unique proteins. More than 60% of the 48 protein hits have been previously linked to Parkinson's Disease through proteomics studies in animal models(167-170, 172-175). The proteomics studies identified either the exact protein as differentially expressed or

an isoform, different subunit or closely related protein. These proteomics studies quantified changes in the protein expression levels due to genetic and chemically induced PD progression. Interestingly, this amount of overlap is on the same order as a previous study that compared SPROX thermodynamic stability hits and proteins with altered protein expression levels of breast cancer cell lines(37). The work described here connects the biophysical property of thermodynamic stability to the altered expression level measured in PD. This is an important step in the understanding of PD development because thermodynamic stability measurements can be targeted with specific molecular chaperones.

4.4.5.3 Protein Networks in Hits

The relationships between the protein hits identified in this work were evaluated using STRING (version 10.0)(176). Shown in **Figure 23** are the STRING analyses of the four protein hit categories.

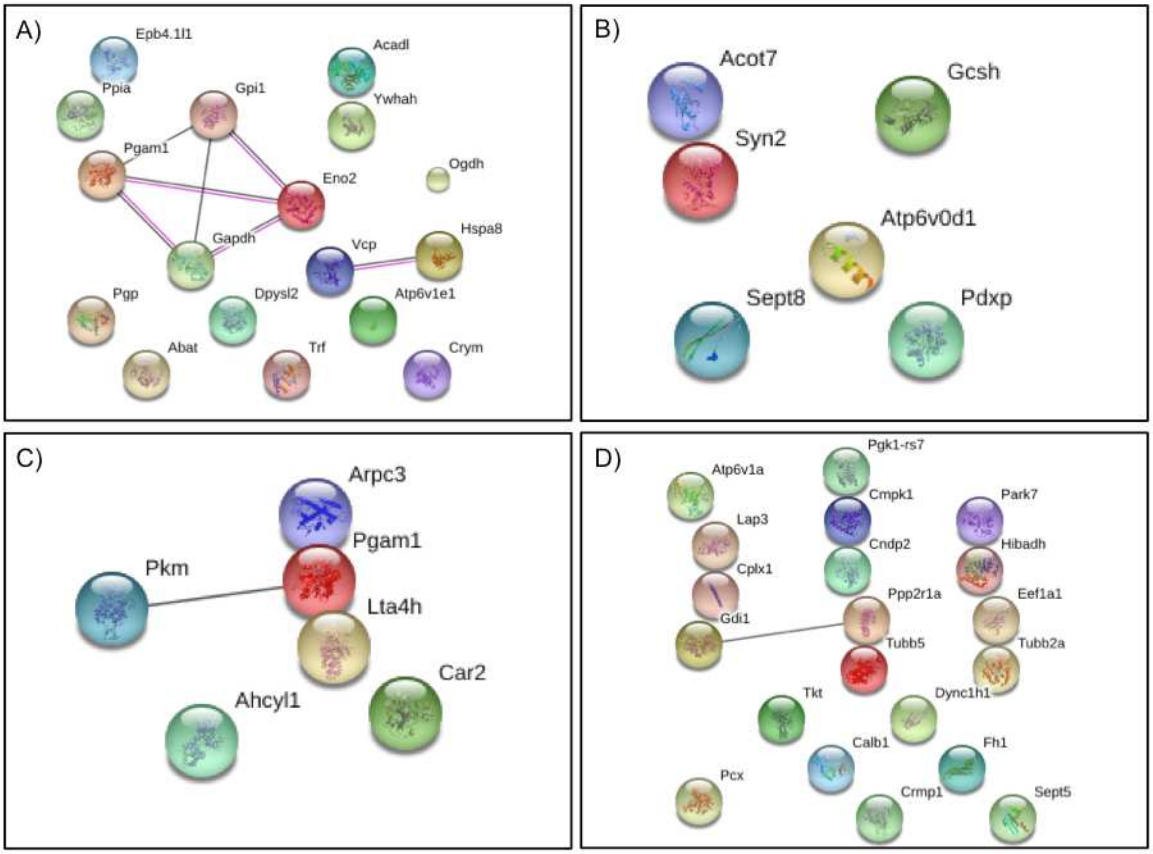

Figure 23: STRING analysis of the four protein hit categories: A) Early, B) Late, C) Gradual, D) No Trend. The STRING analysis was conducted using medium confidence and data from experiments and co-expression studies.

Only the early thermodynamic stability shift protein hits have a significant number of protein-protein interactions (indicated by lines connecting the proteins in **Figure 23**). The four proteins in the cluster (Pgam1, Gpi1, Eno2 and Gapdh) are involved in the glucose metabolism pathway. The inability to break down glucose has been shown to lead to oxidative stress and is of great importance in the development of neurodegenerative disorders(177). Recently, dysregulation of glucose metabolism was measured in human brain tissues of patients with PD(178). The ties between PD and

glycolysis are so strong that small molecules targeting the up-regulation of glucose are being studied as potential treatment options for patients with the disease(179). The thermodynamic stability results reported here add support to the targeting of this pathway in the early stages of PD development and identifies specific proteins that could serve as targets. Furthermore, this work identified specific proteins with a biophysical property that can be targeted via small molecule chaperones to rescue protein function.

4.5 Conclusion

This work highlights a successful application of the iTRAQ-SPROX technique to quantify and characterize the thermodynamic stability of thousands of proteins in A53T mutated α-synuclein disease progression. Through this study 52 peptides from 48 proteins were identified as hits in multiple comparisons and are of particular interest for continued study. Over 90% of the hits in the early, late and gradual disease progression states showed a decrease in thermodynamic stability with disease progression. This is particularly interesting due to earlier work showing a trend of decreased thermodynamic stability with age in control mice. Sixty percent of the proteins identified as hits in this work have been linked to Parkinson's disease through protein expression level studies. This lends support to the claim that we have measured disease related thermodynamic stability differences. More interestingly, this work has linked a biophysical property of proteins Parkinson's Disease progression. Furthermore, this

work proves that there are pre-symptomatic thermodynamic stability differences that are measureable in proteins. Identifying proteins that have measurable differences early in disease development is of extreme interest for the identification of biomarkers for early diagnosis and treatments of earlier stages of the disease. This work identified proteins that are implicated in Parkinson's Disease progression and proteins/pathways that are possible targets for symptomatic drug treatment attempts. These proteins are of the interest for their indication of consistent disease development and may highlight pathways for future understanding of the natural of Parkinson's disease progression.

5. Conclusions and Future Directions

This thesis was designed to study the disease states of aging and Parkinson's Disease while also testing the applications of the SPROX technique on three different styles of mouse models. An important first question in the application of SPROX to mouse models of disease is whether or not there is a significant degree of biological variability in the folding behavior of proteins from mouse to mouse. Through this work, it was determined that the biological variability measured in mouse models is generally low and within the technical variability of SPROX. This is a crucial finding for future SPROX studies on mouse models because it indicates the possibility of parsing out true-positives from false positives due to technical errors.

Chapter 2 describes work conducted to study LRRK2 protein-protein interactions. This set of experiments was structured as a mouse model 'mimic' of the traditional SPROX ligand-binding experiments by using a control mouse, a mouse with overexpression of the LRRK2 protein and a mouse with overexpression of a LRRK2-mutated protein. These mice were not aged to disease progression but all sacrificed at the same time in order to study the impact of the protein overexpression 'ligand' on protein thermodynamic stabilities. The goal of the work in this chapter was to identify protein targets of LRRK2 via overexpression of the wildtype protein and mutation specific interactions via overexpression of an R1441G mutant. Of the hundreds of proteins assayed in these experiments only 1-2% indicated hit behavior. This low hit

rate demonstrates the difficulty of probing hit proteins affected by the excess of a single protein in a mouse model of disease. A 5-fold excess of a single protein (LRRK2 in this case) is likely not large enough to mimic the high levels of free ligand that are usually spiked into a cellular lysate in a more traditional SPROX ligand binding experiment. However, even with such a small hit rate, four proteins (dihydropyrimidinase related protein 2, eukaryotic translation initiation factor 4A2, Rap1 GTP-GDP dissociation stimulator 1 and myelin basic protein, were found to have consistent thermodynamic stability measurements in multiple mice within a biological state and appeared in multiple comparative analyses between the mouse models. Additional experiments are required to validate if the thermodynamic stability measurements are true positives and are due to the overexpression of LRRK2 or the R1441G mutation. Further validation, such as pull-down studies or enzymatic assays, is also needed to understand the biological significance of the ligand-induced stability changes.

The SPROX analyses on the mouse model of aging (Chapter 3) were the first application of the SPROX technique to differentiate between biological states in a mouse model. The mice used in this study were the same base strain (C57BL/6) but simply different ages (6 months and 18 months). As such, any protein hits identified are due to the natural aging process. As part of this work 89 peptide hits from 83 proteins were identified with differential thermodynamic stability. The age related differences were generally destabilizations with age and of small magnitudes. This provides an

interesting avenue for future longevity drug discovery such as small molecules that can 'rescue' protein folding behavior.

The last mouse model studied in this thesis, described in Chapter 4, is one of genetically induced Parkinson's Disease progression. This model was chosen in order to study three separate stages of the neurodegenerative disease. Through a study of the initial time point (1 Month), pre-symptomatic median time point (6 Months), and the symptomatic final stage of disease (10-16 months) hundreds of proteins were assayed. In this study 52 peptides from 48 proteins were discovered as the strongest hits due to their large thermodynamic stability shifts identification in multiple comparisons within the experiment. More than 90% of the peptides showing a disease trend show a decrease in thermodynamic stability with disease progression, an interesting correlation with the natural aging process. A large majority of these proteins (60%) have been previously linked to Parkinson's Disease via expression level studies in animal models. This highlights that thermodynamic stability and expression level studies can often provide complimentary information on the same system. The thermodynamic stability measurements can also provide a biophysical property that is a key piece of information on the disease importance of these proteins. This study also measured thermodynamic stability shifts occurring in the pre-symptomatic time point that are of interest for use as biomarkers for early diagnosis.

This thesis demonstrates the ability of the SPROX technique to analyze, characterize and differentiate three types of mouse models. This is an exciting step in the field of disease state analysis with thermodynamic stability measurements because it indicates an ability to study systems of high biological complexity. However, this discovery based technique still has the same difficulties as previous works—mainly a need for validation of the thermodynamic stability differences and their impact on the protein functionality. This becomes even more important as the ultimate goal of transferring the SPROX technique into a clinical setting gets closer.

Appendix A: Supplemental Tables

Supplemental Table 1: Peptide hits from normal aging study of mouse brains (Chapter 3). These peptides were identified with differential thermodynamic stabilities in the young and old mice via a Student's two-tailed t-test. The p-value reported is from the t-test. The protein turnover rate (PT) is from reference(159). The net charge was determined via the procedure in(112).

Sequence	Gene Name	p.value	Log d-1 (PT)	Seq Length	Net Charge	Young C1/2	Old C1/2	ΔC½	ΔΔG
ADIGVAMGI AGSDVSK	Atp1a3	0.0495	-1.434	1013	19	1.32	1.49	-0.17	0.45
AENLLLDAD MNIK	Mark3	0.0390	NA	753	35.2	1.81	1.27	0.54	-1.41
AFVHWYVG EGMEEGEFSE AR	Tuba3a	0.0218	NA	450	17.8	1.59	1.35	0.24	-0.62
AIPMYK	Atp6v1e1	0.0061	-1.087	226	2.4	1.74	1.42	0.32	-0.83
ALIEHEMK	Lypla2	0.0377	-0.852	231	2.6	1.62	1.32	0.30	-0.79
ALMEEFFR	Pde1b	0.0128	NA	535	11.8	1.65	1.42	0.23	-0.61
AMDLVQEEF LQR	Myg1	0.0297	NA	380	2.6	1.92	1.35	0.57	-1.49
ANEVEQMIR	Dync1h1	0.0309	-0.904	4644	19	1.84	1.52	0.33	-0.85
ASPDLVPMG EWTAR	Ap2a1	0.0249	NA	977	3.4	1.68	1.50	0.18	-0.46
DDAMLLK	Hspd1	0.0175	NA	573	2.4	1.87	1.55	0.32	-0.83
DLYANTVLS GGTTMYPGI ADR	Actb	0.0269	-1.343	375	8.4	1.57	1.28	0.29	-0.74
EGNDLYHE MIESGVINLK	Atp5b	0.0474	-1.759	529	12	1.51	1.42	0.10	-0.26
ELDPTNMTYI TNQAAVHFE K	Stip1	0.0093	-1.045	543	0.6	1.73	1.32	0.41	-1.06
ELGTVMR	Tnnc2	0.0498	NA	160	28.6	1.68	1.47	0.21	-0.53
ELLQQMER	Lancl1	0.0452	-0.880	399	7.6	1.65	1.31	0.34	-0.88
EMASGVNTR	Atp6v0a1	0.0319	NA	839	1	1.71	1.42	0.29	-0.75
EMSLYASLAS EK	Map1b	0.0314	-0.480	2464	147.8	1.70	1.36	0.33	-0.87
EPVQQLTQA	Srm	0.0397	NA	302	6.8	1.35	1.18	0.17	-0.44

QVEQMQLK									
EQMAISGGFIR	Snap25	0.0333	NA	206	13.6	1.56	1.31	0.24	-0.63
EVALMVQER	Aldh7a1	0.0245	NA	539	4.4	1.54	1.27	0.27	-0.70
EVFEMATR	Rhoa	0.0217	-1.264	193	1.2	1.58	1.33	0.24	-0.63
EYFGGFGEVESIELPMDNK	Hnrnpd	0.0361	NA	355	3	1.71	1.26	0.44	-1.15
FALSAMDMEQR	Gls	0.0461	NA	674	11.2	1.85	1.52	0.34	-0.88
FLSQPFQVAEVFTGHMGK	Atp5b	0.0153	-1.759	529	12	1.55	1.33	0.23	-0.59
FPLGGDDEVMSSTLQQFSK	Appl1	0.0030	-1.960	707	16.4	1.50	1.27	0.24	-0.62
GGELGLAMASFLK	Acot1	0.0361	NA	419	1	1.86	1.42	0.44	-1.15
GGQVVNLMNQR	Aak1	0.0048	NA	959	0	1.63	1.08	0.54	-1.42
GHEFSIPFVEMK	Tnr	0.0151	-1.740	1358	54.2	1.07	1.22	-0.15	0.40
GLVTSKPTLATMSVR	Nisch	0.0447	NA	1593	59.4	1.54	1.33	0.21	-0.54
GMAAVPK	Gad1	0.0322	-0.669	593	4	1.59	1.33	0.26	-0.67
GMPGFSTSK	Ivd	0.0260	-1.662	424	7.2	1.43	1.29	0.14	-0.36
GMYDGPVFDLTTTPK	Dpysl3	0.0463	-1.681	570	1.8	1.65	1.33	0.31	-0.82
GQATDIAIQAEEIMK	Clpp	0.0026	-0.558	272	2.8	1.53	1.22	0.32	-0.83
GQSLPSVMGSVPEGVLEDIK	Actr10	0.0044	NA	417	4.2	1.79	1.25	0.54	-1.40
GVNSFQVYMAYK	Crmp1	0.0336	-1.712	572	3.8	1.76	1.56	0.20	-0.51
IENPNQFVPLYTDPQEVLDMR	Add2	0.0144	NA	725	5.6	1.53	1.24	0.29	-0.75
IMDPNIVGNEHYDVAR	Atp5b	0.0222	-1.759	529	12	1.65	1.27	0.37	-0.97
KDLYANTVLSGGTTMYPGIADR	Actb	0.0480	-1.343	375	8.4	1.66	1.37	0.29	-0.76
LADLMER	Aldh1a7	0.0218	NA	501	5.4	1.61	1.23	0.39	-1.00
LAIQEMVSLTSPSAPASSR	Ppfia3	0.0283	NA	1194	20.6	1.82	1.50	0.31	-0.82

LAVNMVPFPR	Tubb2a	0.0118	-1.868	445	21	1.75	1.56	0.19	-0.49
LGPALATGNVVVMK	Aldh2	0.0173	-0.946	519	3.8	1.64	1.42	0.22	-0.57
LLLATMEALNGGK	Aldh1a1	0.0349	NA	501	6.4	1.75	1.38	0.37	-0.97
LPAYLTIQMVR	Usp14	0.0353	-1.143	493	11.4	1.94	1.59	0.36	-0.92
LPLMECVQVTK	Pfkm	0.0395	NA	780	12	1.81	1.47	0.35	-0.91
LPTVPLSGMYNK	Ubfd1	0.0163	NA	368	9	1.38	1.29	0.09	-0.23
LQQTQAQVEEVVDIMR	Vamp1	0.0174	NA	118	0	1.66	1.25	0.41	-1.06
LTDSQNFDEYMK	Fabp7	0.0074	-1.253	132	1.6	1.51	1.34	0.16	-0.42
MADMYTR	Ivd	0.0207	-1.662	424	7.2	1.52	1.33	0.19	-0.49
MAGNEYVGFSNATFQSER	Gls	0.0404	NA	674	11.2	1.54	1.30	0.24	-0.63
MALDDMISTLK	Cct3	0.0177	-0.979	545	0	1.79	1.53	0.27	-0.69
MDSTEPPYSQK	Eef1a1	0.0224	-0.938	462	15	1.43	1.20	0.23	-0.60
MEIGLPDEK	Nsf	0.0425	-1.137	744	1.8	1.43	1.28	0.15	-0.40
MLEIDPQK	Acat1	0.0076	-1.784	424	7.8	1.49	1.33	0.15	-0.40
MLFKDDYPSSPPK	Ube2i	0.0037	NA	158	4.8	1.24	1.13	0.11	-0.28
MQHLIAR	Pkm	0.0290	-1.083	531	4.8	1.48	1.17	0.30	-0.79
MQHNVLVAEVTQQLK	Cul3	0.0261	NA	768	15.6	1.44	1.22	0.22	-0.58
MVVDSAYEVIK	Ldhb	0.0186	-1.227	334	3.2	1.66	1.51	0.15	-0.39
MVVNEGADGGQSVYHIHLHVLGGR	Hint1	0.0312	-0.551	126	0.8	1.23	1.54	-0.31	0.81
NALPTPSDDPTALMTDPK	Gpx1	0.0104	NA	201	0.8	1.50	1.31	0.20	-0.51
NFTTEQVTAMLLSK	Hspa4	0.0442	-1.002	841	23.6	1.53	1.39	0.14	-0.37
NIEVMNSFELLSHTVEEK	Cops6	0.0164	-0.187	324	7.2	1.81	1.53	0.28	-0.72
NPEISHLLNNPDIMR	Ubqln2	0.0330	NA	638	7.4	1.64	1.24	0.40	-1.04

NVEGQDMLYQSLK	Ap2b1	0.0168	NA	937	19.6	1.54	1.27	0.27	-0.71
QFYDQALQQAVMDDDANNAK	Cd81	0.0141	-1.666	236	1.8	1.97	1.29	0.67	-1.75
QLIMANPQMQQLIQR	Ubqln1	0.0426	NA	582	13.6	1.62	1.25	0.38	-0.98
QSTEPSIVMPSIGLSAEPPAPK	Map2	0.0277	-0.929	1828	98	1.65	1.35	0.30	-0.77
RDEMLR	Dnm1	0.0204	-1.118	867	6.6	1.78	1.44	0.34	-0.90
SPLTQEQLIPNLAMK	Stub1	0.0372	NA	304	4.4	1.11	1.48	-0.37	0.96
SQAFIEMETR	Matr3	0.0406	-0.680	846	7.4	1.59	1.39	0.20	-0.52
SQPDMAIMAVNSFVK	Ap2b1	0.0187	NA	937	19.6	1.85	1.63	0.22	-0.56
SVMDQANLQR	Hspa4l	0.0320	-0.979	838	13.2	1.61	1.21	0.40	-1.05
TDPPIIEGNMESAK	Cntn1	0.0434	-1.459	1020	8.2	1.08	1.36	-0.28	0.72
TIPGTALVEMGDEYAVER	Hnrnpll	0.0077	NA	591	8.4	1.07	1.24	-0.16	0.43
TISASTQVQGGDFNLYENMR	Dpysl5	0.0378	-1.533	564	4.8	1.73	1.53	0.20	-0.53
TLNFNEEGDAEEAMVDNWRPAQPLK	Ca2	0.0325	-1.414	260	2.2	1.04	1.11	-0.07	0.19
TPGTWSHITEQIGMFSFTGLNPK	Got1	0.0269	-1.177	413	1.8	1.95	1.83	0.12	-0.30
VAIQLNDTHPALSIPELMR	Pygb	0.0306	-1.175	843	0.4	1.89	1.66	0.23	-0.60
VCMDLNDTVPEYK	Gda	0.0076	-1.252	454	10.2	1.54	1.30	0.24	-0.63
VDILENQLMDNR	Gstm7	0.0027	NA	218	0.2	1.68	1.30	0.37	-0.97
VGAEDADGIDMAYR	Aars	0.0124	-0.838	968	14.6	1.66	1.39	0.27	-0.70
VGEQAQVVIIDMNDPSNPIR	Cltc	0.0300	-1.472	1675	27	1.60	1.30	0.30	-0.77
VIDVFAMPQ	Psmd14	0.0238	NA	310	1.2	1.54	1.36	0.18	-0.46

SGTGVSVEAVDPVFQAK									
VLVVDQLSMR	Stxbp1	0.0029	-1.509	594	2.4	1.60	1.40	0.20	-0.52
VMLDHSHGLAAFR	Ggact	0.0376	NA	149	6.8	1.62	1.33	0.28	-0.74
VTTMDAELEFAIQPNTTGK	Rdx	0.0093	NA	583	4.6	1.72	1.49	0.23	-0.60
YFDSFGDLSSASAIMGNAK	Hbb-b1	0.0378	-1.416	147	3.6	1.55	1.39	0.16	-0.43
YLLTMDK	Uba2	0.0282	-1.517	638	19.2	1.75	1.54	0.21	-0.55
YVHKDETMTPSTAFQVK	Cntn1	0.0212	-1.459	1020	8.2	1.06	1.09	-0.04	0.09

Supplemental Table 2: Peptide hits from PD 1 Month vs 6 Month Comparison (Chapter 4). These peptides were identified with differential thermodynamic stability measurements between the 1 Month and 6 Months PD progression states by the Student's two tailed t-test. Reported in the 1 Month and 6 Month columns are the average $C_{1/2}$ value measurement from all mice within a time point. The p-value was calculated from a Student's two tailed t-test.

Sequence	Protein	p.value	1 Month	6 Month
AALAGGTTMIIDHVVPEPGSSLLTSFEK	P97427	0.0003	1.67	1.17
AAPAAAAAAMAPPGPR	Q8BMF4	0.0017	1.82	1.14
AEMNGLAAQGR	P05063	0.0002	1.64	1.10
AGLELSPEMK	P12658	0.0290	1.65	1.07
AHSSMVGVNLPQK	P09411	0.0036	1.47	1.10
AKFEELNMDLFR	P20029	0.0045	1.64	1.10
ALPAMMQWIR	Q8BLJ3	0.0212	1.23	1.75
ALPDMEVVGLNFSSATTPELLLK	Q9JHU4	0.0108	1.61	1.04
AMEAVAAQGK	Q9DBJ1	0.0317	1.69	1.08
AMNLTLEPEIFPAATDSR	Q99JW2	0.0143	1.61	1.06
AMTGVEQWPYR	P80318	0.0164	1.71	1.11
AVDFQEAQSYADDNSLLFMETSAK	Q9CQD1	0.0080	1.49	1.03
AYHEQLSVAEITNACFEPANQMVK	P05214	0.0220	1.56	1.11
DAALMVTNDGATILK	P80314	0.0471	1.71	1.12
DLLNMYIETEGK	Q61699	0.0474	1.69	1.13
DSLLQDGEFTMDLR	P62962	0.0269	1.62	1.26
EAAQMDMVNDGVEDLR	P19157	0.0219	1.62	1.18
EAEAQAAMEANSEGSLTRPK	P63040	0.0078	1.57	1.06
EAINQGMDEELERDEK	Q9D051	0.0026	1.68	1.10
EGMNIVEAMER	P17742	0.0203	1.57	1.12
EHMQPTHPIR	P68510	0.0031	1.61	1.25
EIEIAEQDMSALISLR	Q80SW1	0.0490	1.69	1.31
ELIPNIPFQMLLR	Q05920	0.0060	1.58	1.25
EMGTPLADTPTRPVTR	Q9EQF6	0.0196	1.65	1.18
EVYMGNVIQGGEGQAPTR	Q8QZT1	0.0244	1.63	1.09
FAAYFQQGDMESNGK	P06745	0.0165	1.61	1.27
FIPQMTAGK	P51174	0.0081	1.67	1.15
FSMVIDNGIVK	P99029-2	0.0001	1.67	1.19
FSNEEIAMATVTALR	P05064	0.0054	1.63	1.39
FVSEMLQK	Q9R111	0.0239	1.42	1.62
GGAEVQIFAPDVPQMHVIDHTK	Q9D172	0.0286	1.68	1.25

GGIMLPEK	Q64433	0.0418	1.51	1.13
GGNMKEVFTR	Q04447	0.0271	1.57	1.27
GIAQMLEK	P67871	0.0307	1.47	1.91
GIVNGAAPELPVPTGGPMAGAR	P62814	0.0018	1.80	1.09
GMTPGEAEIHFLENAK	Q9Z2H5-3	0.0075	1.62	1.33
GMYDGPVFDLTTTPK	Q62188	0.0184	1.69	1.10
GPGYPQAEALLAEAMLK	Q62420	0.0094	1.58	1.10
GQATDIAIQAEEIMK	O88696	0.0083	1.69	1.11
GVIDMGNSLIER	P16546	0.0373	1.63	1.11
GVMLAVDAVIAELK	P63038-1	0.0073	1.60	1.10
HGMFLVR	P47941	0.0196	1.41	1.74
HLMESPANEMTPTR	Q9CPY7-1	0.0053	1.52	1.10
IAPALISSGISVVEQEKLDNLMLELDGTENK	P17183	0.0176	1.79	1.20
IAVGSDADVVIWDPDKMK	P97427	0.0000	1.72	1.12
IEVIEIMTDR	P49312-1	0.0104	1.75	1.38
IHIMPSLNPDGFEK	Q00493	0.0028	1.68	1.15
IHQIEYAMEAVK	Q9R1P4	0.0137	1.79	1.42
ILEMGITGPEGHALSRPEELEAEAVFR	P97427	0.0451	1.74	1.08
LAMQEFMILPVGAESFR	P17183	0.0024	1.82	1.30
LAQENGWGVMVSHR	P17183	0.0062	1.54	1.17
LDLIAQQMMPEVR	P50518	0.0052	1.71	1.23
LDNLMLELDGTENK	P17183	0.0288	1.74	1.36
LEQGQAIDDLMPAQK	Q04447	0.0228	1.62	1.36
LIGNMALLPLR	Q9JM76	0.0170	1.70	1.43
LMFEELR	Q99LF4	0.0226	1.43	1.32
LMIEMDGTENK	P17182	0.0084	1.62	1.35
LRFPAEDEFPDLSSHNNHMAK	Q04447	0.0166	1.62	1.03
LVPDMIPEVVSEQVSSYLSK	Q9D1A2	0.0016	1.32	1.59
MAGSAFDFENMKR	P50396	0.0095	1.41	1.84
MAVTFIGNSTAIQELFK	P99024	0.0000	1.70	1.21
MDATANDVPSPYEVK	P27773	0.0002	1.67	1.01
MESPIPILPLPTPDAETEK	Q9Z2Q6	0.0153	1.74	1.10
MFAIYDGFEGFANGQIK	Q9WUA3-1	0.0205	1.68	1.39
MFASFPTTK	P01942	0.0023	1.59	1.02
MGDHLWIAR	P15105	0.0168	1.63	1.25
MINLSVPDTIDER	Q61233	0.0068	1.59	1.77
MKDTDSEEEIREAFR	P62204	0.0006	1.61	1.09
MKPLVVFVLGGPGAGK	Q9DBP5	0.0153	1.68	1.12

MLHDYIGDKDFK	Q11011	0.0088	1.55	1.92
MLPTIIADNAGYDSADLVAQLR	P80314	0.0455	1.57	1.05
MNEVISLWK	P16546	0.0084	1.35	1.81
MNFSDFLTVMTQK	Q9R1K9	0.0153	1.36	1.68
MPIPVIQAFGILK	P97807-1	0.0015	1.88	1.11
MPLFEHYTR	Q9CPY7-1	0.0017	1.58	1.11
MPTPPSYK	P40142	0.0116	1.69	1.26
MSATFIGNSTAIQELFK	Q7TMM9	0.0428	1.63	1.30
MSDGLFLQK	Q9D6R2-2	0.0020	1.66	1.15
MSESLDTADPAVTGAK	P63011	0.0037	1.66	1.11
MSGDWELEVNGTEAK	O35658	0.0090	1.64	1.13
MSVIWDK	O08553	0.0027	1.64	1.27
MSVQPTVSLGGFEITPPVVLR	Q61937	0.0009	1.83	1.03
MTDQEAIQDLWQWR	Q61937	0.0033	1.39	0.97
MTLSDPSEMDELMSEEAYEK	Q91WK5	0.0097	1.50	1.93
MVIGMDVAASEFYR	P17183	0.0006	1.80	1.16
MVIPGGIDVHTR	O08553	0.0482	1.61	1.19
MVLAAAGGVEHQQLLDLAQK	Q9CZ13	0.0472	1.87	1.28
MVPDFYVDSIADLLPALQG	Q8CHP8	0.0224	1.79	1.08
MVVNEGADGGQSVYHIHLHVLGGR	P70349	0.0378	1.42	1.07
NAVEEYVYEMR	Q61316	0.0286	1.85	1.34
NLKPIKPMQFLGDEETVR	Q9DBJ1	0.0077	1.72	1.32
NMEEEVAITR	Q60597-4	0.0042	1.71	1.04
NSLESYAFNMK	P63017	0.0076	1.63	1.19
NVETMNYADIER	Q9D2G2-2	0.0147	1.73	1.11
QEMQEVQSSR	O88569-3	0.0018	1.80	1.13
QMDTNNDGKLSLEEFIR	P84075	0.0362	1.58	1.06
QQAAMGSQGNLSAEVEQATR	Q9WTT4	0.0052	1.50	1.07
RDHFEEAMR	Q01853	0.0074	1.55	1.03
RFDEILEASDGIMVAR	P52480	0.0062	1.74	1.21
RISEQFTAMFR	Q7TMM9	0.0466	1.58	1.18
SANEFSETESMLK	P24527	0.0331	1.58	1.31
SGASTATAVTDVPSGNLAGAGEAGKLEEVMQELR	Q9WUM3	0.0020	1.62	1.11
SGLGELILPENEPGSSIMPGK	P97807-1	0.0045	1.86	1.10
SGMNVAR	P52480	0.0025	1.77	1.41
SITDIINIGIGGSDLGPLMVTEALKPYSK	P06745	0.0155	1.63	1.39
SLGMAVEDLVAAK	O54983	0.0417	1.65	1.26
SPGAFDMSGVGGSLAESVGSPPPAATPTPTPP	Q80VP1-2	0.0095	1.65	1.05

TR				
SVPMSTVFYPSDGVATEK	P40142	0.0002	1.68	1.08
SYDVPPPPMEPDHPFYSNISK	Q9DBJ1	0.0008	1.76	1.10
TAFDEAIAELDTLNEDSYKDSTLIMQLLR	P68254-1	0.0331	1.59	1.24
TDLVPAFQNLMK	Q76MZ3	0.0060	1.60	1.30
TILMMGR	P58252	0.0109	1.54	1.74
TILSLMTR	Q91V92	0.0038	1.49	1.79
TLNFNEEGDAEEAMVDNWRPAQPLK	P00920	0.0473	1.68	1.34
TLVMAVYDFDR	P46096	0.0345	1.49	1.62
TMVVHEK	P08228	0.0070	1.56	1.09
TPVGFIGLGNMGNPMAK	Q99L13	0.0017	1.47	1.97
TQGPYDVVVLPGGNLGAQNLSESPMVK	Q99LX0	0.0010	1.79	1.10
TVGMLSNMISFYDMAR	P50516-1	0.0376	1.50	1.78
VDIEFDYDGPLMK	P61922	0.0054	1.72	1.09
VETGVLKPGMVVTFAPVNVTTEVK	P10126	0.0003	1.62	1.05
VGNIEIKDLMVGDEASELR	P61161	0.0236	1.89	1.15
VIHDNFGIVEGLMTTVHAITATQK	P16858	0.0431	1.56	1.34
VIPELNGKLTGMAFR	P16858	0.0016	1.69	1.08
VKEGMNIVEAMER	P17742	0.0259	1.67	1.12
VMAGALEGDLFIGPK	Q8R5C5	0.0188	1.71	1.14
VSVTIRPGMTLLMNK	O35215	0.0032	1.72	1.12
VTGADVPMPYAK	Q9D051	0.0139	1.60	1.12
VTNGELLAQYMAEAASELGPSTPYGK	Q8R3V5-3	0.0248	1.65	1.14
VVPEMTEILK	Q99LC5	0.0034	1.75	1.08
WMIPPEAK	Q9D6R2	0.0039	1.73	1.11
YDDMASAMK	P68510	0.0014	1.65	1.01
YGDLANWMIPGK	Q9D0K2	0.0045	1.67	1.13
YGKIETIEVMEDR	Q8BG05-2	0.0147	1.65	1.11
YGMGTSVER	P35486	0.0043	1.86	1.14
YLGAEYMQSVGNMR	Q921I1	0.0006	1.34	1.71
YLPGPLQDMFK	P84086	0.0136	1.72	1.12

Supplemental Table 3: Peptide hits from 1 Month vs Symptomatic comparison (Chapter 4). These peptides were identified with differential thermodynamic stability measurements between the 1 Month and Symptomatic PD progression states by the Student's two tailed t-test. Reported in the 1 Month and Symp columns are the average $C_{1/2}$ value measurement from all mice within a time point. The p-value was calculated from a Student's two tailed t-test.

Sequence	Protein	p.value	1 Month	Symp
AALAGGTTMIIDHVVPEPGSSLLTSFEK	P97427	0.0052	1.67	1.39
AEEYEFLTPMEEAPK	Q99PT1	0.0156	1.55	1.77
AGGFLMK	P09411	0.0418	1.73	1.38
AGLELSPEMK	P12658	0.0036	1.65	1.85
AGYTDQVVIGMDVAASEFYR	P17182	0.0268	1.62	1.23
AHSSMVGVNLPQK	P09411	0.0057	1.47	1.77
AITGASLADIMAK	Q8BP67	0.0496	1.59	1.46
AKPVFEEPPNPTNVEASLQQMK	Q9JKK7	0.0112	1.45	1.16
AMEAVAAQGK	Q9DBJ1	0.0022	1.69	1.26
AMLESIGVPLEK	Q91WQ3	0.0423	1.69	1.87
AMLWVSEK	P12382	0.0380	1.56	1.68
ATAVMPDGQFK	P35700	0.0172	1.47	1.68
AVDLIPWMEYEFR	P12960	0.0169	1.50	1.15
AVMEIMTK	Q62420	0.0078	1.64	1.19
AYAEGMNR	Q9CZU6	0.0066	1.45	1.71
DAGTIAGLNVMR	P20029	0.0010	1.52	1.06
DKEEDMLEVLLDATK	Q8BYI9	0.0017	1.45	1.65
DLTDYLMK	Q8BFZ3	0.0411	1.59	1.88
DLTSWVTEMK	P16546	0.0003	1.68	1.88
DLVPHYYVESIADLMEGLED	P60487	0.0132	1.38	1.17
DMAAVQR	P37804	0.0336	1.56	1.85
DMDDEESWIK	P16546	0.0226	1.38	1.32
DVMPEVNR	P06745	0.00001	1.70	1.04
EEIFGPVMQILK	P47738	0.0475	1.60	1.45
EGMNIVEAMER	P17742	0.0024	1.57	1.02
EHGLIFMETSAK	P53994	0.0278	1.48	1.13
EHMQPTHPIR	P68510	0.0011	1.61	1.08
EIEIAEQDMSALISLR	Q80SW1	0.0018	1.69	1.06
EKEQLMASDDFGR	P16546	0.0023	1.73	1.95

EMDQTMAANAQK	Q9DBP5	0.0012	1.61	1.05
EMNDAATFYTNR	Q9CYT6	0.0089	1.64	1.12
EMQPTHPIR	P68254-1	0.0280	1.55	1.06
EVDEQMLSVQSK	Q9D6F9	0.0142	1.56	1.71
EVMQMLVELAK	P06745	0.0154	1.52	1.09
FAEDMGIPQVPVEK	Q8C0M9	0.0241	1.56	1.21
FDLMYAK	P05214	0.0264	1.48	1.69
FFGPGEFDPSVDVYAMK	Q80XI4	0.0215	1.42	1.17
FGVEQDVDMVFASFIR	P52480	0.0007	1.82	1.08
FIPQMTAGK	P51174	0.0363	1.67	1.31
FLMANGQLVK	Q61598-2	0.0492	1.55	1.66
FVVDLSDQVAPTDIEEGMR	P46471	0.0290	1.61	1.18
GAEEMETVIPVDVMR	Q99LX0	0.0033	1.59	1.09
GDGAALQEMTSQINQK	Q8C8T8	0.0033	1.65	1.88
GEISSTQDAMMEEIFR	Q8R016	0.0435	1.58	1.43
GFIGPGIDVPAPDMSTGER	P26443	0.0091	1.58	1.92
GMALYEEEQVER	P47708	0.0174	1.78	1.13
GMTPGEAEIHFLENAK	Q9Z2H5-3	0.0214	1.62	1.22
GTTASQMAQALALDK	Q60854	0.0255	1.63	1.75
GYTSWAIGLSVADLAESIMK	P06151	0.0202	1.47	1.83
HMGLFDHAAK	Q9D6R2-2	0.0070	1.66	1.84
HQGVMVGMGQK	Q8BFZ3	0.0228	1.67	1.43
IDAMHGVVGPYVK	Q9D0F9	0.0377	1.63	1.84
IDKTDYMVGSYGPR	Q99PT1	0.0318	1.51	1.80
IMIPLK	O55126	0.0362	1.44	1.21
INMCGLTTK	P05201	0.0068	1.73	2.03
IPNIYAIGDVVAGPMLAHK	O08749	0.0417	1.66	1.49
ISEQFTAMFR	Q7TMM9	0.0095	1.58	1.80
IVNDDQSFYADIYMEDGLIK	O08553	0.0445	1.71	1.29
IYPEEMIQTGISAIDGMNSIAR	P62814	0.0110	1.46	1.04
KLAVNMVPFPR	Q7TMM9	0.0023	1.32	1.66
LDLIAQQMMPEVR	P50518	0.0145	1.71	1.43
LDNLMLELDGTENK	P17183	0.0399	1.74	1.29
LFRPDLNMDR	P24288	0.0204	1.63	1.09
LGAGYPMGPFELLDYVGLDTTK	Q61425	0.0304	1.52	1.27
LIGNMALLPLR	Q9JM76	0.0002	1.70	1.14
LIMGIGHR	Q91V92	0.0417	1.61	1.95

LLFDQFMK	Q3UUI3	0.0291	1.64	1.89
LMADVLR	Q8R071	0.0319	1.57	1.69
LMVHNWEYLGK	Q8BVE3	0.0372	1.45	1.65
LPAYLTIQMVR	Q9JMA1	0.0056	1.68	1.95
LSAIMEK	Q9R0Y5-2	0.0443	1.61	1.40
LSFDKDAMVAR	Q93092	0.0170	1.56	1.80
LTGMAFR	Q64467	0.0248	1.75	1.50
LTPVDYLLGVADLTGELMR	Q9QZE7	0.0219	1.34	1.63
LVEDMENK	P47757-1	0.0051	1.52	1.41
MAVTFIGNSTAIQELFK	P99024	0.0389	1.70	1.89
MESALDQLK	Q93092	0.0351	1.71	1.68
MIEEAGAIISTR	Q91V12-3	0.0392	1.53	1.21
MISSYVGENAEFER	Q9D0K2	0.0083	1.74	1.11
MNQLLSR	Q64332	0.0438	1.64	1.32
MPLIGLGTWK	Q9JII6	0.0322	1.68	1.05
MSLFYAEATPMLK	Q921M7	0.0018	1.51	1.07
MSVIWDK	O08553	0.0039	1.64	1.32
MTLSDPSEMDELMSEEAYEK	Q91WK5	0.0350	1.50	1.75
MVPDFYVDSIADLLPALQG	Q8CHP8	0.0131	1.79	1.26
MVVEFR	P51863	0.0298	1.51	1.20
NDFMGAMSFGVSELLK	P63318	0.0372	1.49	1.67
NFDDYMK	P11404	0.0020	1.63	1.91
NLKPIKPMQFLGDEETVR	Q9DBJ1	0.0010	1.72	1.04
NLVDSYMAIVNK	P39053	0.0305	1.61	1.82
NMEEEVAITR	Q60597-4	0.0488	1.71	1.20
NMGLYGER	P05202	0.0202	1.48	1.20
NSLESYAFNMK	P63017	0.0007	1.63	1.08
QMNLQQQPK	O88643	0.0067	1.67	1.14
RDHFEEAMR	Q01853	0.0092	1.55	1.10
RFDEILEASDGIMVAR	P52480	0.0047	1.74	1.05
RPDLLTMVVDYR	Q62048-2	0.0096	1.54	1.16
RVHPISTMIK	P06151	0.0256	1.54	1.75
SANEFSETESMLK	P24527	0.0015	1.58	1.08
SAYSGLQSSSYLMSAR	P08551	0.0419	1.75	1.23
SGLGELILPENEPGSSIMPGK	P97807-1	0.0044	1.86	1.51
SGSHGYDMSTFIR	Q61548	0.0087	1.62	1.82
SITDIINIGIGGSDLGPLMVTEALKPYSK	P06745	0.0052	1.63	1.23

SLDLVTMK	Q8CHH9-2	0.0313	1.54	1.20
SLGMAVEDLVAAK	O54983	0.0493	1.65	1.44
SMGFIGHYLDQK	Q91V92	0.0056	1.72	1.98
SYDVPPPPMEPDHPFYSNISK	Q9DBJ1	0.0024	1.76	1.04
TAGWNIPMGMLYNR	Q921I1	0.0405	1.36	1.60
TGLFTPDMAFETIVK	P39053	0.0448	1.61	1.51
TLNFNEEGDAEEAMVDNWRPAQPLK	P00920	0.0002	1.68	1.05
TMADGNEK	P68510	0.0020	1.73	1.04
TMQTLLSLVK	P00493	0.0038	1.60	1.78
TVPQSSLTMGQLYEK	P60521	0.0066	1.58	2.03
VAEQVGIDKGDIPDLTQAPSSLMETLEQHLNTLEGK	Q61548	0.0172	1.69	1.84
VALVYGQMNEPPGAR	P56480	0.0210	1.53	1.14
VDIEFDYDGPLMK	P61922	0.0196	1.72	1.27
VEAFLITMEK	Q9JHR7	0.0051	1.56	1.83
VETGILRPGMVVTFAPVNITTEVK	P62631	0.0082	1.77	1.27
VHPISTMIK	P06151	0.0472	1.61	1.81
VIHDNFGIVEGLMTTVHAITATQK	P16858	0.0424	1.56	1.34
VIMATNR	P62196	0.0384	1.54	1.14
VIPELNGKLTGMAFR	P16858	0.0151	1.69	1.19
VLDFEHFLPMLQTVAK	Q60605	0.0224	1.67	1.15
VLIMHGGLFSEDGVTLDDIR	Q60676	0.0015	1.55	1.12
VLNNMEIGTSLYDEEGAK	P09411	0.0201	1.63	1.26
VSMELGGLAPFIVFDSANVDQAVAGAMASK	Q8BWF0	0.0238	1.62	1.85
WVDTQVVLAMPYDTPVPGYR	Q9WUB3	0.0086	1.72	1.23
YDDMASAMK	P68510	0.0009	1.65	1.02
YDDMATCMK	P68254-1	0.0011	1.59	1.11
YLGAEYMQSVGNMR	Q921I1	0.0026	1.34	1.60
YLMAEK	P16125	0.0468	1.54	1.76
YMHSGPVVAMVWEGLNVVK	P15532	0.0066	1.43	1.71
YSMVGGNLVINNPDKQK	P12960	0.0474	1.62	1.79

Supplemental Table 4: Peptide hits from 6 Month vs. Symptomatic PD Comparison (Chapter 4). These peptides were identified with differential thermodynamic stability measurements between the 6 Months PD and Symptomatic time points by the Student's two tailed t-test. Reported in the 6 Month and Symp columns are the average $C_{1/2}$ value measurement from all mice within a time point. The p-value was calculated from a Student's two tailed t-test.

Sequence	Protein	p.value	6Month	Symp
AALAGGTTMIIDHVVPEPGSSLLTSFEK	P97427	0.0285	1.17	1.39
AALDGTPGMIGYGMAK	Q8BVI4	0.0031	1.07	1.82
AGLELSPEMK	P12658	0.0157	1.07	1.85
AHSSMVGVNLPQK	P09411	0.0083	1.10	1.77
ALPDMEVVGLNFSSATTPELLLK	Q9JHU4	0.0103	1.04	1.71
AQYDAAMTFGPSQIAK	P50428	0.0016	1.08	1.85
DAGMQLQGYR	P05202	0.0151	1.44	1.19
DLVPHYYVESIADLMEGLED	P60487	0.0362	1.45	1.17
EAEAQAAMEANSEGSLTRPK	P63040	0.0143	1.06	1.54
ELIPNIPFQMLLR	Q05920	0.0348	1.25	1.64
LIGNMALLPLR	Q9JM76	0.0132	1.43	1.14
LVPDMIPEVVSEQVSSYLSK	Q9D1A2	0.0037	1.59	1.29
MAGSAFDFENMKR	P50396	0.0193	1.84	1.40
MASTFIGNSTAIQELFK	Q922F4	0.0487	1.38	1.68
MAVTFIGNSTAIQELFK	P99024	0.0167	1.21	1.89
MESPIPILPLPTPDAETEK	Q9Z2Q6	0.0027	1.10	1.54
MIEEAGAIISTR	Q91V12-3	0.0362	1.56	1.21
MIVVLGEIGGTEEYK	Q91V92	0.0143	1.16	1.81
MKPLVVFVLGGPGAGK	Q9DBP5	0.0357	1.12	1.60
MNQLLSR	Q64332	0.0318	1.62	1.32
MPLFEHYTR	Q9CPY7-1	0.0039	1.11	1.77
MSATFIGNSTAIQELFK	Q7TMM9	0.0298	1.30	1.69
MTLSDPSEMDELMSEEAYEK	Q91WK5	0.0477	1.93	1.75
MVVEFR	P51863	0.0095	1.61	1.20
RFDEILEASDGIMVAR	P52480	0.0448	1.21	1.05
SGLGELILPENEPGSSIMPGK	P97807-1	0.0062	1.10	1.51
SLDLVTMK	Q8CHH9-2	0.0268	1.47	1.20
SVPMSTVFYPSDGVATEK	P40142	0.0433	1.08	1.55

TDLVPAFQNLMK	Q76MZ3	0.0157	1.30	1.63
TLMSPLGITR	P07758	0.0148	1.60	1.22
TPVGFIGLGNMGNPMAK	Q99L13	0.0119	1.97	1.61
TQGPYDVVVLPGGNLGAQNLSESPMVK	Q99LX0	0.0307	1.10	1.56
TVGMLSNMISFYDMAR	P50516-1	0.0291	1.78	1.47
VETGVLKPGMVVTFAPVNVTTEVK	P10126	0.0428	1.05	1.53
YLGAEYMQSVGNMR	Q921I1	0.0331	1.71	1.60

Supplemental Table 5: Peptide hits from 6 Month Control vs 6 Month PD (Chapter 4). These peptides were identified with differential thermodynamic stability measurements between the 6 Month Normal Aging (Control) and 6 Months PD progression states by the Student's two tailed t-test. Reported in the 6 Month Control and 6 Month PD columns are the average $C_{1/2}$ value measurement from all mice within a time point. The p-value was calculated from a Student's two tailed t-test.

Sequence	Protein	p.value	6month Control	6 month PD
AALDGTPGMIGYGMAK	Q8BVI4	0.0008	1.74	1.07
ADEDPIMGFHQMFLLK	P61971	0.0304	1.67	1.53
AGLELSPEMK	P12658	0.0074	1.81	1.07
AHSSMVGVNLPQK	P09411	0.0097	1.57	1.10
AMEAVAAQGK	Q9DBJ1	0.0287	1.52	1.08
AMTGVEQWPYR	P80318	0.0169	1.45	1.11
AQYDAAMTFGPSQIAK	P50428	0.0005	1.81	1.08
AVDFQEAQSYADDNSLLFMETSAK	Q9CQD1	0.0029	1.52	1.03
AYSMAK	Q9JJV2-1	0.0155	1.22	1.56
DAGMQLQGYR	P05202	0.0153	1.20	1.44
DIQEGADMLMVKPGLPYLDMVR	P10518	0.0046	1.80	1.11
DLEALMLDR	Q9D0F9	0.0012	1.19	1.44
DNMFSGSK	P06745	0.0385	1.04	1.34
EAEAQAAMEANSEGSLTRPK	P63040	0.0279	1.63	1.06
EHMQPTHPIR	P68510	0.0177	1.10	1.25
EVYMGNVIQGGEGQAPTR	Q8QZT1	0.0169	1.72	1.09
FVSEMLQK	Q9R111	0.0037	1.37	1.62
GIVNGAAPELPVPTGGPMAGAR	P62814	0.0025	1.58	1.09
GMYDGPVFDLTTTPK	Q62188	0.0029	1.65	1.10
GVIDMGNSLIER	P16546	0.0429	1.43	1.11
HLMESPANEMTPTR	Q9CPY7-1	0.0234	1.41	1.10
IAVGSDADVVIWDPDKMK	P97427	0.0212	1.50	1.12
KDLYANTVLSGGTTMYPGIADR	P60710	0.0053	1.66	1.07
LAMQEFMILPVGASSFR	P17182	0.0455	1.11	1.38
LDLMDEGTDARDVLENK	P39053	0.0335	1.57	1.11
LEQGQAIDDLMPAQK	Q04447	0.0276	1.09	1.36
LIDDMVAQAMK	O88844	0.0057	1.36	1.56
LKTQPTDEEMLFIYSHFK	P31786	0.0180	1.51	1.05

LMFEELR	Q99LF4	0.0019	1.12	1.32
LMVHTVATFNSIK	P16546	0.0337	1.26	1.41
LNITYPMLFK	P70362	0.0401	1.31	1.79
LTPITYPQGLAMAK	P63001	0.0168	1.26	1.53
MAGSAFDFENMKR	P50396	0.0219	1.49	1.84
MAVTFIGNSTAIQELFK	P99024	0.0008	1.73	1.21
MDELQLFR	Q01853	0.0302	1.18	1.50
MFASFPTTK	P01942	0.0029	1.44	1.02
MFIGGLSWDTTK	Q60668-1	0.0251	1.25	1.50
MGDHLWIAR	P15105	0.0002	1.75	1.25
MINLSVPDTIDER	Q61233	0.0152	1.57	1.77
MKDTDSEEEIREAFR	P62204	0.0490	1.71	1.09
MLHDYIGDKDFK	Q11011	0.0132	1.49	1.92
MNEVISLWK	P16546	0.0296	1.63	1.81
MNQLLSR	Q64332	0.0403	1.33	1.62
MSATFIGNSTAIQELFK	Q7TMM9	0.0469	1.60	1.30
MSDGLFLQK	Q9D6R2-2	0.0029	1.60	1.15
MSESLDTADPAVTGAK	P63011	0.0014	1.54	1.11
MSVQPTVSLGGFEITPPVVLR	Q61937	0.0362	1.52	1.03
MTDQEAIQDLWQWR	Q61937	0.0011	1.51	0.97
MTLSDPSEMDELMSEEAYEK	Q91WK5	0.0077	1.47	1.93
MTVVWDK	P97427	0.0001	1.16	1.44
MVVEFR	P51863	0.0135	1.35	1.61
NVETMNYADIER	Q9D2G2-2	0.0247	1.58	1.11
SGASTATAVTDVPSGNLAGAGEAGKLEEVMQELR	Q9WUM3	0.0111	1.69	1.11
SGLGELILPENEPGSSIMPGK	P97807-1	0.0086	1.54	1.10
SGMNVAR	P52480	0.0092	1.08	1.41
SLDLVTMK	Q8CHH9-2	0.00002	1.16	1.47
SVPMSTVFYPSDGVATEK	P40142	0.0095	1.54	1.08
TLMSPLGITR	P07758	0.0384	1.32	1.60
TMVVHEK	P08228	0.0021	1.59	1.09
TPVGFIGLGNMGNPMAK	Q99L13	0.0022	1.60	1.97
TQGPYDVVVLPGGNLGAQNLSESPMVK	Q99LX0	0.0004	1.54	1.10
TTLTDLVPGTEYGVGISAVMNSK	Q8BYI9	0.0214	1.06	1.42
VDSGIQPGSDISIYYDPMISK	Q91ZA3	0.0036	1.37	1.11
VETGVLKPGMVVTFAPVNVTTEVK	P10126	0.0002	1.54	1.05

VSVTIRPGMTLLMNK	O35215	0.0063	1.56	1.12
VTGADVPMPYAK	Q9D051	0.0368	1.42	1.12
VVLPMELPIR	P00405	0.0361	1.32	1.53
VVPEMTEILK	Q99LC5	0.0141	1.57	1.08
VYINYYDMNAANVGWNGSTFA	P34884	0.0351	1.54	1.09
WLAVDHENVRPDMVLLGK	P29758	0.0405	1.21	1.60
WMIPPEAK	Q9D6R2	0.0073	1.67	1.11
YGDLANWMIPGK	Q9D0K2	0.0168	1.42	1.13
YLPGPLQDMFK	P84086	0.0042	1.71	1.12

Supplemental Table 6: Peptide hits from 18 month control vs. symptomatic comparison (Chapter 4). These peptides were identified with differential thermodynamic stability measurements between the 18 Month Normal Aging (Control) and Symptomatic PD progression states by the Student's two tailed t-test. Reported in the 18Month Control and Symp columns are the average $C_{1/2}$ value measurement from all mice within a time point. The p-value was calculated from a Student's two tailed t-test.

Sequence	Protein	p.value	18 month control	Symp
AALDGTPGMIGYGMAK	Q8BVI4	0.0080	1.53	1.82
ADYAQLLEDMQNAFR	P50516-1	0.0485	1.34	1.63
AEEYEFLTPMEEAPK	Q99PT1	0.0205	1.59	1.77
AHSSMVGVNLPQK	P09411	0.0162	1.44	1.77
AIEIYEQVGANTMDNPLLK	P28663	0.0463	1.50	1.14
ALMEEFFR	Q01065	0.0139	1.42	1.73
ALTVPELTQQMFDSK	Q7TMM9	0.0493	1.47	1.59
AMADPEVQQIMSDPAMR	Q60864	0.0244	1.22	1.09
AMLWVSEK	P12382	0.0002	1.49	1.68
APSWIDTGLSEMR	P23927	0.0389	1.18	1.03
ASPDLVPMGEWTAR	P17426-2	0.0444	1.50	1.63
ATSNVFAMFDQSQIQEFK	Q9CQ19	0.0212	1.35	1.77
AYAEGMNR	Q9CZU6	0.0229	1.52	1.71
DHIIEVVGSSMPLIGDHQDEDK	O88935-3	0.0150	1.42	1.64
DMAAVQR	P37804	0.0323	1.61	1.85
DMLYQVLAAEEPSVR	Q64105	0.0077	1.37	1.69
DNLTLWTSDMQGDGEEQNKEALQDVEDENQ	P62259	0.0363	1.11	1.55
DVYIVQDLMETDLYK	Q63844	0.0171	1.37	1.51
EEAQMEVEQYR	Q9WTT4	0.0465	1.29	1.73
EFSVYMTK	P05202	0.0153	1.30	1.44
EGLQNMEAR	Q60864	0.0360	1.39	1.61
ENPTTFMGHYLHEVAR	P07724	0.0043	1.55	1.65
EVDEQMLNVQNK	Q7TMM9	0.0337	1.54	1.68
FDLMYAK	P05214	0.0383	1.48	1.69
FLMANGQLVK	Q61598-2	0.0069	1.48	1.66
FMEQVIFK	Q99JY9	0.0230	1.72	1.91
GFIGPGIDVPAPDMSTGER	P26443	0.0029	1.50	1.92

GVIIMGEDDDSHPSEMR	Q8BWR2-2	0.0345	1.85	1.47
HGIVEDWDLMER	Q641P0	0.0073	1.48	1.75
IDKTDYMVGSYGPR	Q99PT1	0.0002	1.49	1.80
IDSLMDEIAFLK	P08551	0.0066	1.65	1.85
ILSDMFSTEK	P23953	0.0234	1.43	1.78
IMLNTPEDVQALVSGK	Q8BG32	0.0005	1.36	1.88
ITMPVIFNEPLSFLQR	Q91XL9	0.0204	1.37	1.70
IYDMDKDGYISNGELFQVLK	Q63810-2	0.0435	1.66	1.76
LEMYVLNPVK	P14873	0.0062	1.66	1.85
LGLSEMSR	Q08331	0.0090	1.32	1.56
LIMGIGHR	Q91V92	0.0226	1.58	1.95
LLDMDGIIVEK	P23116	0.0215	1.46	1.66
LLLATMEALNGGK	P24549	0.0017	1.38	1.66
LMMNLLR	Q06138	0.0447	1.55	1.77
LPAYLTIQMVR	Q9JMA1	0.0394	1.59	1.95
LSFDKDAMVAR	Q93092	0.0212	1.61	1.80
MAGNEYVGFSNATFQSER	D3Z7P3-2	0.0211	1.30	1.59
MAVTFIGNSTAIQELFK	P99024	0.0179	1.71	1.89
MDSTEPPYSQK	P10126	0.0234	1.20	1.43
MIGGLFIYNHK	P84091	0.0191	1.57	1.89
MLLEYTDSSYDEK	P10649	0.0017	1.32	1.47
MMVGNNLK	Q63810-2	0.0047	1.45	1.70
MPLFEHYTR	Q9CPY7-1	0.0305	1.50	1.77
MTLSDPSEMDELMSEEAYEK	Q91WK5	0.0033	1.45	1.75
NFTTEQVTAMLLSK	Q61316	0.0149	1.39	1.55
QSTEPSIVMPSIGLSAEPPAPK	P20357	0.0355	1.35	1.47
RFDEILEASDGIMVAR	P52480	0.0171	1.16	1.05
SFMNNWEVYK	P47857-3	0.0101	1.44	1.68
SMEIEVLVDADPVVDNSQK	Q91V12-3	0.0442	1.30	1.47
SMGFIGHYLDQK	Q91V92	0.0472	1.82	1.98
SQDSGIAEMEELPVPHNIK	Q8BGT8-2	0.0102	1.27	1.75
SWIEEQEMGSFLSVAK	Q9CPY7-1	0.0113	1.54	1.09
TMLESLIADK	Q7TMB8-1	0.0454	1.47	1.80
TMQTLLSLVK	P00493	0.0332	1.59	1.78
TTVLLADMNDFGTVNEIYK	P52760	0.0406	1.53	1.84
TVEEAAQLALDYMK	Q8C0M9	0.0482	1.36	1.60
TVPQSSLTMGQLYEK	P60521	0.0343	1.74	2.03

VALVYGQMNEPPGAR	P56480	0.0468	1.33	1.14
VESIMK	P50516-1	0.0292	1.16	1.53
VLVVDQLSMR	O08599	0.0204	1.40	1.62
VMLDHSHGLAAFR	Q923B0-1	0.0073	1.33	1.57
VPEANSSWMDTVIR	Q8BMF4	0.0330	1.42	1.65
VQAMYIWVDGTGEGLR	P15105	0.0131	1.22	1.46
WVDTQVVLAMPYDTPVPGYR	Q9WUB3	0.0323	1.63	1.23

References

1. Roberts, J. H.; Liu, F.; Karnuta, J. M.; Fitzgerald, M. C., Discovery of Age-Related Protein Folding Stability Differences in the Mouse Brain Proteome. *Journal of Proteome Research* **2016**.

2. van 't Veer, L. J.; Dai, H.; van de Vijver, M. J.; He, Y. D.; Hart, A. A. M.; Mao, M.; Peterse, H. L.; van der Kooy, K.; Marton, M. J.; Witteveen, A. T.; Schreiber, G. J.; Kerkhoven, R. M.; Roberts, C.; Linsley, P. S.; Bernards, R.; Friend, S. H., Gene expression profiling predicts clinical outcome of breast cancer. *Nature* **2002,** 415, (6871), 530-536.

3. Alizadeh, A. A.; Eisen, M. B.; Davis, R. E.; Ma, C.; Lossos, I. S.; Rosenwald, A.; Boldrick, J. C.; Sabet, H.; Tran, T.; Yu, X.; Powell, J. I.; Yang, L.; Marti, G. E.; Moore, T.; Hudson, J.; Lu, L.; Lewis, D. B.; Tibshirani, R.; Sherlock, G.; Chan, W. C.; Greiner, T. C.; Weisenburger, D. D.; Armitage, J. O.; Warnke, R.; Levy, R.; Wilson, W.; Grever, M. R.; Byrd, J. C.; Botstein, D.; Brown, P. O.; Staudt, L. M., Distinct types of diffuse large B-cell lymphoma identified by gene expression profiling. *Nature* **2000,** 403, (6769), 503-511.

4. Geiger, T.; Madden, S. F.; Gallagher, W. M.; Cox, J.; Mann, M., Proteomic Portrait of Human Breast Cancer Progression Identifies Novel Prognostic Markers. *Cancer Research* **2012,** 72, (9), 2428-2439.

5. Walther, D. M.; Mann, M., Accurate Quantification of More Than 4000 Mouse Tissue Proteins Reveals Minimal Proteome Changes During Aging. *Molecular & Cellular Proteomics* **2011,** 10, (2).

6. Lomenick, B.; Hao, R.; Jonai, N.; Chin, R. M.; Aghajan, M.; Warburton, S.; Wang, J.; Wu, R. P.; Gomez, F.; Loo, J. A.; Wohlschlegel, J. A.; Vondriska, T. M.; Pelletier, J.; Herschman, H. R.; Clardy, J.; Clarke, C. F.; Huang, J., Target identification using drug affinity responsive target stability (DARTS). *Proceedings of the National Academy of Sciences* **2009,** 106, (51), 21984-21989.

7. Feng, Y.; De Franceschi, G.; Kahraman, A.; Soste, M.; Melnik, A.; Boersema, P. J.; de Laureto, P. P.; Nikolaev, Y.; Oliveira, A. P.; Picotti, P., Global analysis of protein structural changes in complex proteomes. *Nat Biotech* **2014,** 32, (10), 1036-1044.

8. Liu, P.-F.; Kihara, D.; Park, C., Energetics-Based Discovery of Protein–Ligand Interactions on a Proteomic Scale. *Journal of Molecular Biology* **2011,** 408, (1), 147-162.

9. West, G. M.; Tucker, C. L.; Xu, T.; Park, S. K.; Han, X.; Yates, J. R.; Fitzgerald, M. C., Quantitative proteomics approach for identifying protein–drug interactions in complex mixtures using protein stability measurements. *Proceedings of the National Academy of Sciences* **2010,** 107, (20), 9078-9082.

10. Savitski, M. M.; Reinhard, F. B.; Franken, H.; Werner, T.; Savitski, M. F.; Eberhard, D.; Molina, D. M.; Jafari, R.; Dovega, R. B.; Klaeger, S., Tracking cancer drugs in living cells by thermal profiling of the proteome. *Science* **2014,** 346, (6205), 1255784.

11. Peng, H.; Guo, H.; Pogoutse, O.; Wan, C.; Hu, L. Z.; Ni, Z.; Emili, A., An Unbiased Chemical Proteomics Method Identifies FabI as the Primary Target of 6-OH-BDE-47. *Environmental Science & Technology* **2016,** 50, (20), 11329-11336.

12. Park, H.; Ha, J.; Koo, J. Y.; Park, J.; Park, S. B., Label-free target identification using in-gel fluorescence difference via thermal stability shift. *Chemical Science* **2017,** 8, (2), 1127-1133.

13. Reinhard, F. B.; Eberhard, D.; Werner, T.; Franken, H.; Childs, D.; Doce, C.; Savitski, M. F.; Huber, W.; Bantscheff, M.; Savitski, M. M., Thermal proteome profiling monitors ligand interactions with cellular membrane proteins. *Nature methods* **2015**.

14. Huber, K. V.; Olek, K. M.; Müller, A. C.; Tan, C. S. H.; Bennett, K. L.; Colinge, J.; Superti-Furga, G., Proteome-wide drug and metabolite interaction mapping by thermal-stability profiling. *Nature methods* **2015,** 12, (11), 1055-1057.

15. Chang, Y.; Schlebach, J. P.; VerHeul, R. A.; Park, C., Simplified proteomics approach to discover protein–ligand interactions. *Protein Science* **2012,** 21, (9), 1280-1287.

16. Adhikari, J.; Fitzgerald, M. C., SILAC-Pulse Proteolysis: A Mass Spectrometry-Based Method for Discovery and Cross-Validation in Proteome-Wide Studies of Ligand Binding. *Journal of The American Society for Mass Spectrometry* **2014,** 25, (12), 2073-2083.

17. Trindade, R. V.; Pinto, A. F. M.; Santos, D. S.; Bizarro, C. V., Pulse Proteolysis and Precipitation for Target Identification. *Journal of Proteome Research* **2016,** 15, (7), 2236-2245.

18. Zeng, L.; Shin, W.-H.; Zhu, X.; Park, S. H.; Park, C.; Tao, W. A.; Kihara, D., Discovery of NAD-Binding Proteins in the E. coli Proteome Using Combined Energetic-Based and Structural-Bioinformatics-Based Approach. *Journal of Proteome Research* **2016**.

19. DeArmond, P. D.; Xu, Y.; Strickland, E. C.; Daniels, K. G.; Fitzgerald, M. C., Thermodynamic Analysis of Protein–Ligand Interactions in Complex Biological Mixtures using a Shotgun Proteomics Approach. *Journal of Proteome Research* **2011,** 10, (11), 4948-4958.

20. Tran, D. T.; Adhikari, J.; Fitzgerald, M. C., Stable Isotope Labeling with Amino Acids in Cell Culture (SILAC)-Based Strategy for Proteome-Wide Thermodynamic Analysis of Protein-Ligand Binding Interactions. *Molecular & Cellular Proteomics* **2014,** 13, (7), 1800-1813.

21. Geer, M. A.; Fitzgerald, M. C., Characterization of the Saccharomyces cerevisiae ATP-Interactome using the iTRAQ-SPROX Technique. *Journal of The American Society for Mass Spectrometry* **2016,** 27, (2), 233-243.

22. Xu, Y.; Wallace, M. A. G.; Fitzgerald, M. C., Thermodynamic Analysis of the Geldanamycin–Hsp90 Interaction in a Whole Cell Lysate Using a Mass Spectrometry-Based Proteomics Approach. *Journal of The American Society for Mass Spectrometry* **2016,** 27, (10), 1670-1676.

23. Vartanian, S.; Ma, T. P.; Lee, J.; Haverty, P. M.; Kirkpatrick, D. S.; Yu, K.; Stokoe, D., Application of mass spectrometry profiling to establish brusatol as an inhibitor of global protein synthesis. *Molecular & Cellular Proteomics* **2016,** 15, (4), 1220-1231.

24. Tohda, C.; Urano, T.; Umezaki, M.; Nemere, I.; Kuboyama, T., Diosgenin is an exogenous activator of 1,25D3-MARRS/Pdia3/ERp57 and improves Alzheimer's disease pathologies in 5XFAD mice. *Scientific Reports* **2012,** 2, 535.

25. Wang, H.; Zhang, L.; Silva, A. J.; Benitez, J. A., A Quinazoline-2,4-Diamino Analog Suppresses Vibrio cholerae Flagellar Motility by Interacting with Motor Protein PomB and Induces Envelope Stress. *Antimicrobial Agents and Chemotherapy* **2013,** 57, (8), 3950-3959.

26. Gong, F.; Peng, X.; Sang, Y.; Qiu, M.; Luo, C.; He, Z.; Zhao, X.; Tong, A., Dichloroacetate induces protective autophagy in LoVo cells: involvement of cathepsin D/thioredoxin-like protein 1 and Akt-mTOR-mediated signaling. *Cell Death Dis* **2013,** 4, e913.

27. Robinson, T.; Pai, M.; Liu, J.; Vizeacoumar, F.; Sun, T.; Egan, S.; Datti, A.; Huang, J.; Zacksenhaus, E., High-throughput screen identifies disulfiram as a potential therapeutic for triple-negative breast cancer cells: Interaction with IQ motif-containing factors. *Cell Cycle* **2013,** 12, (18), 3013-3024.

28. Sun, W.; Tanaka, T. Q.; Magle, C. T.; Huang, W.; Southall, N.; Huang, R.; Dehdashti, S. J.; McKew, J. C.; Williamson, K. C.; Zheng, W., Chemical signatures and new drug targets for gametocytocidal drug development. *Scientific Reports* **2014,** 4, 3743.

29. Chin, R. M.; Fu, X.; Pai, M. Y.; Vergnes, L.; Hwang, H.; Deng, G.; Diep, S.; Lomenick, B.; Meli, V. S.; Monsalve, G. C.; Hu, E.; Whelan, S. A.; Wang, J. X.; Jung, G.; Solis, G. M.; Fazlollahi, F.; Kaweeteerawat, C.; Quach, A.; Nili, M.; Krall, A. S.; Godwin, H. A.; Chang, H. R.; Faull, K. F.; Guo, F.; Jiang, M.; Trauger, S. A.; Saghatelian, A.; Braas, D.; Christofk, H. R.; Clarke, C. F.; Teitell, M. A.; Petrascheck, M.; Reue, K.; Jung, M. E.; Frand, A. R.; Huang, J., The metabolite [agr]-ketoglutarate extends lifespan by inhibiting ATP synthase and TOR. *Nature* **2014,** 510, (7505), 397-401.

30. Gao, W.; Kim, J.-Y.; Anderson, J. R.; Akopian, T.; Hong, S.; Jin, Y.-Y.; Kandror, O.; Kim, J.-W.; Lee, I.-A.; Lee, S.-Y.; McAlpine, J. B.; Mulugeta, S.; Sunoqrot, S.; Wang, Y.; Yang, S.-H.; Yoon, T.-M.; Goldberg, A. L.; Pauli, G. F.; Suh, J.-W.; Franzblau, S. G.; Cho, S., The Cyclic Peptide Ecumicin Targeting ClpC1 Is Active against Mycobacterium tuberculosis In Vivo. *Antimicrobial Agents and Chemotherapy* **2015,** 59, (2), 880-889.

31. Kost, G. C.; Yang, M. Y.; Li, L.; Zhang, Y.; Liu, C.-y.; Kim, D. J.; Ahn, C.-H.; Lee, Y. B.; Liu, Z.-R., A Novel Anti-Cancer Agent, 1-(3,5-Dimethoxyphenyl)-4-[(6-Fluoro-2-Methoxyquinoxalin-3-yl)Aminocarbonyl] Piperazine (RX-5902), Interferes With β-Catenin Function Through Y593 Phospho-p68 RNA Helicase. *Journal of Cellular Biochemistry* **2015,** 116, (8), 1595-1601.

32. Dal Piaz, F.; Vera Saltos, M. B.; Franceschelli, S.; Forte, G.; Marzocco, S.; Tuccinardi, T.; Poli, G.; Nejad Ebrahimi, S.; Hamburger, M.; De Tommasi, N.; Braca, A., Drug Affinity Responsive Target Stability (DARTS) Identifies Laurifolioside as a New Clathrin Heavy Chain Modulator. *Journal of Natural Products* **2016,** 79, (10), 2681-2692.

33. Kim, D.; Hwang, H.-Y.; Kim, J. Y.; Lee, J. Y.; Yoo, J. S.; Marko-Varga, G.; Kwon, H. J., FK506, an Immunosuppressive Drug, Induces Autophagy by Binding to the V-ATPase Catalytic Subunit A in Neuronal Cells. *Journal of Proteome Research* **2016**.

34. Qu, Y.; Gharbi, N.; Yuan, X.; Olsen, J. R.; Blicher, P.; Dalhus, B.; Brokstad, K. A.; Lin, B.; Øyan, A. M.; Zhang, W.; Kalland, K.-H.; Ke, X., Axitinib blocks Wnt/β-catenin signaling and directs asymmetric cell division in cancer. *Proceedings of the National Academy of Sciences* **2016,** 113, (33), 9339-9344.

35. Geiger, R.; Rieckmann, Jan C.; Wolf, T.; Basso, C.; Feng, Y.; Fuhrer, T.; Kogadeeva, M.; Picotti, P.; Meissner, F.; Mann, M.; Zamboni, N.; Sallusto, F.; Lanzavecchia, A., L-Arginine Modulates T Cell Metabolism and Enhances Survival and Anti-tumor Activity. *Cell* **2016,** 167, (3), 829-842.e13.

36. Geer Wallace, M. A.; Kwon, D.-Y.; Weitzel, D. H.; Lee, C.-T.; Stephenson, T. N.; Chi, J.-T.; Mook, R. A.; Dewhirst, M. W.; Hong, J.; Fitzgerald, M. C., Discovery of Manassantin A Protein Targets Using Large-Scale Protein Folding and Stability Measurements. *Journal of Proteome Research* **2016,** 15, (8), 2688-2696.

37. Adhikari, J.; West, G. M.; Fitzgerald, M. C., Global Analysis of Protein Folding Thermodynamics for Disease State Characterization. *Journal of Proteome Research* **2015,** 14, (5), 2287-2297.

38. Ogburn, R. N.; Randall, T. A.; Xu, Y.; Roberts, J. H.; Mebrahtu, B.; Karnuta, J. M.; Rider, S. D.; Kissling, G. E.; London, R. E.; Pomés, A.; Arlian, L.; Fitzgerald, M. C.; Mueller, G. A., Are dust mite allergens more abundant and/or more stable than other Dermatophagoides pteronyssinus proteins? *Journal of Allergy and Clinical Immunology*.

39. Liu, F.; Fitzgerald, M. C., Large-Scale Analysis of Breast Cancer-Related Conformational Changes in Proteins Using Limited Proteolysis. *Journal of Proteome Research* **2016**.

40. Tang, H.; Tian, E.; Liu, C.; Wang, Q.; Deng, H., Oxidative Stress Induces Monocyte Necrosis with Enrichment of Cell-Bound Albumin and Overexpression of Endoplasmic Reticulum and Mitochondrial Chaperones. *PLOS ONE* **2013,** 8, (3), e59610.

41. Hvidt, A.; Nielsen, S. O., Hydrogen Exchange in Proteins. In *Advances in Protein Chemistry*, C.B. Anfinsen, M. L. A. J. T. E.; Frederic, M. R., Eds. Academic Press: 1966; Vol. Volume 21, pp 287-386.

42. Strickland, E. C.; Geer, M. A.; Tran, D. T.; Adhikari, J.; West, G. M.; DeArmond, P. D.; Xu, Y.; Fitzgerald, M. C., Thermodynamic analysis of protein-ligand binding interactions in complex biological mixtures using the stability of proteins from rates of oxidation. *Nat. Protocols* **2013,** 8, (1), 148-161.

43. West, G. M.; Tang, L.; Fitzgerald, M. C., Thermodynamic analysis of protein stability and ligand binding using a chemical modification-and mass spectrometry-based strategy. *Analytical chemistry* **2008,** 80, (11), 4175-4185.

44. Xu, Y.; Strickland, E. C.; Fitzgerald, M. C., Thermodynamic Analysis of Protein Folding and Stability Using a Tryptophan Modification Protocol. *Analytical Chemistry* **2014,** 86, (14), 7041-7048.

45. Jin, L.; Wang, D.; Gooden, D. M.; Ball, C. H.; Fitzgerald, M. C., Targeted Mass Spectrometry-Based Approach for Protein–Ligand Binding Analyses in Complex Biological Mixtures Using a Phenacyl Bromide Modification Strategy. *Analytical Chemistry* **2016,** 88, (22), 10987-10993.

46. Hekimi, S.; Lapointe, J.; Wen, Y., Taking a "good" look at free radicals in the aging process. *Trends in Cell Biology* **2011,** 21, (10), 569-576.

47. Balaban, R. S.; Nemoto, S.; Finkel, T., Mitochondria, Oxidants, and Aging. *Cell* **2005,** 120, (4), 483-495.

48. Reeg, S.; Grune, T., Protein oxidation in aging: Does it play a role in aging progression? *Antioxidants & redox signaling* **2014**.

49. Lindner, H.; Helliger, W., Age-dependent deamidation of asparagine residues in proteins. *Experimental gerontology* **2001,** 36, (9), 1551-1563.

50. Gaczynska, M.; Osmulski, P. A.; Ward, W. F., Caretaker or undertaker? The role of the proteasome in aging. *Mechanisms of Ageing and Development* **2001,** 122, (3), 235-254.

51. Carrard, G.; Bulteau, A.-L.; Petropoulos, I.; Friguet, B., Impairment of proteasome structure and function in aging. *The International Journal of Biochemistry & Cell Biology* **2002,** 34, (11), 1461-1474.

52. Chondrogianni, N.; Gonos, E. S., Proteasome dysfunction in mammalian aging: Steps and factors involved. *Experimental Gerontology* **2005,** 40, (12), 931-938.

53. Friguet, B.; Bulteau, A.-L.; Chondrogianni, N.; Conconi, M.; Petropoulos, I., Protein Degradation by the Proteasome and Its Implications in Aging. *Annals of the New York Academy of Sciences* **2000,** 908, (1), 143-154.

54. Walther, Dirk M.; Kasturi, P.; Zheng, M.; Pinkert, S.; Vecchi, G.; Ciryam, P.; Morimoto, Richard I.; Dobson, Christopher M.; Vendruscolo, M.; Mann, M.; Hartl, F. U., Widespread Proteome Remodeling and Aggregation in Aging C. elegans. *Cell* **2015,** 161, (4), 919-932.

55. Ori, A.; Toyama, B. H.; Harris, M. S.; Bock, T.; Iskar, M.; Bork, P.; Ingolia, N. T.; Hetzer, M. W.; Beck, M., Integrated Transcriptome and Proteome Analyses Reveal Organ-Specific Proteome Deterioration in Old Rats. *Cell Systems* **2015,** 1, (3), 224-237.

56. Wyman, J.; Gill, S. J., *Binding and linkage: functional chemistry of biological macromolecules*. University Science Books: 1990.

57. Schellman, J. A., Macromolecular binding. *Biopolymers* **1975,** 14, (5), 999-1018.

58. Baraibar, M. A.; Liu, L.; Ahmed, E. K.; Friguet, B., Protein oxidative damage at the crossroads of cellular senescence, aging, and age-related diseases. *Oxidative medicine and cellular longevity* **2012,** 2012.

59. Baraibar, M. A.; Ladouce, R.; Friguet, B., Proteomic quantification and identification of carbonylated proteins upon oxidative stress and during cellular aging. *Journal of proteomics* **2013,** 92, 63-70.

60. Baraibar, M. A.; Friguet, B., Oxidative proteome modifications target specific cellular pathways during oxidative stress, cellular senescence and aging. *Experimental gerontology* **2013,** 48, (7), 620-625.

61. David, D. C.; Ollikainen, N.; Trinidad, J. C.; Cary, M. P.; Burlingame, A. L.; Kenyon, C., Widespread protein aggregation as an inherent part of aging in C. elegans. *PLoS biology* **2010,** 8, (8), 1925.

62. Apetri, A. C.; Surewicz, K.; Surewicz, W. K., The effect of disease-associated mutations on the folding pathway of human prion protein. *Journal of Biological Chemistry* **2004,** 279, (17), 18008-18014.

63. Chiti, F.; Taddei, N.; Bucciantini, M.; White, P.; Ramponi, G.; Dobson, C. M., Mutational analysis of the propensity for amyloid formation by a globular protein. *The EMBO journal* **2000,** 19, (7), 1441-1449.

64. Liemann, S.; Glockshuber, R., Influence of amino acid substitutions related to inherited human prion diseases on the thermodynamic stability of the cellular prion protein. *Biochemistry* **1999,** 38, (11), 3258-3267.

65. Ma, J.; Wollmann, R.; Lindquist, S., Neurotoxicity and neurodegeneration when PrP accumulates in the cytosol. *Science* **2002,** 298, (5599), 1781-1785.

66. Qu, B.-H.; Thomas, P. J., Alteration of the Cystic Fibrosis Transmembrane Conductance Regulator Folding Pathway EFFECTS OF THE ΔF508 MUTATION ON THE THERMODYNAMIC STABILITY AND FOLDING YIELD OF NBD1. *Journal of Biological Chemistry* **1996,** 271, (13), 7261-7264.

67. Varani, L.; Hasegawa, M.; Spillantini, M. G.; Smith, M. J.; Murrell, J. R.; Ghetti, B.; Klug, A.; Goedert, M.; Varani, G., Structure of tau exon 10 splicing regulatory element RNA and destabilization by mutations of frontotemporal dementia and parkinsonism linked to chromosome 17. *Proceedings of the National Academy of Sciences* **1999,** 96, (14), 8229-8234.

68. Bullock, A. N.; Henckel, J.; DeDecker, B. S.; Johnson, C. M.; Nikolova, P. V.; Proctor, M. R.; Lane, D. P.; Fersht, A. R., Thermodynamic stability of wild-type and mutant p53 core domain. *Proceedings of the National Academy of Sciences* **1997,** 94, (26), 14338-14342.

69. Mayer, S.; Rüdiger, S.; Ang, H. C.; Joerger, A. C.; Fersht, A. R., Correlation of levels of folded recombinant p53 in Escherichia coli with thermodynamic stability in vitro. *Journal of molecular biology* **2007,** 372, (1), 268-276.

70. György, B.; Tóth, E.; Tarcsa, E.; Falus, A.; Buzás, E. I., Citrullination: a posttranslational modification in health and disease. *The international journal of biochemistry & cell biology* **2006,** 38, (10), 1662-1677.

71. Proctor, E. A.; Ding, F.; Dokholyan, N. V., Structural and thermodynamic effects of post-translational modifications in mutant and wild type Cu, Zn superoxide dismutase. *Journal of molecular biology* **2011,** 408, (3), 555-567.

72. Fan, J. Q.; Ishii, S.; Asano, N.; Suzuki, Y., Accelerated transport and maturation of lysosomal alpha-galactosidase A in Fabry lymphoblasts by an enzyme inhibitor. *Nat Med* **1999,** 5, (1), 112-5.

73. Hammarstrom, P.; Wiseman, R. L.; Powers, E. T.; Kelly, J. W., Prevention of transthyretin amyloid disease by changing protein misfolding energetics. *Science* **2003,** 299, (5607), 713-6.

74. Sawkar, A. R.; Cheng, W. C.; Beutler, E.; Wong, C. H.; Balch, W. E.; Kelly, J. W., Chemical chaperones increase the cellular activity of N370S beta -glucosidase: a therapeutic strategy for Gaucher disease. *Proc Natl Acad Sci U S A* **2002,** 99, (24), 15428-33.

75. Lindquist, S. L.; Kelly, J. W., Chemical and biological approaches for adapting proteostasis to ameliorate protein misfolding and aggregation diseases: progress and prognosis. *Cold Spring Harb Perspect Biol* **2011,** 3, (12).

76. Powers, E. T.; Morimoto, R. I.; Dillin, A.; Kelly, J. W.; Balch, W. E., Biological and chemical approaches to diseases of proteostasis deficiency. *Annu Rev Biochem* **2009,** 78, 959-91.

77. Mecozzi, V. J.; Berman, D. E.; Simoes, S.; Vetanovetz, C.; Awal, M. R.; Patel, V. M.; Schneider, R. T.; Petsko, G. A.; Ringe, D.; Small, S. A., Pharmacological chaperones stabilize retromer to limit APP processing. *Nature chemical biology* **2014,** 10, (6), 443-449.

78. Parkinson, J., An essay on the shaking palsy. . *Whittingham and Rowland for Sherwood, Needly and Jones, London* **1817**.

79. George, J. L.; Mok, S.; Moses, D.; Wilkins, S.; Bush, A. I.; Cherny, R. A.; Finkelstein, D. I., Targeting the Progression of Parkinson's Disease. *Current Neuropharmacology* **2009,** 7, (1), 9-36.

80. Polymeropoulos, M. H.; Lavedan, C.; Leroy, E.; Ide, S. E.; Dehejia, A.; Dutra, A.; Pike, B.; Root, H.; Rubenstein, J.; Boyer, R.; Stenroos, E. S.; Chandrasekharappa, S.; Athanassiadou, A.; Papapetropoulos, T.; Johnson, W. G.; Lazzarini, A. M.; Duvoisin, R. C.; Di Iorio, G.; Golbe, L. I.; Nussbaum, R. L., Mutation in the α-Synuclein Gene Identified in Families with Parkinson's Disease. *Science* **1997,** 276, (5321), 2045-2047.

81. Spillantini, M. G.; Schmidt, M. L.; Lee, V. M. Y.; Trojanowski, J. Q.; Jakes, R.; Goedert, M., [alpha]-Synuclein in Lewy bodies. *Nature* **1997,** 388, (6645), 839-840.

82. Blesa, J.; Phani, S.; Jackson-Lewis, V.; Przedborski, S., Classic and New Animal Models of Parkinson's Disease. *Journal of Biomedicine and Biotechnology* **2012,** 2012, 10.

83. Ulmer, T. S.; Bax, A.; Cole, N. B.; Nussbaum, R. L., Structure and dynamics of micelle-bound human alpha-synuclein. *J Biol Chem* **2005,** 280, (10), 9595-603.

84. Tuttle, M. D.; Comellas, G.; Nieuwkoop, A. J.; Covell, D. J.; Berthold, D. A.; Kloepper, K. D.; Courtney, J. M.; Kim, J. K.; Barclay, A. M.; Kendall, A.; Wan, W.; Stubbs, G.; Schwieters, C. D.; Lee, V. M.; George, J. M.; Rienstra, C. M., Solid-state NMR structure of a pathogenic fibril of full-length human alpha-synuclein. *Nat Struct Mol Biol* **2016,** 23, (5), 409-15.

85. Conway, K. A.; Lee, S.-J.; Rochet, J.-C.; Ding, T. T.; Williamson, R. E.; Lansbury, P. T., Acceleration of oligomerization, not fibrillization, is a shared property of both α-synuclein mutations linked to early-onset Parkinson's disease: Implications for pathogenesis and therapy. *Proceedings of the National Academy of Sciences* **2000,** 97, (2), 571-576.

86. Fredenburg, R. A.; Rospigliosi, C.; Meray, R. K.; Kessler, J. C.; Lashuel, H. A.; Eliezer, D.; Lansbury, P. T., The Impact of the E46K Mutation on the Properties of α-Synuclein in Its Monomeric and Oligomeric States. *Biochemistry* **2007,** 46, (24), 7107-7118.

87. Taylor, J. P.; Mata, I. F.; Farrer, M. J., LRRK2: a common pathway for parkinsonism, pathogenesis and prevention? *Trends in Molecular Medicine* **2006,** 12, (2), 76-82.

88. Greggio, E.; Zambrano, I.; Kaganovich, A.; Beilina, A.; Taymans, J.-M.; Daniëls, V.; Lewis, P.; Jain, S.; Ding, J.; Syed, A.; Thomas, K. J.; Baekelandt, V.; Cookson, M. R., The Parkinson Disease-associated Leucine-rich Repeat Kinase 2 (LRRK2) Is a Dimer That Undergoes Intramolecular Autophosphorylation. *Journal of Biological Chemistry* **2008,** 283, (24), 16906-16914.

89. Guaitoli, G.; Raimondi, F.; Gilsbach, B. K.; Gómez-Llorente, Y.; Deyaert, E.; Renzi, F.; Li, X.; Schaffner, A.; Jagtap, P. K. A.; Boldt, K.; von Zweydorf, F.; Gotthardt, K.; Lorimer, D. D.; Yue, Z.; Burgin, A.; Janjic, N.; Sattler, M.; Versées, W.; Ueffing, M.; Ubarretxena-Belandia, I.; Kortholt, A.; Gloeckner, C. J., Structural model of the dimeric Parkinson's protein LRRK2 reveals a compact architecture involving distant interdomain contacts. *Proceedings of the National Academy of Sciences* **2016,** 113, (30), E4357-E4366.

90. Berger, Z.; Smith, K. A.; LaVoie, M. J., Membrane Localization of LRRK2 Is Associated with Increased Formation of the Highly Active LRRK2 Dimer and Changes in Its Phosphorylation. *Biochemistry* **2010,** 49, (26), 5511-5523.

91. Thaler, A.; Ash, E.; Gan-Or, Z.; Orr-Urtreger, A.; Giladi, N., The LRRK2 G2019S mutation as the cause of Parkinson's disease in Ashkenazi Jews. *Journal of Neural Transmission* **2009,** 116, (11), 1473.

92. West, A. B.; Moore, D. J.; Biskup, S.; Bugayenko, A.; Smith, W. W.; Ross, C. A.; Dawson, V. L.; Dawson, T. M., Parkinson's disease-associated mutations in leucine-rich repeat kinase 2 augment kinase activity. *Proceedings of the National Academy of Sciences of the United States of America* **2005,** 102, (46), 16842-16847.

93. Lewis, P. A.; Greggio, E.; Beilina, A.; Jain, S.; Baker, A.; Cookson, M. R., The R1441C mutation of LRRK2 disrupts GTP hydrolysis. *Biochemical and biophysical research communications* **2007,** 357, (3), 668-671.

94. Li, Y.; Dunn, L.; Greggio, E.; Krumm, B.; Jackson, G. S.; Cookson, M. R.; Lewis, P. A.; Deng, J., THE R1441C MUTATION ALTERS THE FOLDING PROPERTIES OF THE ROC DOMAIN OF LRRK2. *Biochimica et biophysica acta* **2009,** 1792, (12), 1194-1197.

95. Ito, G.; Okai, T.; Fujino, G.; Takeda, K.; Ichijo, H.; Katada, T.; Iwatsubo, T., GTP Binding Is Essential to the Protein Kinase Activity of LRRK2, a Causative Gene Product for Familial Parkinson's Disease. *Biochemistry* **2007,** 46, (5), 1380-1388.

96. Sheng, Z.; Zhang, S.; Bustos, D.; Kleinheinz, T.; Le Pichon, C. E.; Dominguez, S. L.; Solanoy, H. O.; Drummond, J.; Zhang, X.; Ding, X.; Cai, F.; Song, Q.; Li, X.; Yue, Z.; van der Brug, M. P.; Burdick, D. J.; Gunzner-Toste, J.; Chen, H.; Liu, X.; Estrada, A. A.; Sweeney, Z. K.; Scearce-Levie, K.; Moffat, J. G.; Kirkpatrick, D. S.; Zhu, H., Ser¹²⁹² Autophosphorylation Is an Indicator of LRRK2 Kinase Activity and Contributes to the Cellular Effects of PD Mutations. *Science Translational Medicine* **2012,** 4, (164), 164ra161-164ra161.

97. Taymans, J.-M., The GTPase function of LRRK2. *Biochemical Society Transactions* **2012,** 40, (5), 1063-1069.

98. Cookson, M. R., Cellular functions of LRRK2 implicate vesicular trafficking pathways in Parkinson's disease. *Biochemical Society Transactions* **2016,** 44, (6), 1603-1610.

99. Schapansky, J.; Nardozzi, J. D.; Felizia, F.; LaVoie, M. J., Membrane recruitment of endogenous LRRK2 precedes its potent regulation of autophagy. *Human Molecular Genetics* **2014,** 23, (16), 4201-4214.

100. Liu, Z.; Mobley, J. A.; DeLucas, L. J.; Kahn, R. A.; West, A. B., LRRK2 autophosphorylation enhances its GTPase activity. *The FASEB Journal* **2016,** 30, (1), 336-347.

101. Li, Y.; Liu, W.; Oo, T. F.; Wang, L.; Tang, Y.; Jackson-Lewis, V.; Zhou, C.; Geghman, K.; Bogdanov, M.; Przedborski, S.; Beal, M. F.; Burke, R. E.; Li, C., Mutant LRRK2(R1441G) BAC transgenic mice recapitulate cardinal features of Parkinson's disease. *Nature neuroscience* **2009,** 12, (7), 826-828.

102. Strickland, E. C.; Geer, M. A.; Hong, J.; Fitzgerald, M. C., False-Positive Rate Determination of Protein Target Discovery using a Covalent Modification- and Mass Spectrometry-Based Proteomics Platform. *Journal of The American Society for Mass Spectrometry* **2014,** 25, (1), 132-140.

103. Nelder, J. A.; Mead, R., A Simplex Method for Function Minimization. *The Computer Journal* **1965,** 7, (4), 308-313.

104. Myers, J. K.; Pace, C. N.; Scholtz, J. M., Denaturant m values and heat capacity changes: relation to changes in accessible surface areas of protein unfolding. *Protein Science : A Publication of the Protein Society* **1995,** 4, (10), 2138-2148.

105. Castegna, A.; Aksenov, M.; Thongboonkerd, V.; Klein, J. B.; Pierce, W. M.; Booze, R.; Markesbery, W. R.; Butterfield, D. A., Proteomic identification of oxidatively modified proteins in Alzheimer's disease brain. Part II: dihydropyrimidinase-related protein 2, α-enolase and heat shock cognate 71. *Journal of Neurochemistry* **2002,** 82, (6), 1524-1532.

106. Wakatsuki, S.; Saitoh, F.; Araki, T., ZNRF1 promotes Wallerian degeneration by degrading AKT to induce GSK3B-dependent CRMP2 phosphorylation. *Nat Cell Biol* **2011,** 13, (12), 1415-1423.

107. Takai, Y.; Sasaki, T.; Matozaki, T., Small GTP-Binding Proteins. *Physiological Reviews* **2001,** 81, (1), 153-208.

108. Lewis, P. A., Assaying the Kinase Activity of LRRK2 in vitro. *Journal of Visualized Experiments : JoVE* **2012**, (59), 3495.

109. Webber, P. J.; Smith, A. D.; Sen, S.; Renfrow, M. B.; Mobley, J. A.; West, A. B., Autophosphorylation in the Leucine-Rich Repeat Kinase 2 (LRRK2) GTPase Domain Modifies Kinase and GTP-Binding Activities. *Journal of molecular biology* **2011,** 412, (1), 94-110.

110. Morimoto, R. I., Proteotoxic stress and inducible chaperone networks in neurodegenerative disease and aging. *Genes Dev* **2008,** 22, (11), 1427-38.

111. Berlett, B. S.; Stadtman, E. R., Protein oxidation in aging, disease, and oxidative stress. *J Biol Chem* **1997,** 272, (33), 20313-6.

112. de Graff, Adam M. R.; Hazoglou, Michael J.; Dill, Ken A., Highly Charged Proteins: The Achilles' Heel of Aging Proteomes. *Structure* 24, (2), 329-336.

113. Eppig, J. T.; Blake, J. A.; Bult, C. J.; Kadin, J. A.; Richardson, J. E.; The Mouse Genome Database, G., The Mouse Genome Database (MGD): facilitating mouse as a model for human biology and disease. *Nucleic Acids Research* **2015,** 43, (Database issue), D726-D736.

114. Meany, D. L.; Xie, H.; Thompson, L. V.; Arriaga, E. A.; Griffin, T. J., Identification of carbonylated proteins from enriched rat skeletal muscle mitochondria using affinity chromatography-stable isotope labeling and tandem mass spectrometry. *Proteomics* **2007,** 7, (7), 1150-1163.

115. Umstead, T. M.; Freeman, W. M.; Chinchilli, V. M.; Phelps, D. S., Age-related changes in the expression and oxidation of bronchoalveolar lavage proteins in the rat. *American Journal of Physiology - Lung Cellular and Molecular Physiology* **2009,** 296, (1), L14-L29.

116. Piec, I.; Listrat, A.; Alliot, J.; Chambon, C.; Taylor, R. G.; Bechet, D., Differential proteome analysis of aging in rat skeletal muscle. *The FASEB Journal* **2005,** 19, (9), 1143-1145.

117. Wenzel, P.; Schuhmacher, S.; Kienhöfer, J.; Müller, J.; Hortmann, M.; Oelze, M.; Schulz, E.; Treiber, N.; Kawamoto, T.; Scharffetter-Kochanek, K.; Münzel, T.; Bürkle, A.; Bachschmid, M. M.; Daiber, A., Manganese superoxide dismutase and aldehyde dehydrogenase deficiency increase mitochondrial oxidative stress and aggravate age-dependent vascular dysfunction. *Cardiovascular Research* **2008,** 80, (2), 280-289.

118. Waldera-Lupa, D. M.; Kalfalah, F.; Florea, A.-M.; Sass, S.; Kruse, F.; Rieder, V.; Tigges, J.; Fritsche, E.; Krutmann, J.; Busch, H.; Boerries, M.; Meyer, H. E.; Boege, F.; Theis, F.; Reifenberger, G.; Stuhler, K., Proteome-wide analysis reveals an age-associated cellular phenotype of in situ aged human fibroblasts. *Aging (Albany NY)* **2014,** 6, (10), 856-872.

119. Fu, Y.; Zhao, D.; Pan, B.; Wang, J.; Cui, Y.; Shi, F.; Wang, C.; Yin, X.; Zhou, X.; Yang, L., Proteomic Analysis of Protein Expression Throughout Disease Progression in a Mouse Model of Alzheimer's Disease. *Journal of Alzheimer's Disease* **2015,** 47, 915-926.

120. Martínez, A.; Portero-Otin, M.; Pamplona, R.; Ferrer, I., Protein Targets of Oxidative Damage in Human Neurodegenerative Diseases with Abnormal Protein Aggregates. *Brain Pathology* **2010,** 20, (2), 281-297.

121. Fu, Y.-J.; Xiong, S.; Lovell, M. A.; Lynn, B. C., Quantitative Proteomic Analysis of Mitochondria in Aging PS-1 Transgenic Mice. *Cellular and Molecular Neurobiology* **2009,** 29, (5), 649-664.

122. Pamplona, R.; Dalfó, E.; Ayala, V.; Bellmunt, M. J.; Prat, J.; Ferrer, I.; Portero-Otín, M., Proteins in human brain cortex are modified by oxidation, glycoxidation, and lipoxidation Effects of Alzheimer disease and identification of lipoxidation targets. *Journal of Biological Chemistry* **2005,** 280, (22), 21522-21530.

123. Bosetti, F.; Brizzi, F.; Barogi, S.; Mancuso, M.; Siciliano, G.; Tendi, E. A.; Murri, L.; Rapoport, S. I.; Solaini, G., Cytochrome c oxidase and mitochondrial F1F0-ATPase (ATP synthase) activities in platelets and brain from patients with Alzheimer's disease. *Neurobiology of Aging* **2002,** 23, (3), 371-376.

124. Sultana, R.; Perluigi, M.; Newman, S. F.; Pierce, W. M.; Cini, C.; Coccia, R.; Butterfield, D. A., Redox proteomic analysis of carbonylated brain proteins in mild cognitive impairment and early Alzheimer's disease. *Antioxidants & redox signaling* **2010,** 12, (3), 327-336.

125. Cabiscol, E.; Levine, R. L., Carbonic Anhydrase III. OXIDATIVE MODIFICATION IN VIVO AND LOSS OF PHOSPHATASE ACTIVITY DURING AGING. *Journal of Biological Chemistry* **1995,** 270, (24), 14742-14747.

126. Zhang, J.; Goodlett, D. R.; Peskind, E. R.; Quinn, J. F.; Zhou, Y.; Wang, Q.; Pan, C.; Yi, E.; Eng, J.; Aebersold, R. H.; Montine, T. J., Quantitative proteomic analysis of age-related changes in human cerebrospinal fluid. *Neurobiology of Aging* **2005,** 26, (2), 207-227.

127. Bota, D. A.; Davies, K. J. A., Protein degradation in mitochondria: implications for oxidative stress, aging and disease:: a novel etiological classification of mitochondrial proteolytic disorders. *Mitochondrion* **2001,** 1, (1), 33-49.

128. Dencher, N. A.; Frenzel, M.; Reifschneider, N. H.; Sugawa, M.; Krause, F., Proteome Alterations in Rat Mitochondria Caused by Aging. *Annals of the New York Academy of Sciences* **2007,** 1100, (1), 291-298.

129. Poon, H. F.; Vaishnav, R. A.; Getchell, T. V.; Getchell, M. L.; Butterfield, D. A., Quantitative proteomics analysis of differential protein expression and oxidative modification of specific proteins in the brains of old mice. *Neurobiology of Aging* **2006,** 27, (7), 1010-1019.

130. Chapple, S. J.; Siow, R. C. M.; Mann, G. E., Crosstalk between Nrf2 and the proteasome: Therapeutic potential of Nrf2 inducers in vascular disease and aging. *The International Journal of Biochemistry & Cell Biology* **2012,** 44, (8), 1315-1320.

131. Lee, C. H.; Won, M.-H., Increased Dynamin-1 and -2 Protein Expression in the Aged Gerbil Hippocampus. *Cellular and Molecular Neurobiology* **2014,** 34, (6), 791-796.

132. Kimura, N.; Imamura, O.; Ono, F.; Terao, K., Aging attenuates dynactin–dynein interaction: Down-regulation of dynein causes accumulation of endogenous tau and amyloid precursor protein in human neuroblastoma cells. *Journal of Neuroscience Research* **2007,** 85, (13), 2909-2916.

133. Reed, T. T., Lipid peroxidation and neurodegenerative disease. *Free Radical Biology and Medicine* **2011,** 51, (7), 1302-1319.

134. Shephard, F.; Greville-Heygate, O.; Marsh, O.; Anderson, S.; Chakrabarti, L., A mitochondrial location for haemoglobins—Dynamic distribution in ageing and Parkinson's disease. *Mitochondrion* **2014,** 14, 64-72.

135. Stanley, D. P.; Shetty, A. K., Aging in the rat hippocampus is associated with widespread reductions in the number of glutamate decarboxylase-67 positive interneurons but not interneuron degeneration. *Journal of Neurochemistry* **2004,** 89, (1), 204-216.

136. Sorolla, M. A.; Reverter-Branchat, G.; Tamarit, J.; Ferrer, I.; Ros, J.; Cabiscol, E., Proteomic and oxidative stress analysis in human brain samples of Huntington disease. *Free Radical Biology and Medicine* **2008,** 45, (5), 667-678.

137. Oelze, M.; Kröller-Schön, S.; Steven, S.; Lubos, E.; Doppler, C.; Hausding, M.; Tobias, S.; Brochhausen, C.; Li, H.; Torzewski, M.; Wenzel, P.; Bachschmid, M.; Lackner, K. J.; Schulz, E.; Münzel, T.; Daiber, A., <div xmlns="http://www.w3.org/1999/xhtml" xmlns:hwp="http://schema.highwire.org/Journal hwp:id="article-title-1" class="article-title">Glutathione Peroxidase-1 Deficiency Potentiates Dysregulatory Modifications of Endothelial Nitric Oxide Synthase and Vascular Dysfunction in AgingNovelty and Significance . *Hypertension* **2014,** 63, (2), 390-396.

138. Chaudhuri, A. R.; de Waal, E. M.; Pierce, A.; Van Remmen, H.; Ward, W. F.; Richardson, A., Detection of protein carbonyls in aging liver tissue: A fluorescence-based proteomic approach. *Mechanisms of ageing and development* **2006,** 127, (11), 849-861.

139. Heydari, A. R.; Wu, B.; Takahashi, R.; Strong, R.; Richardson, A., Expression of heat shock protein 70 is altered by age and diet at the level of transcription. *Molecular and Cellular Biology* **1993,** 13, (5), 2909-2918.

140. Trougakos, I. P.; Gonos, E. S., Regulation of clusterin/apolipoprotein J, a functional homologue to the small heat shock proteins, by oxidative stress in ageing and age-related diseases. *Free Radical Research* **2006,** 40, (12), 1324-1334.

141. Hondius, D. C.; van Nierop, P.; Li, K. W.; Hoozemans, J. J. M.; van der Schors, R. C.; van Haastert, E. S.; van der Vies, S. M.; Rozemuller, A. J. M.; Smit, A. B., Profiling the human hippocampal proteome at all pathologic stages of Alzheimer's disease. *Alzheimer's & Dementia* **2016,** 12, (6), 654-668.

142. Reed, T.; Perluigi, M.; Sultana, R.; Pierce, W. M.; Klein, J. B.; Turner, D. M.; Coccia, R.; Markesbery, W. R.; Butterfield, D. A., Redox proteomic identification of 4-hydroxy-2-nonenal-modified brain proteins in amnestic mild cognitive impairment: insight into the role of lipid peroxidation in the progression and pathogenesis of Alzheimer's disease. *Neurobiology of disease* **2008,** 30, (1), 107-120.

143. Benice, T. S.; Rizk, A.; Kohama, S.; Pfankuch, T.; Raber, J., Sex-differences in age-related cognitive decline in C57BL/6J mice associated with increased brain microtubule-associated protein 2 and synaptophysin immunoreactivity. *Neuroscience* **2006,** 137, (2), 413-423.

144. Johnson, J. O.; Pioro, E. P.; Boehringer, A.; Chia, R.; Feit, H.; Renton, A. E.; Pliner, H. A.; Abramzon, Y.; Marangi, G.; Winborn, B. J.; Gibbs, J. R.; Nalls, M. A.; Morgan, S.; Shoai, M.; Hardy, J.; Pittman, A.; Orrell, R. W.; Malaspina, A.; Sidle, K. C.; Fratta, P.; Harms, M. B.; Baloh, R. H.; Pestronk, A.; Weihl, C. C.; Rogaeva, E.; Zinman, L.; Drory, V. E.; Borghero, G.; Mora, G.; Calvo, A.; Rothstein, J. D.; Italsgen; Drepper, C.; Sendtner, M.; Singleton, A. B.; Taylor, J. P.; Cookson, M. R.; Restagno, G.; Sabatelli, M.; Bowser, R.; Chiò, A.; Traynor, B. J., Mutations in the Matrin 3 gene cause familial amyotrophic lateral sclerosis. *Nature neuroscience* **2014,** 17, (5), 664-666.

145. Perluigi, M.; Di Domenico, F.; Giorgi, A.; Schininà, M. E.; Coccia, R.; Cini, C.; Bellia, F.; Cambria, M. T.; Cornelius, C.; Butterfield, D. A.; Calabrese, V., Redox proteomics in aging rat brain: Involvement of mitochondrial reduced glutathione status and mitochondrial protein oxidation in the aging process. *Journal of Neuroscience Research* **2010,** 88, (16), 3498-3507.

146. Ortega-Molina, A.; Serrano, M., PTEN in cancer, metabolism, and aging. *Trends in Endocrinology & Metabolism* **2013,** 24, (4), 184-189.

147. Favre, C.; Aguilar, P. S.; Carrillo, M. C., Oxidative stress and chronological aging in glycogen-phosphorylase-deleted yeast. *Free Radical Biology and Medicine* **2008,** 45, (10), 1446-1456.

148. Parisiadou, L.; Xie, C.; Cho, H. J.; Lin, X.; Gu, X.-L.; Long, C.-X.; Lobbestael, E.; Baekelandt, V.; Taymans, J.-M.; Sun, L.; Cai, H., Phosphorylation of ERM Proteins by LRRK2 Promotes the Rearrangement of Actin Cytoskeleton in Neuronal Morphogenesis. *The Journal of neuroscience : the official journal of the Society for Neuroscience* **2009,** 29, (44), 13971-13980.

149. Shimohama, S.; Fujimoto, S.; Sumida, Y.; Akagawa, K.; Shirao, T.; Matsuoka, Y.; Taniguchi, T., Differential Expression of Rat Brain Synaptic Proteins in Development and Aging. *Biochemical and Biophysical Research Communications* **1998,** 251, (1), 394-398.

150. Song, H.-O.; Lee, W.; An, K.; Lee, H.-s.; Cho, J. H.; Park, Z.-Y.; Ahnn, J., C. elegans STI-1, the Homolog of Sti1/Hop, Is Involved in Aging and Stress Response. *Journal of Molecular Biology* **2009,** 390, (4), 604-617.

151. Zhang, G.-R.; Cheng, X.-R.; Zhou, W.-X.; Zhang, Y.-X., Age-related expression of STUB1 in senescence-accelerated mice and its response to anti-Alzheimer's disease traditional Chinese medicine. *Neuroscience Letters* **2008,** 438, (3), 371-375.

152. Boyd-Kimball, D.; Castegna, A.; Sultana, R.; Poon, H. F.; Petroze, R.; Lynn, B. C.; Klein, J. B.; Butterfield, D. A., Proteomic identification of proteins oxidized by Aβ(1–42) in synaptosomes: Implications for Alzheimer's disease. *Brain Research* **2005,** 1044, (2), 206-215.

153. Sarge, K. D.; Park-Sarge, O.-K., Sumoylation and human disease pathogenesis. *Trends in Biochemical Sciences* **2009,** 34, (4), 200-205.

154. Carrano, A. C.; Liu, Z.; Dillin, A.; Hunter, T., A conserved ubiquitination pathway determines longevity in response to diet restriction. *Nature* **2009,** 460, (7253), 396-399.

155. Haapasalo, A.; Viswanathan, J.; Bertram, L.; Soininen, H.; Tanzi, Rudolph E.; Hiltunen, M., Emerging role of Alzheimer's disease-associated ubiquilin-1 in protein aggregation. *Biochemical Society Transactions* **2010,** 38, (1), 150-155.

156. Zhang, K. Y.; Yang, S.; Warraich, S. T.; Blair, I. P., Ubiquilin 2: A component of the ubiquitin–proteasome system with an emerging role in neurodegeneration. *The International Journal of Biochemistry & Cell Biology* **2014,** 50, 123-126.

157. Gong, B., Leznik, Elena, The Role of Ubiquitin C-Terminal Hydrolase L1 in Neurodegenerative Disorders. *Drug News Perspect* **2007,** 20, (6).

158. Anagnostou, G.; Akbar, M. T.; Paul, P.; Angelinetta, C.; Steiner, T. J.; de Belleroche, J., Vesicle associated membrane protein B (VAPB) is decreased in ALS spinal cord. *Neurobiology of Aging* **2010,** 31, (6), 969-985.

159. Price, J. C.; Guan, S.; Burlingame, A.; Prusiner, S. B.; Ghaemmaghami, S., Analysis of proteome dynamics in the mouse brain. *Proc Natl Acad Sci U S A* **2010,** 107, (32), 14508-13.

160. Fà, M.; Staniszewski, A.; Saeed, F.; Francis, Y. I.; Arancio, O., Dynamin 1 Is Required for Memory Formation. *PLoS ONE* **2014,** 9, (3), e91954.

161. Song, Y.; Masison, D. C., Independent Regulation of Hsp70 and Hsp90 Chaperones by Hsp70/Hsp90-organizing Protein Sti1 (Hop1). *The Journal of biological chemistry* **2005,** 280, (40), 34178-34185.

162. Hsu, A.-L.; Murphy, C. T.; Kenyon, C., Regulation of Aging and Age-Related Disease by DAF-16 and Heat-Shock Factor. *Science* **2003,** 300, (5622), 1142.

163. Muñoz, M. J., Longevity and heat stress regulation in Caenorhabditis elegans. *Mechanisms of Ageing and Development* **2003,** 124, (1), 43-48.

164. Min, J.-N.; Whaley, R. A.; Sharpless, N. E.; Lockyer, P.; Portbury, A. L.; Patterson, C., CHIP Deficiency Decreases Longevity, with Accelerated Aging Phenotypes Accompanied by Altered Protein Quality Control. *Molecular and Cellular Biology* **2008,** 28, (12), 4018-4025.

165. Saez, I.; Vilchez, D., The Mechanistic Links Between Proteasome Activity, Aging and Age-related Diseases. *Current Genomics* **2014,** 15, (1), 38-51.

166. Lee, M. K.; Stirling, W.; Xu, Y.; Xu, X.; Qui, D.; Mandir, A. S.; Dawson, T. M.; Copeland, N. G.; Jenkins, N. A.; Price, D. L., Human α-synuclein-harboring familial Parkinson's disease-linked Ala-53 → Thr mutation causes neurodegenerative disease with α-synuclein aggregation in transgenic mice. *Proceedings of the National Academy of Sciences* **2002,** 99, (13), 8968-8973.

167. Diedrich, M.; Mao, L.; Bernreuther, C.; Zabel, C.; Nebrich, G.; Kleene, R.; Klose, J., Proteome analysis of ventral midbrain in MPTP-treated normal and L1cam transgenic mice. *PROTEOMICS* **2008,** 8, (6), 1266-1275.

168. Van Laar, V. S.; Dukes, A. A.; Cascio, M.; Hastings, T. G., Proteomic analysis of rat brain mitochondria following exposure to dopamine quinone: Implications for Parkinson disease. *Neurobiology of Disease* **2008,** 29, (3), 477-489.

169. Periquet, M.; Corti, O.; Jacquier, S.; Brice, A., Proteomic analysis of parkin knockout mice: alterations in energy metabolism, protein handling and synaptic function. *Journal of Neurochemistry* **2005,** 95, (5), 1259-1276.

170. Jin, J.; Meredith, G. E.; Chen, L.; Zhou, Y.; Xu, J.; Shie, F.-S.; Lockhart, P.; Zhang, J., Quantitative proteomic analysis of mitochondrial proteins: relevance to Lewy body formation and Parkinson's disease. *Molecular Brain Research* **2005,** 134, (1), 119-138.

171. Gibson, G. E.; Park, L. C. H.; Sheu, K.-F. R.; Blass, J. P.; Calingasan, N. Y., The α-ketoglutarate dehydrogenase complex in neurodegeneration. *Neurochemistry International* **2000,** 36, (2), 97-112.

172. Zhang, X.; Yin, X.; Yu, H.; Liu, X.; Yang, F.; Yao, J.; Jin, H.; Yang, P., Quantitative proteomic analysis of serum proteins in patients with Parkinson's disease using an isobaric tag for relative and absolute quantification labeling, two-dimensional liquid chromatography, and tandem mass spectrometry. *Analyst* **2012,** 137, (2), 490-495.

173. Xun, Z.; Sowell, R. A.; Kaufman, T. C.; Clemmer, D. E., Lifetime Proteomic Profiling of an A30P α-Synuclein Drosophila Model of Parkinson's Disease. *Journal of Proteome Research* **2007,** 6, (9), 3729-3738.

174. Fai Poon, H.; Frasier, M.; Shreve, N.; Calabrese, V.; Wolozin, B.; Butterfield, D. A., Mitochondrial associated metabolic proteins are selectively oxidized in A30P α-synuclein transgenic mice—a model of familial Parkinson's disease. *Neurobiology of Disease* **2005,** 18, (3), 492-498.

175. Licker, V.; Côte, M.; Lobrinus, J. A.; Rodrigo, N.; Kövari, E.; Hochstrasser, D. F.; Turck, N.; Sanchez, J.-C.; Burkhard, P. R., Proteomic profiling of the substantia nigra demonstrates CNDP2 overexpression in Parkinson's disease. *Journal of Proteomics* **2012,** 75, (15), 4656-4667.

176. Szklarczyk, D.; Franceschini, A.; Wyder, S.; Forslund, K.; Heller, D.; Huerta-Cepas, J.; Simonovic, M.; Roth, A.; Santos, A.; Tsafou, K. P.; Kuhn, M.; Bork, P.; Jensen, L. J.; von Mering, C., STRING v10: protein–protein interaction networks, integrated over the tree of life. *Nucleic Acids Research* **2015,** 43, (Database issue), D447-D452.

177. Chen, X.; Guo, C.; Kong, J., Oxidative stress in neurodegenerative diseases. *Neural Regeneration Research* **2012,** 7, (5), 376-385.

178. Dunn, L.; Allen, G. F. G.; Mamais, A.; Ling, H.; Li, A.; Duberley, K. E.; Hargreaves, I. P.; Pope, S.; Holton, J. L.; Lees, A.; Heales, S. J.; Bandopadhyay, R., Dysregulation of glucose metabolism is an early event in sporadic Parkinson's disease(). *Neurobiology of Aging* **2014,** 35, (5), 1111-1115.

179. Aviles-Olmos, I.; Dickson, J.; Kefalopoulou, Z.; Djamshidian, A.; Ell, P.; Soderlund, T.; Whitton, P.; Wyse, R.; Isaacs, T.; Lees, A.; Limousin, P.; Foltynie, T., Exenatide and the treatment of patients with Parkinson's disease. *The Journal of Clinical Investigation* **2013,** 123, (6), 2730-2736.

Biography

Julia Hamilton Roberts was born on June 7, 1990 in Cumberland, Maryland. She was raised in Frostburg, Maryland by her parents Ken and Margaret Roberts with her younger sister Kathryn. She attended Georgetown University in Washington, DC from 2008-2012 and graduated with a Bachelors of Science in Chemistry with a minor in Psychology. She started her graduate career in 2012 at Duke University and worked as a graduate assistant in the lab of Michael C. Fitzgerald. She graduated with her PhD in Chemistry in the spring of 2017. Throughout her time at Duke she was awarded the Kathleen Zielek Fellowship (2015) and the GAANN Fellowship to further her goals of teaching at the college level (2016-2017). She was a member of the American Chemical Society from 2014-present and the U.S. Human Proteome Organization 2016-present. She served as the co-President of Duke's Women in Science and Engineering (WiSE) graduate student organization for the 2016-2017 academic year.

Publications

1). **Roberts JH**, Liu F, Karnuta JM, Fitzgerld MC. Discovery of Age-Related Protein Folding Stability Differences in the Mouse Brain Proteome. Journal of Proteome Research. Published online: November 2, 2016 DOI: 10.1021/acs.jproteome.6b00927

2). Ogburn RN, Randall TA, Xu Y, **Roberts JH** et al. Are dust mite allergens more abundant or more stable than other Dermatophagoides pteronyssinus proteins? Letter to

the Editor. The Journal of allergy and clinical immunology. Published online: August 2016. DOI: http://dx.doi.org/10.1016/j.jaci.2016.08.016

3). **Roberts JH,** Fitzgerald MC. A Study of Protein Folding Stability Differences Caused by Parkinson's Disease Progression in Mice. *Manuscript in Progress*